MATHEMATICAL MODELLING OF ADVECTION-DIFFUSION-REACTION IN ETHANOL PRODUCTION

AHMAD IZUL FAKHRUDDIN B. AZIMI

DOCTOR OF PHILOSOPHY

UNIVERSITI MALAYSIA PAHANG
AL-SULTAN ABDULLAH

UNIVERSITI MALAYSIA PAHANG AL-SULTAN ABDULLAH

DECLARATION OF THESIS AND COPYRIGHT

Author's Full Name : AHMAD IZUL FAKHRUDDIN B. AZIMI
Date of Birth : 24th October 1989
Title : MATHEMATICAL MODELLING OF ADVECTION-DIFFUSION-REACTION IN ETHANOL PRODUCTION
Academic Session : SEMESTER II SESSION 2023/2024

I declare that this thesis is classified as:

☐	CONFIDENTIAL	(Contains confidential information under the Official Secret Act 1997)*
☐	RESTRICTED	(Contains restricted information as specified by the organization where research was done)*
☒	OPEN ACCESS	I agree that my thesis to be published as online open access (Full Text)

I acknowledge that Universiti Malaysia Pahang Al-Sultan Abdullah reserves the following rights:

1. The Thesis is the Property of Universiti Malaysia Pahang Al-Sultan Abdullah
2. The Library of Universiti Malaysia Pahang Al-Sultan Abdullah has the right to make copies of the thesis for the purpose of research only.
3. The Library has the right to make copies of the thesis for academic exchange.

Certified by:

_______________________	_______________________
(Student's Signature)	(Supervisor's Signature)
_______________________	Ts. Dr. Norazaliza Binti Mohd Jamil
New IC	Name of Supervisor
Date: 25 July 2024	Date: 25/7/2024

NOTE : * If the thesis is CONFIDENTIAL or RESTRICTED, please attach a thesis declaration letter.

SUPERVISOR’S DECLARATION

We hereby declare that We have checked this thesis and, in our opinion, this thesis is adequate in terms of scope and quality for the award of the degree of Doctor of Philosophy.

(Supervisor’s Signature)

Full Name : TS. DR. NORAZALIZA BINTI MOHD JAMIL

Position : Senior Lecturer

Date : 25/7/2024

(Co-supervisor’s Signature)

Full Name : PROFESOR ChM DR. MOHD HASBI BIN AB RAHIM

Position : Professor

Date : 25/7/2024

STUDENT'S DECLARATION

I hereby declare that the work in this thesis is based on my original work except for quotations and citations which have been duly acknowledged. I also declare that it has not been previously or concurrently submitted for any other degree at Universiti Malaysia Pahang Al-Sultan Abdullah or any other institutions.

(Student's Signature)

Full Name : AHMAD IZUL FAKHRUDDIN BIN AZIMI

ID Number : PSS17001

Date : 25 July 2024

MATHEMATICAL MODELLING OF ADVECTION-DIFFUSION-REACTION IN ETHANOL PRODUCTION

AHMAD IZUL FAKHRUDDIN B. AZIMI

Thesis submitted in fulfillment of the requirements
for the award of the degree of
Doctor of Philosophy

Centre for Mathematical Sciences

UNIVERSITI MALAYSIA PAHANG AL-SULTAN ABDULLAH

JULY 2024

ACKNOWLEDGEMENTS

I have interacted with numerous researchers, academics, and practitioners while completing my thesis. They contributed to my comprehension and thought processes. In particular, I would like to thank my main supervisor, Ts. Dr. Norazaliza Binti Mohd Jamil, for her unwavering support throughout my Ph.D. studies and related research, as well as for her patience, motivation, and vast knowledge. Throughout my research and writing of this thesis, her assistance has been extremely valuable.

I would also like to convey my deepest gratitude to my parents, Azimi Bin Ismail and Wan Fauziah Binti Wan Agil, for their prayers and support from the time of my birth to the present.

In addition, I would like to thank the Ministry of Higher Education Malaysia (MOHE) and Universiti Malaysia Pahang Al-Sultan Abdullah (UMPSA) for their financial support via research grants RDU160116 and RDU210329.

I would like to express my gratitude and appreciation to all of the lecturers, laboratory technicians, and staff members at the Centre for Mathematical Sciences, UMPSA.

Not forgotten are all my family members, Mohd Amiridwan, Farah Hanan, Ahmad Khairul, Ezzaty, Ahmad Aiman, Farah Waheeda, Uwais, Aisyah, and Eishal. All of my friends, Dr. Basri, Dr. Amir, Usop, Zahir, Dr. Redwan, and Dr. Nurashiken, for spiritually supporting me and encouraging me to be more patient during my studies.

I could not have completed this thesis without their prayers and support.

ABSTRAK

Etanol yang dihasilkan melalui penapaian merupakan salah satu tenaga boleh diperbaharui dan boleh menjadi alternatif kepada tenaga bahan api fosil konvensional. Walau bagaimanapun, penghasilan etanol pada kadar yang tinggi sukar untuk difahami dan mahal untuk dikendalikan. Oleh itu, penyelidikan yang mendalam diperlukan untuk penghasilan yang optimum. Penggunaan model kinetik adalah salah satu kaedah yang paling mudah untuk bereksperimen dengan pengeluaran. Namun, pembangunan model kinetik praktikal memerlukan pertimbangan yang teliti terhadap banyak faktor. Selain itu, kajian terdahulu telah menunjukkan bahawa parameter pengadukan dalam tangki juga mempunyai kesan ke atas pengeluaran etanol. Objektif kajian ini adalah untuk menyediakan strategi penyelesaian bagi pemodelan dan simulasi pengadukan dalam tangki melalui penambahan dan peningkatan model kinetik. Untuk mendapatkan pemahaman yang lebih mendalam tentang pengeluaran etanol, analisis kestabilan model tanpa dimensi dan analisis parameter telah dilaksanakan. Dalam sistem persamaan matematik ini, tiga titik kestabilan ditemui. Sementara itu, analisis parameter mendedahkan hanya satu parameter dengan kesan positif dan lapan parameter yang akan menghalang proses penapaian etanol. Kajian ini juga mengkaji kesan pergerakan zarah-zarah terhadap proses penapaian etanol. Penggabungan komponen pergerakan zarah-zarah membawa kepada pembentukan tiga sistem persamaan pembezaan separa (PDE) berasingan, yang kesemuanya diselesaikan dengan menggunakan Kaedah Isipadu Terhingga (FVM). Penambahan elemen pergerakan zarah-zarah pada model juga telah menunjukkan bahawa pergerakan jenis alir lintang mempunyai kesan yang ketara ke atas sistem pengeluaran etanol. Kajian ini juga dapat menentukan nilai terbaik untuk alir lintang bagi mengoptimumkan pengeluaran. Penambahbaikan model lanjutan dengan memasukkan unsur-unsur dinamik bendalir dalam kajian ini juga telah membenarkan penyiasatan pengadukan sistem pengeluaran etanol. Kajian mendapati bahawa peningkatan keluasan pusaran permukaan bebas daripada pengadukan dan peningkatan kelajuan pengaduk akan mengurangkan pengeluaran. Analisis kedudukan pengaduk juga telah mendedahkan bahawa pengadukan yang menghasilkan larutan homogen meningkatkan pengeluaran etanol. Kajian ini mampu menghasilkan anggaran yang lebih baik untuk pengeluaran etanol dalam bioreaktor beraduk dan pemahaman yang lebih mendalam tentang tingkah laku zarah-zarah dalam sistem pengeluaran etanol melalui penapaian.

ABSTRACT

Ethanol produced through fermentation is one of the renewable energies that can be an alternative to conventional fossil fuel energy. However, high-volume ethanol production process is difficult to comprehend and expensive to operate. Therefore, in-depth research is required for optimal outcomes. Utilising a kinetic model is one of the most convenient method to experiment with the production of high-volume ethanol. However, the development of a practical kinetic model requires careful consideration of numerous factors. In addition, previous research has shown that the agitation parameters in the tank also have an impact on ethanol production. This study aimed to provide a solution strategy for modelling and simulation of agitation in the tank by extending and enhancing the kinetic model. In order to gain a deeper understanding of ethanol production, stability analysis of the non-dimensional model and parameter analysis were performed. In this system of mathematical equations, three stability points were found. In the meantime, the parameter analysis revealed only one parameter with positive effects and eight parameters that will hinder the ethanol fermentation process. This study additionally studied the impact of particle movement on the process of ethanol fermentation. The incorporation of particle movement components led to the formation of three separate systems of partial differential equations (PDEs), all of which were solved using the Finite Volume Method (FVM). The addition of particle movement elements to the model demonstrated a significant effect of advection-type movements on the ethanol production system. This study also determined the best value for advection to optimise production. The incorporation of fluid dynamics elements in the extended model of this study also allowed for the investigation of the ethanol production system’s agitator. The study found that the increase in the area of the free surface vortex from agitation and the increase in agitator speed reduce the volume of ethanol production. The analysis of the agitator’s position further revealed that agitation resulting in the production of a homogeneous solution increases ethanol production. The findings of this study can result in better estimations of ethanol production in agitated bioreactors and enhance understanding of particle behaviour in ethanol production system through fermentation.

TABLE OF CONTENT

CHAPTER 6 RESULT AND DISCUSSION 75

LIST OF TABLES

LIST OF FIGURES

LIST OF SYMBOLS

$M(t)$	The variable of microbial concentration at time t
$P(t)$	The variable of ethanol concentration at time t
$S(t)$	The variable of substrate concentration at time t
$\mu_{\max}$	Maximum specific rate for microbial growth
K_{SM}	Substrate half-saturation coefficient for microbial growth
K_{IM}	Substrate inhibition coefficient in microbial growth
P_M	Product inhibition coefficient in microbial growth
K_d	Microbial death rate
v_{max}	Maximum specific rate for ethanol production
K_{SP}	Substrate half-saturation coefficient for ethanol production
K_{IP}	Substrate inhibition coefficient in ethanol production
P_P	Product inhibition coefficient in ethanol production
Y_{MS}	Yield coefficient for the substrate used on microbial growth
Y_{PS}	Yield coefficient for the substrate used on ethanol production
m	Maintenance coefficient of microbial
g	The dimensionless variable of microbes
p	The dimensionless variable of ethanol
s	The dimensionless variable of substrate
τ	The dimensionless variable of time
σ	The ratio of maximum specific microbial growth to its death rate
α	The ratio of substrate half-saturation coefficient for microbial growth to its inhibitory effect
β	The ratio of substrate inhibitory effect between ethanol production and microbial growth
λ	The ratio of maximum specific ethanol production and its substrate inhibitory effect to microbial death rate and its product inhibitory effect

ϕ	The ratio of maximum specific ethanol production and its substrate inhibitory effect to microbial death rate and its product inhibitory effect
ρ	The ratio of microbial maintenance coefficient to its death rate
γ	The ratio of substrate half-saturation coefficient for ethanol production and its substrate inhibitory effect towards the product inhibitory effect in microbial growth
κ	The ratio of maximum specific ethanol production and its substrate inhibitory effect towards microbial death rate and the product inhibitory effect in ethanol production
Y_i	Observed values
$\hat{Y}_i$	Predicted values
D	Particle diffusivity coefficient
ω	Shape parameter of gamma distribution
ψ	Scale parameter of gamma distribution
U	Velocity components in the x directions
V	Velocity components in the y directions
pr	Pressure of solution
vis	Viscosity of solution
ρ	Density of water
Re	Reynolds numbers
σ	Standard deviation of normal distribution
μ_x, μ_y	Means of multivariate normal distribution
σ_x, σ_y	Standard deviation of multivariate normal distribution
$Cov(x,y)$	Covariance of multivariate normal distribution
Ag	Agitator speed coefficient

LIST OF ABBREVIATIONS

ASEAN	Association of Southeast Asian Nations
DAFC	Direct Alcohol Fuel Cells
ODE	Ordinary Differential Equations
OPT	Oil Palm Trunk
PDE	Partial Differential Equations
MSE	Mean Square Error
FVM	Finite Volume Method

LIST OF APPENDICES

CHAPTER 1

INTRODUCTION

1.1 Research Background

Energy is one of the most essential requirements for the development of a nation and has attracted much attention over the past several decades. According to Bouzguenda et al. (2019), the energy industry has a significant role in increasing wealth, fostering national development, and ensuring social sustainability. Nonetheless, there has been a significant rise in energy consumption. According to the findings of Malek et al. (2017), Malaysia is among the ASEAN nations that have experienced a threefold increase in energy consumption. In order to reduce carbon dioxide and greenhouse gas emissions while meeting future energy demands, fossil fuels should be replaced by sustainable and green energy sources. Nonetheless, the use of fossil fuels has caused global climate change (Kumar et al., 2020).

Ethanol through fermentation, also known as bioethanol, appears to be a promising alternative to traditional fossil fuel energy sources. As an alternative energy source, it can typically be created through yeast fermentation from agricultural waste. Bioethanol is one of the renewable energies that has grabbed the attention of Malaysian researchers such as Derman et al. (2018) and Phuang et al. (2022), possibly due to the abundance of natural resources, economic considerations, and environmental concerns (Derman et al., 2018). Bioethanol is mostly created by fermenting the sugar, most of which is found in food, with yeasts or bacteria in a reactor. Nevertheless, the utilisation of food as a viable source for bioethanol production is hindered by the escalating market demand and subsequent increase in food prices (Tse et al., 2021). They also mention that this issue has resulted in the creation of bioethanol of the second generation, which replaces feed with low-value materials such as wood chips, crop residues, and waste. Ethanol can also be combined with diesel to create biodiesel, which emits fewer pollutants and greenhouse gases. According to Sokmez et al. (2022), ethanol is one of the sources that can generate electricity using Direct Alcohol Fuel Cells (DAFC) technology. They also stated that ethanol has advantages over other liquid alcohols because it can be produced using renewable resources. According to Phuang et al. (2022), the Malaysian government enacted a B20 biodiesel mandate in 2020, requiring the transportation industry to blend at least 20 per cent oil palm biodiesel with diesel gasoline. In addition, the Feed-in Tariff Mechanism enables the renewable energy industry to sell electricity to the national grid at predetermined prices. The implementation of initiatives such as the Feed-in Tariff Mechanism in Malaysia is expected to enhance the domestic demand for ethanol; thus, emphasising the need for studies to improve ethanol production in Malaysia.

1.2 Problem Statement

The process of ethanol production through fermentation is complex to understand and expensive to operate. One of the convenient ways to experiment with the production is by using kinetic models. According to Phukoetphim et al. (2017), kinetic models can forecast fermentation performance and the influence of environmental conditions on ethanol production. In addition, Germec et al. (2022) state that the study on the kinetic models will enhance understanding of the metabolic nature of a fermentation process, including the behaviour of microbes and the biomass consumed throughout the fermentation process. In order to have a deep understanding of the microbial nature and subsequently optimise the production yield, a lot of consideration has to be made, such as the parameters and significant factors of kinetic models.

Numerous research has been conducted to investigate the various elements that influence ethanol yield and the type of fermentation involved. Tesfaw & Assefa (2014) reported that microbial growth and ethanol production are greatly influenced by temperature, pH, oxygen, initial concentrations of the substrate, by-product acids, solid solubility, and microbe immobilisation. Phisalaphong et al. (2006) also took into account the influence of temperature in his investigation of ethanol production. The study successfully developed a kinetic model and discovered 12 parameters within it. Nevertheless, the study concentrated solely on developing kinetic models for batch fermentation, neglecting other variables that impact ethanol production.

A review by Tse et al. (2021) stated that three types of fermentation to produce ethanol fermentation, namely batch, fed-batch, and continuous fermentations, each can be represented with a different kind of kinetic model. In general, in batch fermentation, all ingredients will be added to the reactor, and only when the reaction is complete will the materials be extracted. In contrast, during fed-batch fermentation, the ingredients are regularly brought into the reactor. Similar to batch fermentation, the material will only be removed from the reactor at the end of the reaction. Meanwhile, continuous fermentation is carried out with the input and removal of material occurring continuously during the fermentation process.

Batch fermentation can be undertaken in a non-shaking or shaking reactor, such as the experiment conducted by Nasir et al. (2017). According to their research, shaking the reactor creates a homogenous mixture that can increase ethanol production. This homogeneous mixture can be linked to hydrodynamic factors like diffusion and advection. Diffusion is the random motion of particles in a fluid, whereas advection is the transport of particles affected by the velocity of the fluid. However, there is no kinetic study related to batch fermentation that includes hydrodynamics factors has been conducted to the extent of the researcher’s knowledge. This might lead to biased prediction results due to the incomprehensive judgment of both chemical and physical phenomena occurring in the ethanol production process.

1.3 Research Question

This research is conducted to answer the following questions:

i. How to improve the predictive capabilities of the existing kinetic model and provide more directed and rational approaches for process design and optimisation?
ii. What are the advection and diffusion effects during the fermentation process?
iii. What is the effect of hydrodynamics in a mathematical model of ethanol production through batch fermentation process?

1.4 Research Objectives

The objectives of this research are:

i. To improve the predictive capabilities of the existing kinetic model and provide more directed and rational approaches for process design and optimisation.
ii. To examine the effects of advection and diffusion during a fermentation process.
iii. To formulate the effect of hydrodynamics in a mathematical model of ethanol production through the batch fermentation process.

1.5 Research Scope

Generally, batch fermentation is conducted in a reactor with no addition or removal initial value of microbial, substrate, and products from the beginning of the operation until the process is completed. According to Tse et al. (2021), this type of fermentation is the cheapest to operate despite the longer downtime between batches because of cleaning, vessel preparation, and sterilisation. For that reason, this research focused on the modelling of ethanol production through batch fermentation only. Experimental data from Abdul Halim (2016) was used in this study due to challenges in gathering data for the validation process. For the computation procedure, MATLAB was utilised for stability analysis, whereas Python was employed for Finite Volume Method.

1.6 Research Significance

This research provided significant contributions to mathematics and its application in terms of the study’s novelty and the findings’ applicability. First, this research proposed a mathematical model for ethanol production through the batch fermentation process with the effect of hydrodynamics by coupling the diffusion-advection-reaction equations with fluid dynamics terms. Then, the developed kinetic model can be used to better predict ethanol production, better explain the fermentation process, and verify experimental output.

1.7 Thesis Outlines

The current thesis consists of seven chapters on fermentation-based ethanol production. Chapter 1 outlines the introduction, the importance of studying ethanol fermentation production, and the existing body of knowledge in this field of study. Chapter 2 discusses microbial growth and its relationship to the reaction kinetic model. This chapter additionally explains the data sources of this study, the necessity of considering particle movement in the ethanol production process, the concepts of diffusion and advection transport phenomena, the introduction of fluid dynamics, and the mathematical equation for fluid flow. Chapter 3 provides an overview of the study and discusses the specific numerical method employed, namely the finite volume method, for both 1D and 2D problems. Chapter 4 examines stability analysis from the chosen model of Phisalaphong et al. (2006) to gain a more comprehensive understanding of the dynamic system of ethanol production. The proposed mathematical models for particle movement and fluid flow in the reactor are then presented in Chapter 5. Chapter 6 primarily focuses on the results and discussion of the study, whilst Chapter 7 presents the conclusions and recommendations for future works.

CHAPTER 2

LITERATURE REVIEW

2.1 Introduction

This chapter begins with a review of microbial growth in the literature. The phases of microbial growth are discussed to understand the kinetic model and parameters involved. This chapter also outlines prior findings related to the elements of particle movement during fermentation and discusses the significance of fluid dynamics in the process of ethanol production through fermentation.

2.2 Microbial Growth

Batch fermentation relates to the rate of microbial growth, substrate usage, and product formation in different environmental conditions (Tse et al., 2021). Microbial growth plays a crucial role in biotechnologies as it elucidates the fundamental aspects of microbial life and understands the utilisation of substrates and the resulting byproducts. Nevertheless, the factors influencing the growth vary depending on microbial species. Figure 2.1 shows the typical microbial growth as seen in Das & Pandit (2021). Microbes undergo various phases of growth in fermentation: (i) lag phase, (ii) exponential phase, (iii) stationary phase, and (iv) death phase. The lag phase follows the introduction of microbial, during which they are introduced and adjusted to the new environment. At this phase, no growth will occur. During the exponential phase, the number of bacteria and their mass increase with the presence of substrate. Then, the stationary phase happens when the growth rate equals the death rate. The death phase is when the death rate is higher than the growth rate. The drop-in growth rate is due to a lack of food and microbial contamination due to toxic or environmental changes, such as temperature or pH.

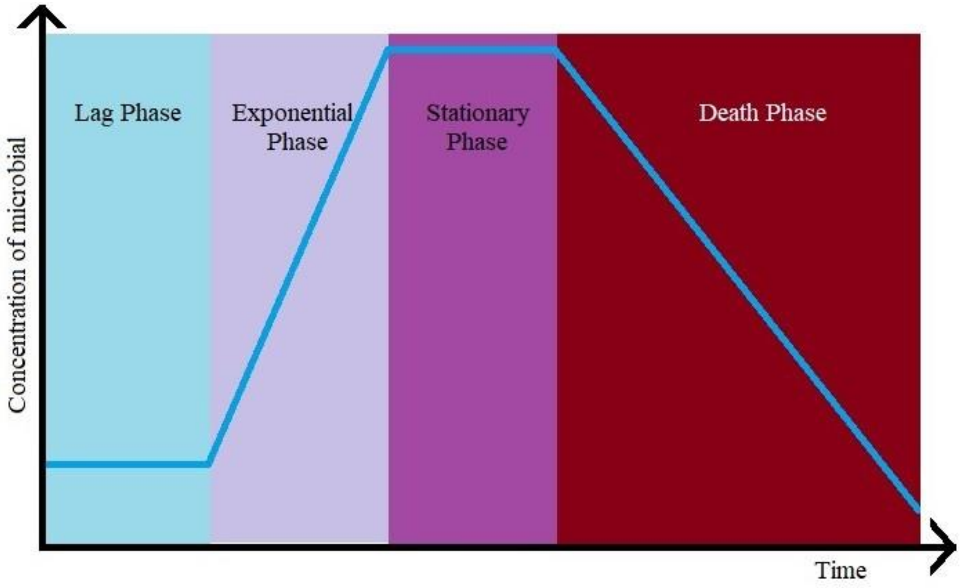

Figure 2.1 Phases in the microbial growth.
Source: Das & Pandit (2021)

2.3 Kinetic Reaction Model for Batch Fermentation

Fermentation is a biological process whereby microbes naturally degrade complex substrate molecules into smaller and simpler molecules. The process leads to the production of many byproducts, including ethanol. During the process of fermentation, microbes undergo cell proliferation, which is referred to as microbial growth. Recently, various mathematical models pertaining to the topic of biotechnology have been documented in the literature, with an extensive array of kinetic models exploring fermentation processes.

Kinetic models are one of the methods that can be used to gain an understanding of microbes. The Monod's (1949) model is the dominant and well-known kinetic model. This model relating to microbial growth was introduced by a French scientist, Jacques Monod, and it becomes the foundation for the most recently developed model.

Equation 2.1 was used by Monod (1949) to explain the behaviour of microbial growth under the conditions of limited substrate availability, where μ is the microbial growth, $\mu_{\max}$ is the maximum specific growth rate, S is the substrate concentration, and K_{SM} is saturation growth constant.

$$\mu = \frac{\mu_{\max} S}{K_{SM} + S} \qquad 2.1$$

Roca et al. (1996) and Birol et al. (1998) are among the researchers in the field of ethanol fermentation who have employed the Monod (1949) model in their studies. While they discovered that Monod's (1949) model had a strong fit with their data from experimentation, the research conducted by Kono (1968) demonstrated that the model needed revision to accurately describe the data obtained from batch fermentation experiments. Kono & Asai (1969) presented a mathematical equation that explains the production of ethanol by incorporating parameters associated with the phase of microbial growth. The parameters are related to the correlation between microbial growth and production under growth and non-growth conditions.

Other studies have demonstrated that a high substrate concentration inhibits microbial growth. Among these studies are those conducted by Yano & Koga (1969), Edwards (1970), and Tseng & Wayman (1975). For example, according to Tseng & Wayman (1975), low levels of substrate concentrations serve as a metabolic resource for microbes, with excessive concentrations of substrate inhibiting microbial growth. In addition, the model proposed by Edwards (1970), inspired by the model proposed by Aiba et al. (1968), incorporated substrate inhibition factors into the study of microbial growth. The factor of product inhibition also has an influence on the process of ethanol production through fermentation. Doble et al. (2004) reported that product inhibition is apparent when the concentration of the product exceeds a specific threshold at the end of the process.

Aiba et al. (1968) effectively incorporated product inhibition effect parameters into the kinetic model in their study on the product inhibition effect in ethanol production. However, the model developed by them did not account for the substrate’s kinetic model. A mathematical model that integrated the effects of substrate inhibition and product inhibition by integrating both factors into a single equation was developed by Levenspiel (1980), but a substrate kinetic model is still missing from the model. Ghaly & El-Taweel (1997) also introduced a model of ethanol production that integrates factors, namely substrate limitation, substrate inhibition, ethanol inhibition, and cell death. The model found that microbes possess the capacity to endure specific amounts of ethanol within their growth medium. Nevertheless, the presence and increase of ethanol production can potentially hinder microbial growth, resulting in a complete cessation of growth. Apart from that, they stated that the effect of osmotic pressure in a medium with a high substrate concentration will also inhibit growth. The microbial growth rate proposed by Ghaly & El-Taweel (1997) is expressed in Equation 2.2,

$$\mu = \frac{\mu_{\max} S}{K_{SM} + S} \frac{P_M}{P_M + P} \frac{K_{IM}}{K_{IM} + S} \tag{2.2}$$

where K_{SM} represents the saturation growth constant and P_M and K_{IM} represent the product inhibition coefficient and substrate inhibition coefficient, respectively. In addition, Ghaly & El-Taweel (1997) used the K_d parameter as a coefficient or the microbial death rate in their model.

In principle, Equation 2.3 represents the mathematical expression for measuring the rate of change of microbial populations.

$$\begin{gathered} \begin{bmatrix} \text{Rate of} \\ \text{change of microbial} \end{bmatrix} = \begin{bmatrix} \text{Microbial} \\ \text{growth rate} \end{bmatrix} - \begin{bmatrix} \text{Microbial} \\ \text{death rate} \end{bmatrix} \\ \frac{dM}{dt} = M \frac{\mu_{\max} S}{K_{SM} + S} \frac{P_M}{P_M + P} \frac{K_{IM}}{K_{IM} + S} - K_d M \end{gathered} \tag{2.3}$$

where the variable M is the microbial concentration ($\mathrm{g\,L^{-1}}$), P is the product concentration ($\mathrm{g\,L^{-1}}$), S is the substrate concentration ($\mathrm{g\,L^{-1}}$) and t is the time (h).

Additionally, Ghaly & El-Taweel (1997) highlighted the significance of the yield coefficient for product on substrate, Y_{PS} , the yield coefficient for microbes on substrate, Y_{MS} , and the rate of change of microbial populations, dM/dt when defining the rate of product formation. Equation 2.4 mathematically illustrates the rate of change of the product.

$$\begin{bmatrix}\text{Rate of}\\ \text{change of product}\end{bmatrix}=\begin{bmatrix}\text{Product}\\ \text{formation rate}\end{bmatrix}$$

$$\frac{dP}{dt}=\frac{Y_{PS}}{Y_{MS}}\frac{dM}{dt} \qquad 2.4$$

$$\frac{dP}{dt}=\frac{Y_{PS}}{Y_{MS}}\left(M\frac{\mu_{\max}S}{K_{SM}+S}\frac{P_M}{P_M+P}\frac{K_{IM}}{K_{IM}+S}-K_dM\right)$$

Ghaly & El-Taweel (1997) also explained three different factors that can affect the rate of substrate change. These factors include the substrate consumption in microbial growth, the substrate consumption for maintenance, and the substrate consumption in product formation. Equation 2.5 explains the rate of change of the substrate in more detail.

$$-\begin{bmatrix}\text{Rate of}\\ \text{change of substrate}\end{bmatrix}=-\begin{bmatrix}\text{Substrate}\\ \text{consumption in}\\ \text{microbial growth}\end{bmatrix}-\begin{bmatrix}\text{Substrate}\\ \text{consumption in}\\ \text{product formation}\end{bmatrix}-\begin{bmatrix}\text{Substrate}\\ \text{consumption in}\\ \text{maintenance}\end{bmatrix} \qquad 2.5$$

Equation 2.5 can be represented as demonstrated in Equation 2.6.

$$-\frac{dS}{dt}=-\frac{1}{Y_{MS}}\left(\frac{dM}{dt}\right)-\frac{1}{Y_{PS}}\left(\frac{dP}{dt}\right)-mM$$

$$\frac{dS}{dt}=\frac{1}{Y_{MS}}\left(\frac{dM}{dt}\right)+\frac{1}{Y_{PS}}\left(\frac{dP}{dt}\right)+mM \qquad 2.6$$

where m is the maintenance coefficient of microbes.

In particular, Equations 2.7, 2.8, and 2.9 represent the kinetic model of Ghaly & El-Taweel (1997), which defines the microbial growth rate, product formation rate, and substrate consumption rate, respectively.

$$\frac{dM}{dt} = M\frac{\mu_{\max} S}{K_{SM}+S}\frac{P_M}{P_M+P}\frac{K_{IM}}{K_{IM}+S} - K_d M \tag{2.7}$$

$$\frac{dP}{dt} = \frac{Y_{PS}}{Y_{MS}}\left(M\frac{\mu_{\max} S}{K_{SM}+S}\frac{P_M}{P_M+P}\frac{K_{IM}}{K_{IM}+S} - K_d M\right) \tag{2.8}$$

$$\frac{dS}{dt} = \frac{1}{Y_{MS}}\left(\frac{dM}{dt}\right) + \frac{1}{Y_{PS}}\left(\frac{dP}{dt}\right) + mM \tag{2.9}$$

Phisalaphong et al. (2006) also developed a mathematical model. Akin to the study conducted by Ghaly & El-Taweel (1997), Phisalaphong et al. (2006) formulated a mathematical model consisting of three equations that explain the dynamics of microbes, products, and substrates during the ethanol fermentation process. These equations, designated as Equations 2.10, 2.11, and 2.12, constitute a system of ordinary differential equations (ODEs). Different from Ghaly & El-Taweel (1997), Phisalaphong et al. (2006) employed a number of parameters to represent inhibition factors in the equation relating to ethanol production. For instance, K_{IP} in ethanol production defines the substrate inhibition coefficient, while K_{IM} quantifies the substrate inhibition coefficient in the context of microbial growth. The model proposed by Phisalaphong et al. (2006) is represented in Equations 2.10, 2.11, and 2.12,

$$\frac{dM}{dt} = \mu_{\max} SM\left(K_{SM}+S+\frac{S^2}{K_{IM}}\right)^{-1}\left(1-\frac{P}{P_M}\right) - K_d M \tag{2.10}$$

$$\frac{dP}{dt} = v_{\max} SM\left(K_{SP}+S+\frac{S^2}{K_{IP}}\right)^{-1}\left(1-\frac{P}{P_P}\right) \tag{2.11}$$

$$\frac{dS}{dt} = -\frac{1}{Y_{MS}}\left(\frac{dM}{dt}\right) - \frac{1}{Y_{PS}}\left(\frac{dP}{dt}\right) - mM \tag{2.12}$$

where the variable M is the microbial concentration ($\mathrm{g\,L^{-1}}$), P is the product concentration ($\mathrm{g\,L^{-1}}$), S is the substrate concentration ($\mathrm{g\,L^{-1}}$) and t is the time (h). The parameters and their meaning are listed in Table 2.1.

Table 2.1 Parameters introduced by Phisalaphong et al. (2006) for ethanol fermentation production.

Parameters	Description	Unit
$\mu_{\max}$	Maximum specific rate for microbial growth	$\mathrm{h^{-1}}$
$v_{\max}$	Maximum specific rate for ethanol production	$\mathrm{h^{-1}}$
K_{SM}	Substrate half-saturation coefficient for microbial growth	$\mathrm{g\,L^{-1}}$
K_{SP}	Substrate half-saturation coefficient for ethanol production	$\mathrm{g\,L^{-1}}$
K_{IM}	Substrate inhibition coefficient in microbial growth	$\mathrm{g\,L^{-1}}$
K_{IP}	Substrate inhibition coefficient in ethanol production	$\mathrm{g\,L^{-1}}$
P_M	Product inhibition coefficient in microbial growth	$\mathrm{g\,L^{-1}}$
P_P	Product inhibition coefficient in ethanol production	$\mathrm{g\,L^{-1}}$
K_d	Microbial death rate	$\mathrm{h^{-1}}$
Y_{MS}	Yield coefficient for the substrate used on microbial growth	dimensionless
Y_{PS}	Yield coefficient for the substrate used on ethanol production	dimensionless
m	Maintenance coefficient of microbes	$\mathrm{h^{-1}}$

2.4 Data Extraction

Oil palm trunk (OPT) is a waste product generated by palm oil operations. Chopped and pressed OPT produces juice that is rich in substrate, making it a suitable metabolic source for ethanol production. Abdul Halim (2016) conducted a comparative analysis in her doctoral dissertation to explore the feasibility of making ethanol from OPT. The study examined multiple factors that contribute to the increase in ethanol production, including shaking. When a shaker was employed, only *Pichia stipitis* showed signs of an increase in ethanol production, with *Saccharomyces cerevisiae* Kyokai no. 7 species exhibited the highest ethanol yield under static conditions in the experiment. According to Abdul Halim (2016), this occurred due to the fact that shaking could increase the surface area in contact with the air. The implementation of this approach significantly reduces anaerobic conditions, a condition that does not require oxygen, within the bioreactor, hence resulting in a drop in ethanol production. Nevertheless, the study provided a basis for investigating a mathematical model related to the production of ethanol through fermentation, under both shaking and non-shaking situations. Hence, the data was used as a reference in this study.

2.5 Particle Movement in Ethanol Production

Using mathematical models is an effective way to understand the complex behaviour of fermentation processes. Understanding the parameters and key factors in fermentation process models will improve the understanding of microbial nature, optimise manufacturing yield, and boost production output. According to Ghaly & El-Taweel (1997), optimal microbial growth requires the transport of nutrients from the medium to the surface of the microbes, which can be defined as the movement of substrate particles in the medium to the microbes, thereby affecting the production of ethanol. On the other hand, Setford et al. (2019) developed a mathematical model to study the anthocyanin dissolved in the grape skin and solution for winemaking. The study found two types of particle movement with the same concept as ethanol fermentation, namely diffusion, the random movement of particles in a fluid, and advection, the transport of substances influenced by fluid velocity.

Nasir et al. (2017) conducted experiments on the isolation of *Saccharomyces cerevisiae*, a common microorganism in ethanol production, and metal ions for the production of ethanol through shaking fermentation and non-shaking fermentation. According to the study, shaking creates a homogenous mixture that improves ethanol production. In addition, a study conducted by Mohd Azhar et al. (2017) concluded that *Saccharomyces cerevisiae* can be inhibited in extreme conditions, such as high temperatures, high ethanol concentrations, and high sugar levels. To prevent such an occurrence, Merger et al. (2017) highlighted particle movement factors in their study. Although their research aimed to optimise the substrate yeast used to produce high-quality wine, the model can also be applied to ethanol fermentation. Recently, Phisalaphong et al. (2006) introduced a mathematical model that considers the inhibition factors in the process of ethanol production through fermentation. Inspired by those studies, the combination of a mathematical model that incorporates an inhibitory impact and a particle movement factor is deemed crucial for optimal ethanol production.

This study aimed to provide an understanding of mathematical models in non-shaking fermentation by considering the inhibition factor in the model of Phisalaphong et al. (2006) and the particle movement element as proposed in the model of Merger et al. (2017). The combination of these two models has led to the development of a mathematical model for fermentation in a shaking reactor. The mathematical model proposed for non-shaking fermentation is named the diffusion-reaction model, while the model for shaking fermentation is named the advection-diffusion-reaction model.

2.6 Diffusion and Advection Transport Phenomena.

There are two methods of fermentation to obtain ethanol, namely non-shaking fermentation and shaking fermentation, as described in Section 2.5. The two forms of fermentation exhibit different particle movements. The first particle movement in non-shaking fermentation involves the natural movement of particles from regions of higher particle concentration to regions of lower particle concentration. Bennett (2012) associates this movement with a diffusion movement. Many researchers have integrated the elements of diffusion with reaction through mathematical equations, for example in the work of Tosun (2007). The representation in mathematics of a coupled diffusion-reaction model is given by Equation 2.13.

$$\text{Accumulation} = \text{Diffusion Element} + \text{Reaction Element} \qquad 2.13$$

The second particle movement to explain transport phenomena, advection, is characterised by bulk movement or flow (Bennett, 2012). The flow created in shaking fermentation has an impact on the movement of particles in the reactor, consequently affecting the ethanol production process (Abdul Halim, 2016). The concept of coupled advection-diffusion-reaction has been widely applied across multiple fields of study. For instance, Cheng & Zheng (2021) conducted a study on disease transmission, Ma & Tang (2023) investigated prey and predator population densities, and Ebrahimijahan et al. (2020) conducted research on the prevention of groundwater contamination.

Tosun (2007) developed a mathematical representation for its couple advection-diffusion-reaction model expressed in Equation 2.14

$$\begin{aligned}\text{Accumulation} = \text{Advection Element} + \text{Diffusion Element}\\ + \text{Reaction Element}\end{aligned} \tag{2.14}$$

The current study believed that the integration of these two fundamental transport phenomena into a system of mathematical equations enables the development of an extensive understanding of the complex relationship between advection and diffusion phenomena.

2.7 Fluid dynamics in Ethanol Production

Understanding the behaviour of large-scale bioreactors is necessary to optimise bioethanol production. For example, Nasir et al. (2017) and Afedzi et al. (2022) indicated that inhomogeneity significantly impacts large-scale systems. However, the majority of research on ethanol production is undertaken in small-scale facilities that ignore inhomogeneity variables in bioreactors.

Saikali et al. (2021) employed the Navier-Stokes equations in their mathematical model to determine velocity profiles when simulating turbulent flow in a stirred tank reactor without baffles. However, the study did not consider the impact of the velocity profile on ethanol fermentation. The equation is a common mathematical model in the field of fluid dynamics. According to Quiroz-Pérez et al. (2019), fluid flow analysis is essential for ensuring and enhancing equipment performance to boost production output. Also, several studies adapted the fluid dynamics model into the ethanol fermentation process. The rheological parameters, including shear rate, were assessed by Um & Hanley (2008) during the process of simultaneous saccharification and co-fermentation. This investigation employed a high solid loading, resulting in a non-Newtonian solution in the tank. Their research found that regions of high shear stress can reduce the viscosity of the tank's liquid. However, Tse et al. (2021) reported that water, a Newtonian solution, is also one of the media in the fermentation process. Therefore, it is believed that a study of fermentation employing a Newtonian solution is required.

Additionally, Nagarajan et al. (2017) have conducted a fluid dynamics investigation on the fermentation of cellulose to produce ethanol. Prior to fermentation, they utilised photocatalysis, which is the process of breaking down cellulose molecules into smaller carbohydrate forms using light. Therefore, the tank wall has to transmit light. In addition, their research revealed that the Rushton impeller was capable of pushing particles against the reactor wall. However, their research only considered mixing aspects and neglected to account for element reactions. In order to contribute value to the study of ethanol production, this chapter combines previous advection-diffusion-reaction models with the fluid flow mathematical equation to illustrate fermentation in a stirred tank reactor.

2.8 Mathematical Equation for Fluid Flow

Studying the velocity profile in reactors require a comprehensive understanding of fluid flow. According to Childs (2011), the continuity equation, the conservation of mass inside a fluid flow, and the Navier-Stokes equation can be used to mathematically express the fluid flow model. According to Childs (2011), the continuity equation can be written as Equation 2.15,

$$-\frac{\partial \rho}{\partial t}=\frac{\partial(\rho u)}{\partial x}+\frac{\partial(\rho v)}{\partial y} \qquad 2.15$$

where ρ represents the density and u and v indicate the velocity components in the x and y axes, respectively. Additionally, Equation 2.15 can be reformulated as Equation 2.16.

$$\frac{\partial \rho}{\partial t} + u\frac{\partial \rho}{\partial x} + v\frac{\partial \rho}{\partial y} + \rho\left(\frac{\partial u}{\partial x} + \frac{\partial v}{\partial y}\right) = 0$$
$$\frac{D\rho}{Dt} + \rho\left(\frac{\partial u}{\partial x} + \frac{\partial v}{\partial y}\right) = 0 \qquad 2.16$$

Childs (2011) further states that in incompressible flow, the density of a fluid particle remains constant as the particle travels. Therefore, Equation 2.16 can be represented as demonstrated in Equation 2.17.

$$\frac{D\rho}{Dt} = \rho\left(\frac{\partial u}{\partial x} + \frac{\partial v}{\partial y}\right) = 0 \qquad 2.17$$

When the $\frac{D\rho}{Dt} = 0$, and Equation 2.17 is divided by the density, ρ, the continuity equation can be expressed in vector notation, as presented in Equation 2.18.

$$\nabla \bullet \mathrm{U} = 0 \quad \text{where } \mathrm{U} = \begin{pmatrix} u \\ v \end{pmatrix} \qquad 2.18$$

Also, Saikali et al. (2021) utilised the Navier-Stokes equation for their velocity profile investigation in the reactor tank. The Navier-Stokes equation is presented in Equation 2.19.

$$\frac{\partial \mathrm{U}}{\partial t} = -\left(\mathrm{U} \bullet \nabla\right)\mathrm{U} + vis\left(\nabla \bullet \nabla\right)\mathrm{U} - \frac{1}{\rho}\nabla pr \quad \text{where } \mathrm{U} = \begin{pmatrix} u \\ v \end{pmatrix} \qquad 2.19$$

In Chapter 5, continuity and the Navier-Stokes equation were utilised to couple advection-diffusion-reaction equations with fluid dynamics.

2.9 Conclusion

Gaining a thorough comprehension of a production process can enhance production output and simultaneously enable a precise mathematical model to be developed. Thus, this chapter begins by discussing microbial growth and its relationship with the reaction kinetic model of ethanol production. This chapter also presents an explanation of the data sources employed in the study. In addition, this chapter delineates the importance of incorporating particle movement into the ethanol production process, as well as the concepts of diffusion and advection. In order to further the investigation of the ethanol production process in a tank, this chapter also includes an introduction to fluid dynamics and the mathematical equations for fluid flow. The methodology of the study plays a crucial role in determining its effectiveness. Hence, the forthcoming chapter will provide a comprehensive explanation of the procedure utilised to achieve the objective of the study.

CHAPTER 3

METHODOLOGY

3.1 Introduction

This chapter explores the structure of research framework and the numerical method for solving PDE problems. The solutions to 1D and 2D spatial problems are described in more detail for all models associated with this investigation.

3.2 Overview of the Research

A structured methodology is essential to ensure systematic and efficient progress towards achieving research objectives. This study employs a flow chart, as shown in Figure 3.1, to enhance the clarity and comprehensiveness of its approach. This visual tool illustrates the sequential steps involved, offering a clear depiction of the process flow from the beginning to the end of the study.

The study started by fitting parameters to the selected model, specifically the one that Phisalaphong et al. (2006) proposed. This method aims to approximate the unknown parameter values in the model based on experimental data. Nelder-Mead serves as the algorithm in this parameter fitting, and Abdul Halim's (2016) study provides the experimental data. In general, using the algorithm, this method can estimate parameter values that minimize the difference between the model and the experimental data. Then, the study continued with stability analysis and parameter analysis on Phisalaphong et al. (2006) model. Using software named XPPAUT, this study conducts a stability analysis to determine the value of equilibrium points in the ethanol production system. In the meantime, the parameter analysis aims to investigate the behavior of the Phisalaphong et al. (2006) model parameters in relation to ethanol production.

The investigation was subsequently continued with an analysis of particle movement factors during fermentation. A model of particle movement based on diffusion has been suggested as a means to depict the non-shaking fermentation process. This is an expansion of the Phisalaphong et al. (2006). The investigation of particle movement has been further expanded with the incorporation of the advection factor into the model. Its objective is to outline the process for shaking fermentation. The fluid dynamic factor is also taken into account in order to ascertain the actual state of particle movement within the tank. A coupled fluid dynamics-advection-diffusion-reaction model was proposed.

The Finite Volume Method was used to solve the three expanded models in this study. This solution has been executed via the Python programming language, enabling the simulation of ethanol production. The final stage of this study involves the analysis of the results, discussion, conclusion, and report writing.

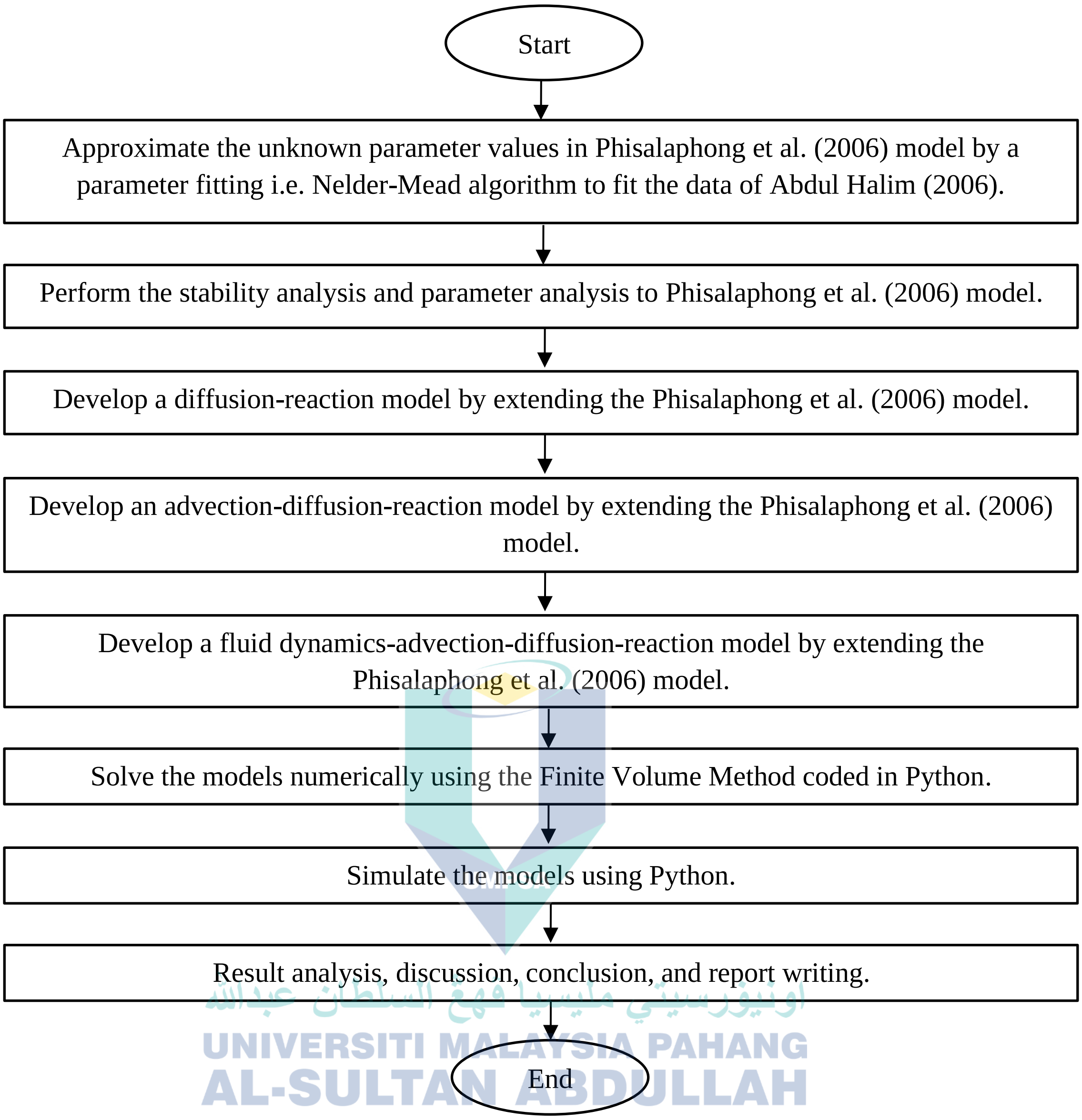

Figure 3.1 Summary of overall research framework.

3.3 Finite Volume Method for 1D Problems

This section provides an overview of the Finite Volume Method (FVM). According to Moroney (2006), the finite volume method is suitable for fluid flow problems since it preserves the conservation law, even when discretized. Furthermore, FVM can be easily implemented on many mesh structures and geometries. In consideration of these benefits, the finite volume method was utilised to solve the partial differential equation models in this study. FVM discretised its calculations using two forms of grids: (i) cell-vertex grid and (ii) cell-centre grid. The cell-vertex grid is used to calculate velocity, while the cell-centre grid is used for variables unrelated to velocity.

In this study, Equations 5.1–5.3 and Equations 5.6–5.8 represent the model for the 1D spatial problem. Both models presumed that the diffusion coefficient, D, and velocity coefficient, U, remained constant throughout the fermentation process. Therefore, FVM calculation was only limited to M, P, and S variables, with the solution for the coupled diffusion-reaction equation and the coupled advection-diffusion equation relying on the cell-centre grid type. Figure 3.2 shows the cell-centre grid. The letter C represents variables, and i is the interpolated value.

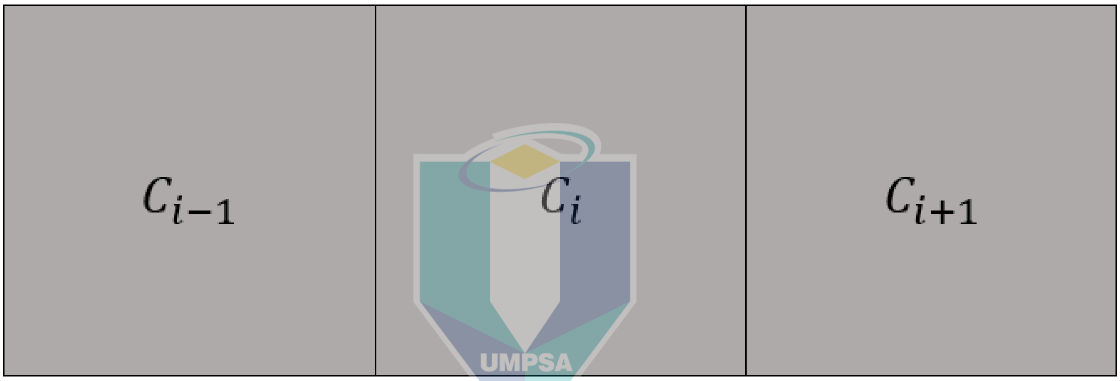

Figure 3.2 Cell-centre grid in 1D problem FVM.

Equations 5.1–5.3 contained temporal, diffusion and reaction components as shown in the following equation.

$$\text{Rate}(M) = \text{Diffusion}(M) + \text{Reaction}(M) \tag{3.1}$$

$$\text{Rate}(P) = \text{Diffusion}(P) + \text{Reaction}(P) \tag{3.2}$$

$$\text{Rate}(S) = \text{Diffusion}(S) + \text{Reaction}(S) \tag{3.3}$$

Then, each component can be solved using the next equations. The letter C is used to represent all variables to avoid repeating writing and the $\forall$ symbol is control volume.

$$\begin{aligned}\mathrm{Rate}(C) &= \int_{n}^{n+1}\int_{\forall}\frac{\partial C}{\partial t}\ \partial\forall\partial t \\ &= \frac{\partial}{\partial t}\left(C_i\Delta\forall\right) \\ &= \left(C_i^{n+1}-C_i^{n}\right)\Delta x\end{aligned}\tag{3.4}$$

$$\begin{aligned}\mathrm{Diffusion}(C) &= \int_{n}^{n+1}\int_{\forall}D\nabla\left(\nabla C\right)\ \partial\forall\partial t \\ &= \left[\left(1-f_t\right)\left(\mathrm{A}\right)^{n}+\left(f_t\right)\left(\mathrm{A}\right)^{n+1}\right]\Delta t\end{aligned}\tag{3.5}$$

where $\mathrm{A}=D\sum_{\mathrm{F}}\nabla C_{\mathrm{F}}\bullet\mathrm{F}$. The letter F is faces and f_t is time factor. The explicit-type computations were chosen to simplify the calculating procedure. Hence, the variable f_t in Equation 3.5 is equal to 0. Equation 3.6 represents the new expression for the diffusion component.

$$\begin{aligned}\mathrm{Diffusion}(C) &= \left(D\sum_{\mathrm{F}}\nabla C_{\mathrm{F}}\bullet\mathrm{F}\right)^{n}\Delta t \\ &= D\left(\frac{C_{i+1}^{n}-C_{i}^{n}}{\Delta x}\bullet(1)+\frac{C_{i-1}^{n}-C_{i}^{n}}{\Delta x}\bullet(-1)\right)\Delta t \\ &= \frac{D\Delta t}{\Delta x}\left(C_{i+1}^{n}-C_{i-1}^{n}\right)\end{aligned}\tag{3.6}$$

The subsequent equation represents the component of the reaction. To simplify writing, the letter R is used to denote reaction component. As a result of the explicit calculation type, f_t in Equation 3.7 once more has the value 0.

$$\begin{aligned}\mathrm{Reaction}(C) &= \int_{n}^{n+1}\int_{\forall}\mathrm{R}(C)\ \partial\forall\partial t \\ &= \left[\left(1-f_t\right)\mathrm{R}\left(C_i^{n}\right)+\left(f_t\right)\mathrm{R}\left(C_i^{n+1}\right)\right]\Delta x\Delta t \\ &= \mathrm{R}\left(C_i^{n}\right)\Delta x\Delta t\end{aligned}\tag{3.7}$$

Subsequently, the reaction variables M, P, and S can be defined by the following equations.

$$\mathrm{R}\left(M_i^n\right)=\frac{\mu_{max}S_i^nM_i^n}{K_{SM}+S_i^n+\left(S_i^n\right)^2\big/K_{IM}}\left(1-\frac{P_i^n}{P_M}\right)-K_dM_i^n \qquad 3.8$$

$$\mathrm{R}\left(P_i^n\right)=\frac{v_{max}S_i^nM_i^n}{K_{SP}+S_i^n+\left(S_i^n\right)^2\big/K_{IP}}\left(1-\frac{P_i^n}{P_P}\right) \qquad 3.9$$

$$\mathrm{R}\left(S_i^n\right)=-\frac{1}{Y_{MS}}\left[\mathrm{R}\left(M_i^n\right)\right]-\frac{1}{Y_{PS}}\left[\mathrm{R}\left(P_i^n\right)\right]-mM_i^n \qquad 3.10$$

Finally, Equation 3.11 can be utilised to determine the values of each variable for the subsequent iteration.

$$C_i^{n+1}=C_i^n+\frac{D\Delta t}{\left(\Delta x\right)^2}\left(C_{i+1}^n-C_{i-1}^n\right)+\mathrm{R}\left(C_i^n\right)\Delta t \qquad 3.11$$

Equations 5.6–5.8 contained temporal, advection, diffusion, and reaction components. For the temporal, diffusion and reaction components of this model, the calculations were similar to Equations 5.1–5.3. Therefore, temporal, diffusion and reaction calculations were not discussed. The following equation were then applied to Equations 5.6–5.8 to solve the advection component.

$$\begin{aligned}\text{Advection}\left(C\right)&=\int_n^{n+1}\int_{\forall}\nabla\left(UC\right)\,\partial\forall\partial t\\&=\left[\left(1-f_t\right)\left(\mathrm{B}\right)^n+\left(f_t\right)\left(\mathrm{B}\right)^{n+1}\right]\Delta t\end{aligned} \qquad 3.12$$

where $\mathrm{B}=\sum_{\mathrm{F}}UC_{\mathrm{F}}\bullet\mathrm{F}$ and $f_t = 0$. Equation 3.13 describes the new expression for the advection component.

$$\begin{aligned}\text{Advection}(C) &= \left(\sum_{\mathrm{F}} UC_{\mathrm{F}} \bullet \mathrm{F}\right)^n \Delta t \\ &= U\left(\frac{C_{i+1}^n + C_i^n}{2} \bullet (1) + \frac{C_{i-1}^n + C_i^n}{2} \bullet (-1)\right)\Delta t \\ &= \frac{U\Delta t}{2}\left(C_{i+1}^n - C_{i-1}^n\right)\end{aligned} \tag{3.13}$$

Finally, Equations 5.6–5.8 were solved using Equation 3.14.

$$C_i^{n+1} = C_i^n + \frac{D\Delta t}{(\Delta x)^2}\left(C_{i+1}^n - C_{i-1}^n\right) + \frac{U\Delta t}{2\Delta x}\left(C_{i+1}^n - C_{i-1}^n\right) + \mathrm{R}\left(C_i^n\right)\Delta t \tag{3.14}$$

3.4 Finite Volume Method for 2D Problems

In this research, the mathematical model for the 2D spatial problem was the coupled fluid dynamics-advection-diffusion-reaction equation. This model assumed that the advection value varied based on the fluid velocity, as commonly used in stirred reactors. Therefore, the FVM calculation employed differed from the 1D spatial problem. In Figure 3.3, the cell-vertex was represented by a white box, whereas the cell-centre was indicated by a shaded box. The variables *U* and *V* related to the velocity profile employed the cell-vertex grid, while the other variables employed the cell-centre grid. The letter $C_{i,j}$ in Figure 3.3 was substituted with pressure (*pr*), microbe (*M*), ethanol (*P*), and substrate (*S*).

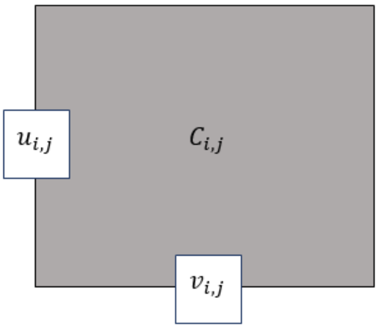

Figure 3.3 Cell-vertex grid and cell-centre grid in FVM.

Figure 3.3 shows a single grid cell. For the proposed model to be solved, the calculation should involve multiple adjacent cells. Figure 3.4 depicts the particular cell and its adjacent cell in the calculation of variable *U* in Equation 5.10.

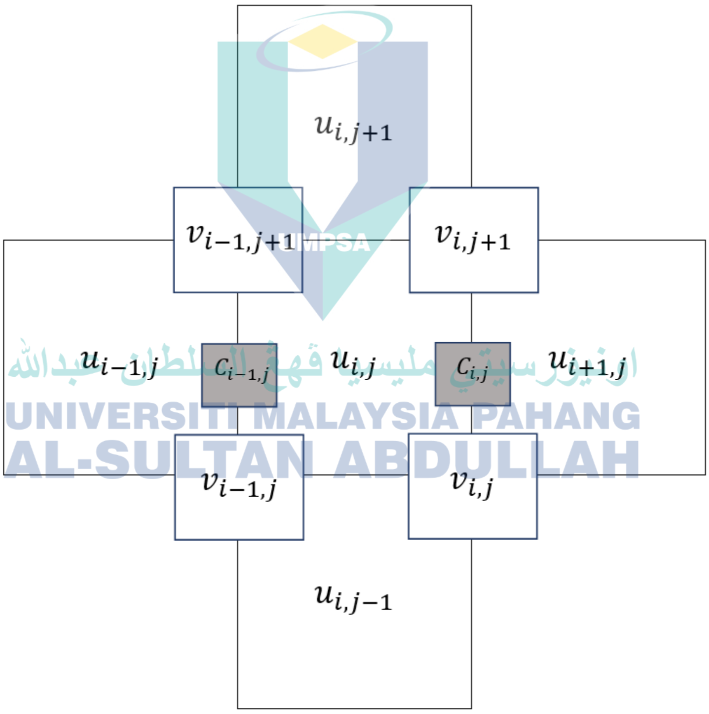

Figure 3.4 The grid cells utilised to solve Equations 5.10.

Equations 5.10–5.11 consisted of temporal, advection, diffusion, and pressure components. In order to simplify the calculation, Equations 5.10–5.11 were split down into their components.

$$\begin{aligned}\text{Rate}(U) &= \int_{n}^{n+1}\int_{\forall}\frac{\partial U}{\partial t}\ \partial\forall\partial t\\ &= \frac{\partial}{\partial t}\left(U_i\Delta\forall\right)\\ &= \left(U_i^{n+1}-U_i^{n}\right)\Delta x\Delta y\end{aligned} \tag{3.15}$$

$$\begin{aligned}\text{Advection}(U) &= \int_{n}^{n+1}\int_{\forall}\left(U\frac{\partial U}{\partial x}+V\frac{\partial U}{\partial y}\right)\ \partial\forall\partial t\\ &= \left(\sum_{\text{F}}\left(UU+VU\right)\bullet\text{F}\right)^{n}\ \Delta t\\ &= \left[\begin{array}{l}\left(\dfrac{U_{i+1,j}^{n}+U_{i,j}^{n}}{2}\right)\left(\dfrac{U_{i+1,j}^{n}+U_{i,j}^{n}}{2}\right)\bullet\left(\Delta y\right)\\ +\left(\dfrac{U_{i-1,j}^{n}+U_{i,j}^{n}}{2}\right)\left(\dfrac{U_{i-1,j}^{n}+U_{i,j}^{n}}{2}\right)\bullet\left(-\Delta y\right)\\ +\left(\dfrac{V_{i-1,j+1}^{n}+V_{i,j+1}^{n}}{2}\right)\left(\dfrac{U_{i,j+1}^{n}+U_{i,j}^{n}}{2}\right)\bullet\left(\Delta x\right)\\ +\left(\dfrac{V_{i-1,j}^{n}+V_{i,j}^{n}}{2}\right)\left(\dfrac{U_{i,j-1}^{n}+U_{i,j}^{n}}{2}\right)\bullet\left(-\Delta x\right)\end{array}\right]\Delta t\end{aligned} \tag{3.16}$$

$$\begin{aligned}\text{Diffusion}(U) &= \int_{n}^{n+1}\int_{\forall}\frac{\partial}{\partial x}\left(\frac{\partial U}{\partial x}\right)+\frac{\partial}{\partial y}\left(\frac{\partial U}{\partial y}\right)\ \partial\forall\partial t\\ &= \left(\sum_{\text{F}}\frac{\partial U_{\text{F}}}{\partial x}\bullet\text{F}+\sum_{\text{F}}\frac{\partial U_{\text{F}}}{\partial y}\bullet\text{F}\right)^{n}\ \Delta t\\ &= \left(\begin{array}{l}\dfrac{U_{i+1,j}^{n}-U_{i,j}^{n}}{\Delta x}\bullet\left(\Delta y\right)+\dfrac{U_{i,j}^{n}-U_{i-1,j}^{n}}{\Delta x}\bullet\left(-\Delta y\right)\\ +\dfrac{U_{i,j+1}^{n}-U_{i,j}^{n}}{\Delta y}\bullet\left(\Delta x\right)+\dfrac{U_{i,j}^{n}-U_{i,j-1}^{n}}{\Delta y}\bullet\left(-\Delta x\right)\end{array}\right)\Delta t\\ &= \frac{\Delta y\Delta t}{\Delta x}\left(U_{i+1,j}^{n}-2U_{i,j}^{n}+U_{i-1,j}^{n}\right)\\ &\quad+\frac{\Delta x\Delta t}{\Delta y}\left(U_{i,j+1}^{n}-2U_{i,j}^{n}+U_{i,j-1}^{n}\right)\end{aligned} \tag{3.17}$$

$$\begin{aligned}\text{Pressure}(U) &= \int_{n}^{n+1}\int_{\forall}\frac{1}{\rho}\frac{\partial pr}{\partial x}\;\partial\forall\partial t\\ &= \left(\frac{1}{\rho}\sum_{\mathrm{F}}\frac{\partial pr_{\mathrm{F}}}{\partial x}\bullet\mathrm{F}\right)^{n}\Delta t\\ &= \frac{1}{\rho}\left(pr_{i,j}^{n}-pr_{i-1,j}^{n}\right)\bullet(\Delta y)\Delta t\\ &= \frac{\Delta y}{\rho}\left(pr_{i,j}^{n}-pr_{i-1,j}^{n}\right)\Delta t\end{aligned}\qquad 3.18$$

Hence, Equation 3.19 showed the calculation for the next iteration for Equations 5.10

$$\begin{aligned}U_{i}^{n+1}=U_{i}^{n}-&\begin{bmatrix}\left(\dfrac{U_{i+1,j}^{n}+U_{i,j}^{n}}{2}\right)\left(\dfrac{U_{i+1,j}^{n}+U_{i,j}^{n}}{2}\right)\bullet\left(\dfrac{1}{\Delta x}\right)\\ -\left(\dfrac{U_{i-1,j}^{n}+U_{i,j}^{n}}{2}\right)\left(\dfrac{U_{i-1,j}^{n}+U_{i,j}^{n}}{2}\right)\bullet\left(\dfrac{1}{\Delta x}\right)\\ +\left(\dfrac{V_{i-1,j+1}^{n}+V_{i,j+1}^{n}}{2}\right)\left(\dfrac{U_{i,j+1}^{n}+U_{i,j}^{n}}{2}\right)\bullet\left(\dfrac{1}{\Delta y}\right)\\ -\left(\dfrac{V_{i-1,j}^{n}+V_{i,j}^{n}}{2}\right)\left(\dfrac{U_{i,j-1}^{n}+U_{i,j}^{n}}{2}\right)\bullet\left(\dfrac{1}{\Delta y}\right)\end{bmatrix}\Delta t\qquad 3.19\\ &+\left(\begin{matrix}\dfrac{vis}{(\Delta x)^{2}}\left(U_{i+1,j}^{n}-2U_{i,j}^{n}+U_{i-1,j}^{n}\right)\\ +\dfrac{vis}{(\Delta y)^{2}}\left(U_{i,j+1}^{n}-2U_{i,j}^{n}+U_{i,j-1}^{n}\right)\end{matrix}\right)\Delta t\\ &-\frac{1}{\rho\Delta x}\left(pr_{i,j}^{n}-pr_{i-1,j}^{n}\right)\Delta t\end{aligned}$$

After that, the calculation cell for the variable V in Equation 5.11 is displayed in Figure 3.5.

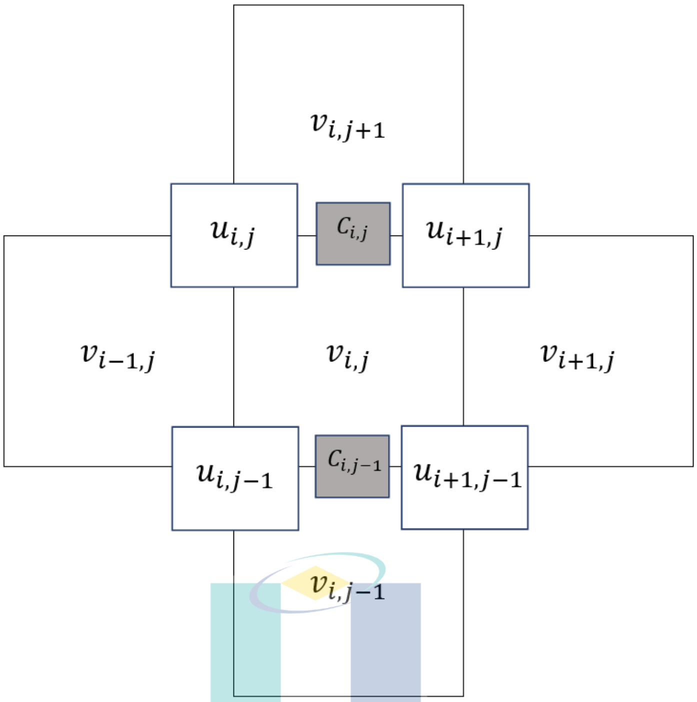

Figure 3.5 The grid cells that were utilised in solving Equation 5.11.

Equation 5.11 was separated into its individual components, which are demonstrated in Equations 3.20, 3.21, 3.22, and 3.23.

$$\begin{aligned}\text{Rate}(V) &= \int_{n}^{n+1}\int_{\forall}\frac{\partial V}{\partial t}\,\partial\forall\partial t\\ &= \frac{\partial}{\partial t}(V_i\Delta\forall)\\ &= \left(V_i^{n+1}-V_i^{n}\right)\Delta x\Delta y\end{aligned} \tag{3.20}$$

$$\text{Advection}\left(V\right)=\int_{n}^{n+1}\int_{\forall}\left(U\frac{\partial V}{\partial x}+V\frac{\partial V}{\partial y}\right)\partial\forall\partial t$$

$$=\left(\sum_{\mathrm{F}}\left(UV+VV\right)\bullet\mathrm{F}\right)^{n}\Delta t$$

$$=\begin{bmatrix}\left(\dfrac{U^{n}_{i+1,j}+U^{n}_{i+1,j-1}}{2}\right)\left(\dfrac{V^{n}_{i+1,j}+V^{n}_{i,j}}{2}\right)\bullet\left(\Delta y\right)\\+\left(\dfrac{U^{n}_{i,j}+U^{n}_{i,j-1}}{2}\right)\left(\dfrac{V^{n}_{i-1,j}+V^{n}_{i,j}}{2}\right)\bullet\left(-\Delta y\right)\\+\left(\dfrac{V^{n}_{i,j+1}+V^{n}_{i,j}}{2}\right)\left(\dfrac{V^{n}_{i,j+1}+V^{n}_{i,j}}{2}\right)\bullet\left(\Delta x\right)\\+\left(\dfrac{V^{n}_{i,j-1}+V^{n}_{i,j}}{2}\right)\left(\dfrac{V^{n}_{i,j-1}+V^{n}_{i,j}}{2}\right)\bullet\left(-\Delta x\right)\end{bmatrix}\Delta t \qquad 3.21$$

$$\text{Diffusion}\left(V\right)=\int_{n}^{n+1}\int_{\forall}\frac{\partial}{\partial x}\left(\frac{\partial V}{\partial x}\right)+\frac{\partial}{\partial y}\left(\frac{\partial V}{\partial y}\right)\partial\forall\partial t$$

$$=\left(\sum_{\mathrm{F}}\frac{\partial V_{\mathrm{F}}}{\partial x}\bullet\mathrm{F}+\sum_{\mathrm{F}}\frac{\partial V_{\mathrm{F}}}{\partial y}\bullet\mathrm{F}\right)^{n}\Delta t$$

$$=\left(\begin{aligned}&\frac{V^{n}_{i+1,j}-V^{n}_{i,j}}{\Delta x}\bullet\left(\Delta y\right)+\frac{V^{n}_{i,j}-V^{n}_{i-1,j}}{\Delta x}\bullet\left(-\Delta y\right)\\&+\frac{V^{n}_{i,j+1}-V^{n}_{i,j}}{\Delta y}\bullet\left(\Delta x\right)+\frac{V^{n}_{i,j}-V^{n}_{i,j-1}}{\Delta y}\bullet\left(-\Delta x\right)\end{aligned}\right)\Delta t \qquad 3.22$$

$$=\frac{\Delta y\Delta t}{\Delta x}\left(V^{n}_{i+1,j}-2V^{n}_{i,j}+V^{n}_{i-1,j}\right)$$

$$+\frac{\Delta x\Delta t}{\Delta y}\left(V^{n}_{i,j+1}-2V^{n}_{i,j}+V^{n}_{i,j-1}\right)$$

$$\begin{aligned}\text{Pressure}(V) &= \int_{n}^{n+1}\int_{\forall}\frac{1}{\rho}\frac{\partial pr}{\partial y}\;\partial\forall\partial t\\ &= \left(\frac{1}{\rho}\sum_{\mathrm{F}}\frac{\partial pr_{\mathrm{F}}}{\partial y}\bullet\mathrm{F}\right)^{n}\Delta t\\ &= \frac{1}{\rho}\left(pr^{n}_{i,j}-pr^{n}_{i,j-1}\right)\bullet\left(\Delta x\right)\Delta t\\ &= \frac{\Delta x}{\rho}\left(pr^{n}_{i,j}-pr^{n}_{i,j-1}\right)\Delta t\end{aligned} \qquad 3.23$$

Thus, the Equation 3.24 could be utilised to calculate the next iteration for *V*.

$$\begin{aligned}V_i^{n+1} = V_i^{n} - &\left[\begin{aligned}&\left(\frac{U^{n}_{i+1,j}+U^{n}_{i+1,j-1}}{2}\right)\left(\frac{V^{n}_{i+1,j}+V^{n}_{i,j}}{2}\right)\bullet\left(\frac{1}{\Delta x}\right)\\ -&\left(\frac{U^{n}_{i,j}+U^{n}_{i,j-1}}{2}\right)\left(\frac{V^{n}_{i-1,j}+V^{n}_{i,j}}{2}\right)\bullet\left(\frac{1}{\Delta x}\right)\\ +&\left(\frac{V^{n}_{i,j+1}+V^{n}_{i,j}}{2}\right)\left(\frac{V^{n}_{i,j+1}+V^{n}_{i,j}}{2}\right)\bullet\left(\frac{1}{\Delta y}\right)\\ -&\left(\frac{V^{n}_{i,j-1}+V^{n}_{i,j}}{2}\right)\left(\frac{V^{n}_{i,j-1}+V^{n}_{i,j}}{2}\right)\bullet\left(\frac{1}{\Delta y}\right)\end{aligned}\right]\Delta t\\ +&\left(\begin{aligned}&\frac{vis}{(\Delta x)^2}\left(V^{n}_{i+1,j}-2V^{n}_{i,j}+V^{n}_{i-1,j}\right)\\ +&\frac{vis}{(\Delta y)^2}\left(V^{n}_{i,j+1}-2V^{n}_{i,j}+V^{n}_{i,j-1}\right)\end{aligned}\right)\Delta t +\\ -&\frac{1}{\rho\Delta y}\left(pr^{n}_{i,j}-pr^{n}_{i,j-1}\right)\Delta t\end{aligned} \qquad 3.24$$

All variables besides *U* and *V* utilised the cell-centre grid. As a result, the calculation of all variables employed the same cell grid, as shown in Figure 3.6. Equation 5.12–5.14 contained components for temporal, advection and diffusion. The variables *M*, *P*, and *S*, which represent the microbes, ethanol and substrate, were consolidated into a single variable (*C*) due to their identical forms.

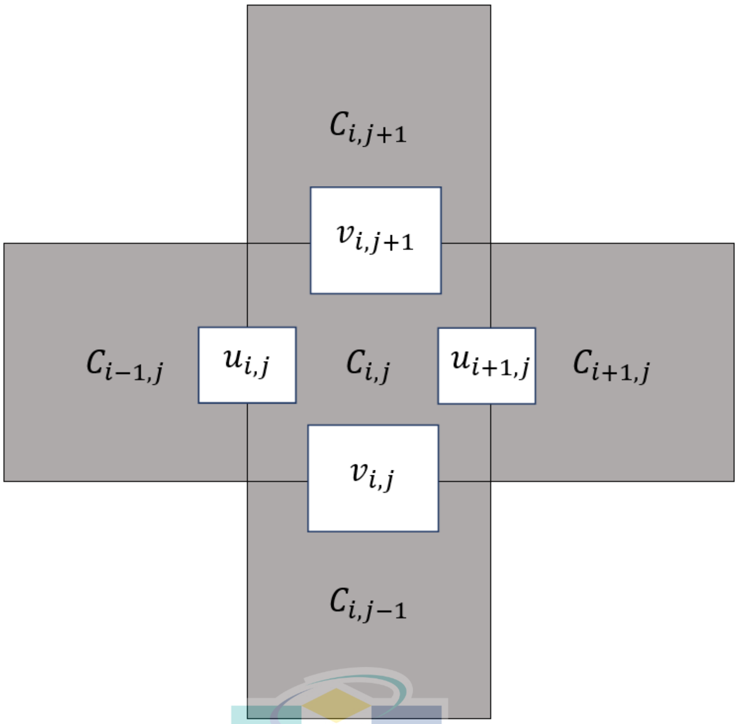

Figure 3.6 The grid cells that were utilised in solving Equation 5.12–5.17.

Equation 3.25–3.27 describes each component of *C*.

$$\begin{aligned}\text{Rate}(C) &= \int_{n}^{n+1}\int_{\forall} \frac{\partial C}{\partial t}\,\partial\forall\partial t \\ &= \frac{\partial}{\partial t}\left(C_{i,j}\Delta\forall\right) \\ &= \left(C_{i,j}^{n+1} - C_{i,j}^{n}\right)\Delta x\Delta y\end{aligned} \qquad 3.25$$

$$
\begin{aligned}
\text{Advection}(C) &= \int_{n}^{n+1}\int_{\forall}\left(U\frac{\partial C}{\partial x}+V\frac{\partial C}{\partial y}\right)\partial\forall\partial t \\
&= \left(\sum_{\mathrm{F}}\left(U_{\mathrm{F}}C_{\mathrm{F}x}+V_{\mathrm{F}}C_{\mathrm{F}y}\right)\bullet\mathrm{F}\right)^{n}\Delta t \\
&= \begin{bmatrix}
U_{i+1,j}^{n}\left(\dfrac{C_{i+1,j}^{n}+C_{i,j}^{n}}{2}\right)\bullet(\Delta y) \\
+U_{i,j}^{n}\left(\dfrac{C_{i-1,j}^{n}+C_{i,j}^{n}}{2}\right)\bullet(-\Delta y) \\
+V_{i,j+1}^{n}\left(\dfrac{C_{i,j+1}^{n}+C_{i,j}^{n}}{2}\right)\bullet(\Delta x) \\
+V_{i,j}^{n}\left(\dfrac{C_{i,j-1}^{n}+C_{i,j}^{n}}{2}\right)\bullet(-\Delta x)
\end{bmatrix}\Delta t
\end{aligned}
\tag{3.26}
$$

$$
\begin{aligned}
\text{Diffusion}(C) &= \int_{n}^{n+1}\int_{\forall}\frac{\partial}{\partial x}\left(\frac{\partial C}{\partial x}\right)+\frac{\partial}{\partial y}\left(\frac{\partial C}{\partial y}\right)\partial\forall\partial t \\
&= \left(\sum_{\mathrm{F}}\frac{\partial C}{\partial x}\bullet\mathrm{F}+\sum_{\mathrm{F}}\frac{\partial C}{\partial y}\bullet\mathrm{F}\right)^{n}\Delta t \\
&= \begin{pmatrix}
\dfrac{C_{i+1,j}^{n}-C_{i,j}^{n}}{\Delta x}\bullet(\Delta y)+\dfrac{C_{i,j}^{n}-C_{i-1,j}^{n}}{\Delta x}\bullet(-\Delta y) \\
+\dfrac{C_{i,j+1}^{n}-C_{i,j}^{n}}{\Delta y}\bullet(\Delta x)+\dfrac{C_{i,j}^{n}-C_{i,j-1}^{n}}{\Delta y}\bullet(-\Delta x)
\end{pmatrix}\Delta t \\
&= \frac{\Delta y\Delta t}{\Delta x}\left(C_{i+1,j}^{n}-2C_{i,j}^{n}+C_{i-1,j}^{n}\right) \\
&\quad+\frac{\Delta x\Delta t}{\Delta y}\left(C_{i,j+1}^{n}-2C_{i,j}^{n}+C_{i,j-1}^{n}\right)
\end{aligned}
\tag{3.27}
$$

Additionally, the reaction variables M , P , and S can be defined by the following equations.

$$\mathrm{R}\left(M_{i,j}^{n}\right)=\frac{\mu_{max}S_{i,j}^{n}M_{i,j}^{n}}{K_{SM}+S_{i,j}^{n}+\left(S_{i,j}^{n}\right)^{2}\Big/K_{IM}}\left(1-\frac{P_{i,j}^{n}}{P_{M}}\right)-K_{d}M_{i,j}^{n} \qquad 3.28$$

$$\mathrm{R}\left(P_{i,j}^{n}\right)=\frac{v_{max}S_{i,j}^{n}M_{i,j}^{n}}{K_{SP}+S_{i,j}^{n}+\left(S_{i,j}^{n}\right)^{2}\Big/K_{IP}}\left(1-\frac{P_{i,j}^{n}}{P_{P}}\right) \qquad 3.29$$

$$\mathrm{R}\left(S_{i,j}^{n}\right)=-\frac{1}{Y_{MS}}\left[\mathrm{R}\left(M_{i,j}^{n}\right)\right]-\frac{1}{Y_{PS}}\left[\mathrm{R}\left(P_{i,j}^{n}\right)\right]-mM_{i,j}^{n} \qquad 3.30$$

As a final step, Equation 3.31 define the values of each variable for the subsequent iteration.

$$\begin{aligned}C_{i,j}^{n+1}=C_{i,j}^{n}-&\left[\begin{array}{l}\dfrac{U_{i+1,j}^{n}}{\Delta x}\left(\dfrac{C_{i+1,j}^{n}+C_{i,j}^{n}}{2}\right)-\dfrac{U_{i,j}^{n}}{\Delta x}\left(\dfrac{C_{i-1,j}^{n}+C_{i,j}^{n}}{2}\right)\\+\dfrac{V_{i,j+1}^{n}}{\Delta y}\left(\dfrac{C_{i,j+1}^{n}+C_{i,j}^{n}}{2}\right)-\dfrac{V_{i,j}^{n}}{\Delta y}\left(\dfrac{C_{i,j-1}^{n}+C_{i,j}^{n}}{2}\right)\end{array}\right]\Delta t\\+&\frac{D}{\left(\Delta x\right)^{2}}\left(C_{i+1,j}^{n}-2C_{i,j}^{n}+C_{i-1,j}^{n}\right)\Delta t\\+&\frac{D}{\left(\Delta y\right)^{2}}\left(C_{i,j+1}^{n}-2C_{i,j}^{n}+C_{i,j-1}^{n}\right)\Delta t+\mathrm{R}\left(C_{i,j}^{n}\right)\Delta t\end{aligned} \qquad 3.31$$

3.5 Conclusion

Research methodology is the primary focus of this chapter, which begins with an overview of research design. The research overview has been organised as a flow chart to simplify the explanation. Besides that, this chapter offers a comprehensive explanation of the numerical method, specifically the finite volume method, for the purpose of solving the mathematical model. This study aims to solve mathematical models with 1D and 2D dimensions. In order to solve those mathematical models, this chapter details two different forms of FVM.

CHAPTER 4

STABILITY ANALYSIS

4.1 Introduction

Phisalaphong et al. (2006) demonstrated the inhibitory effect of high temperatures on cell activity during the fermentation process through a mathematical model. However, the study failed to discuss the stability analysis of the model. This chapter discusses the stability analysis of Phisalaphong et al. (2006) model in Equation 2.10, Equation 2.11, and Equation 2.12 to comprehend the dynamic system of ethanol production. Moreover, the results of this stability analysis can provide an estimate of ethanol production in the long term.

4.2 Parameters in Phisalaphong et al. (2006) Model

There are a total of 12 parameters in the model that Phisalaphong et al. (2006) proposed. The parameter fitting technique was conducted to approximate unknown parameter values in Phisalaphong et al. (2006) model based on the data obtained from the experiment conducted by Abdul Halim (2016). In this study, the parameters in Phisalaphong et al. (2006) model were obtained, as shown in Table 4.1. MATLAB toolbox that utilised the Nelder-Mead method was employed for parameter fitting technique.

Table 4.1 Fitted parameters using experimental data.

Parameters	**Fitted Values**	**Unit**
$\mu_{\max}$	0.7790	h^{-1}
$v_{\max}$	50.1142	h^{-1}
K_{SM}	257.9958	$g\ L^{-1}$
K_{SP}	26.3216	$g\ L^{-1}$
K_{IM}	182.3467	$g\ L^{-1}$
K_{IP}	0.1221	$g\ L^{-1}$
P_M	31.2110	$g\ L^{-1}$
P_P	25.7261	$g\ L^{-1}$
K_d	0.0225	h^{-1}
Y_{MS}	2.7793	dimensionless
Y_{PS}	1.2606	dimensionless
m	0.0017	h^{-1}

Figure 4.1 illustrates the microbial growth, substrate consumption, and ethanol formation during the ethanol fermentation production process by utilising the fitted parameters. The blue line in this graph represents the solution to the Phisalaphong et al. (2006) model using the fourth-order Runge-Kutta method, while the red dot describes experimental data. To have a more comprehensive understanding of the model, mathematical analysis was conducted in the subsequent section.

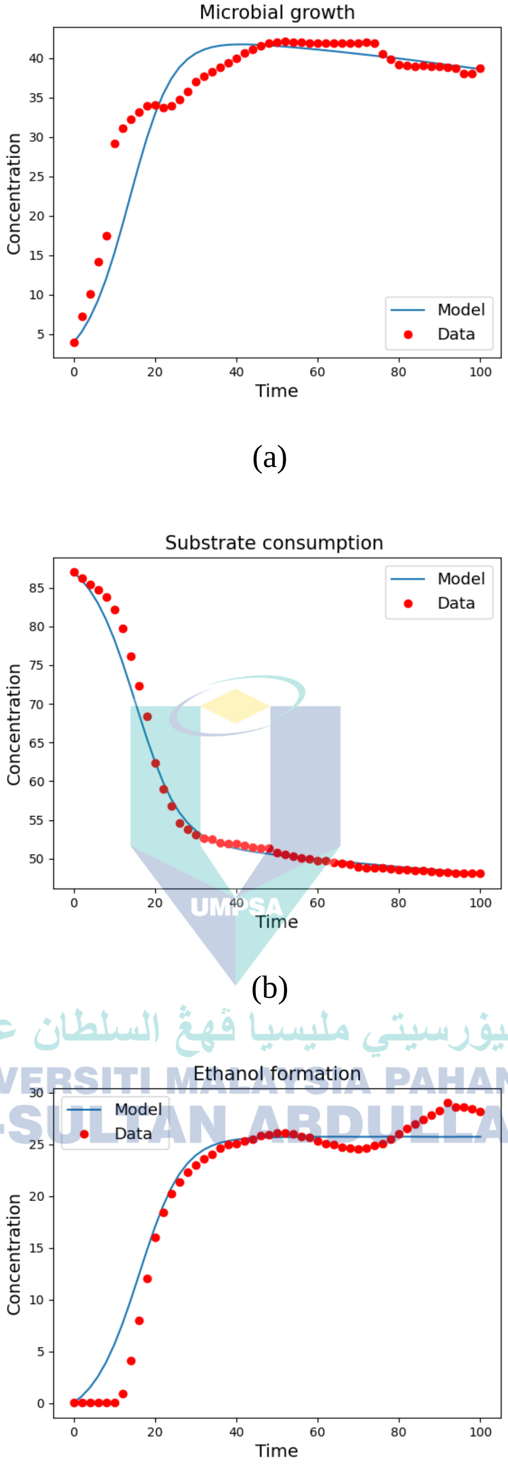

(a)

(b)

(c)

Figure 4.1 The (a) microbial growth, (b), substrate consumption and (c) ethanol formation using Phisalaphong et al. (2006) model.

4.3 Non-dimensional Phisalaphong et al. (2006) Model

Phisalaphong et al. (2006) introduced a mathematical model in their study, which focused on ethanol fermentation by highlighting several inhibitory elements. However, they failed to address the mathematical analysis associated with the model. Therefore, the purpose of this chapter is to provide a mathematical analysis of the Phisalaphong et al. (2006) model.

The mathematical analyses performed in the model are stability analysis and parameter analysis. Before running the analysis, the model was converted to a non-dimensional form. Transforming mathematical models into a non-dimensional form has numerous advantages. In a study on the need for non-dimensional form models of biological processes, Louie et al. (1998) found that the non-dimensional form can reduce the number of model parameters. Furthermore, Langtangen & Pedersen (2016) state that non-dimensional form models can enhance the comprehension of how distinct physical processes could interact in a differential equation model. In this study, Equation 4.1, a transformation equation, was introduced to transform Phisalaphong et al. (2006) model into a non-dimensional form.

$$M = g\left(K_{IM}\right),\quad P = p\left(\frac{v_{\max} K_{IP}}{K_d}\right),\quad S = s\left(K_{IM}\right),\quad t = \tau\left(\frac{1}{K_d}\right) \qquad 4.1$$

The variables g, p, s and τ represent non-dimensional variables for microbes, ethanol, substrate and time, respectively. Hence, the Phisalaphong et al. (2006) model can be rewritten as Equation 4.2–4.5.

$$\frac{dg}{d\tau} = \frac{\left(1-\lambda p\right)\sigma s g}{\alpha + s + s^2} - g \qquad 4.2$$

$$\frac{dp}{d\tau} = \frac{\left(1-\kappa p\right) s g}{\gamma + \beta s + s^2} \qquad 4.3$$

$$\frac{ds}{d\tau} = \frac{\left(\lambda p - 1\right)\sigma s g}{Y_{MS}\left(\alpha + s + s^2\right)} + \frac{\left(\kappa p - 1\right)\phi s g}{Y_{PS}\left(\gamma + \beta s + s^2\right)} + \left(\frac{g}{Y_{MS}} - \rho g\right) \qquad 4.4$$

where

$$\sigma = \frac{\mu_{\max}}{K_d} \qquad \alpha = \frac{K_{SM}}{K_{IM}} \qquad \beta = \frac{K_{IP}}{K_{IM}} \qquad \lambda = \frac{v_{\max} K_{IP}}{K_d P_M}$$

$$\phi = \frac{v_{\max} K_{IP}}{K_d K_{IM}} \qquad \rho = \frac{m}{K_d} \qquad \gamma = \frac{K_{SP} K_{IP}}{K_{IM}{}^2} \qquad \kappa = \frac{v_{\max} K_{IP}}{K_d P_P}. \tag{4.5}$$

The derivation of Equation 4.1–4.4 can be found in Appendix A. Table 4.2 summarises the meaning of these non-dimensional parameters.

Table 4.2 Parameters of non-dimensional Phisalaphong et al. (2006) model.

Parameters	**Description**
σ	The ratio of maximum specific microbial growth to its death rate
α	The ratio of substrate half-saturation coefficient for microbial growth to its inhibitory effect
β	The ratio of substrate inhibitory effect between ethanol production and microbial growth
λ	The ratio of maximum specific ethanol production and its substrate inhibitory effect to microbial death rate and its product inhibitory effect
ϕ	The ratio of maximum specific ethanol production and its substrate inhibitory effect to microbial death rate and its product inhibitory effect
ρ	The ratio of microbial maintenance coefficient to its death rate
γ	The ratio of substrate half-saturation coefficient for ethanol production and its substrate inhibitory effect towards the product inhibitory effect in microbial growth
κ	The ratio of maximum specific ethanol production and its substrate inhibitory effect towards microbial death rate and the product inhibitory effect in ethanol production
Y_{MS}	The yield coefficient for the substrate used on microbial growth
Y_{PS}	The yield coefficient for the substrate used on ethanol production

The subsequent section will describe in detail how stability analysis is conducted.

4.4 Stability Analysis

Brandon (2003) demonstrated how to analyse the stability of a model using the Jacobian matrix's eigenvalues. Equation 4.6 explains the definition of the Jacobian matrix for the non-dimensional model by Phisalaphong et al. (2006).

$$J(g,p,s)=\begin{pmatrix} \frac{\partial\left(dg/d\tau\right)}{\partial g} & \frac{\partial\left(dg/d\tau\right)}{\partial p} & \frac{\partial\left(dg/d\tau\right)}{\partial s} \\ \frac{\partial\left(dp/d\tau\right)}{\partial g} & \frac{\partial\left(dp/d\tau\right)}{\partial p} & \frac{\partial\left(dp/d\tau\right)}{\partial s} \\ \frac{\partial\left(ds/d\tau\right)}{\partial g} & \frac{\partial\left(ds/d\tau\right)}{\partial p} & \frac{\partial\left(ds/d\tau\right)}{\partial s} \end{pmatrix} \qquad 4.6$$

where

$$\frac{\partial\left(dg/d\tau\right)}{\partial g}=\frac{(1-\lambda p)s\sigma}{\alpha+s+s^2} \qquad 4.7$$

$$\frac{\partial\left(dg/d\tau\right)}{\partial p}=-\frac{\lambda s\sigma g}{\alpha+s+s^2} \qquad 4.8$$

$$\frac{\partial\left(dg/d\tau\right)}{\partial s}=\frac{\sigma(1-\lambda p)\left(\alpha-s^2\right)}{\left(\alpha+s+s^2\right)^2} \qquad 4.9$$

$$\frac{\partial\left(dp/d\tau\right)}{\partial g}=\frac{(1-\kappa p)s}{\gamma+\beta s+s^2} \qquad 4.10$$

$$\frac{\partial\left({}^{dp}\!/\!_{d\tau} \right)}{\partial p} = -\frac{\kappa s g}{\gamma + \beta s + s^2} \tag{4.11}$$

$$\frac{\partial\left({}^{dp}\!/\!_{d\tau} \right)}{\partial s} = \frac{g\left(1-\kappa p\right)\left(\gamma - s^2\right)}{\left(\gamma + \beta s + s^2\right)^2} \tag{4.12}$$

$$\frac{\partial\left({}^{ds}\!/\!_{d\tau} \right)}{\partial g} = \frac{\left(\lambda p - 1\right) s\sigma}{Y_{MS}\left(\alpha + s + s^2\right)} + \frac{\left(\kappa p - 1\right) s\phi}{Y_{PS}\left(\gamma + \beta s + s^2\right)} + \left(1-\rho\right) \tag{4.13}$$

$$\frac{\partial\left({}^{ds}\!/\!_{d\tau} \right)}{\partial p} = \frac{\lambda s\sigma g}{Y_{MS}\left(\alpha + s + s^2\right)} + \frac{\kappa s\phi g}{Y_{PS}\left(\gamma + \beta s + s^2\right)} \tag{4.14}$$

$$\frac{\partial\left({}^{ds}\!/\!_{d\tau} \right)}{\partial s} = \frac{\left(\lambda p - 1\right)\sigma g\left(\alpha - s^2\right)}{Y_{MS}\left(\alpha + s + s^2\right)^2} + \frac{\left(\kappa p - 1\right)\phi g\left(\gamma - s^2\right)}{Y_{PS}\left(\gamma + \beta s + s^2\right)^2} \tag{4.15}$$

To find the equilibrium point of the system, Equations 4.2–4.4 were set to zero and solved for g, p, and s. Due to the complexity of the model, the simultaneous equations were solved and coded in MATLAB. Based on the output values, the equilibrium points depended on certain conditions, as shown in Appendix B.

In the current study, the stability study of the fermentation system was investigated using an alternative method, an application called XPPAUT. According to Ermentrout (2002), XPPAUT is a software that simulates, analyses, and animates dynamical systems. This software can also easily generate the direction fields, nullclines, and equilibrium points of dynamical systems. Figure 4.2 depicts the direction field between variables p and g, with red and green lines representing nullclines obtained from the XPPAUT. In this analysis, the value 1 was assigned to variable s. According to Ermentrout (2002), nullclines are curves in the direction field when the rate of change for a particular variable is zero, and when these nullclines intersect, an equilibrium point is formed.

The eigenvalues can be used to determine each equilibrium point’s stability. Stable equilibrium points have only negative real-valued eigenvalues, whereas unstable equilibrium points have positive real-valued eigenvalues. The equilibrium point, nevertheless, takes into account examined dependent variables, expressed as *g*, *p*, *s*, even though XPPAUT presents a two-dimensional image. The oval shape in Figure 4.2, with points at (0, 0.37, 1), represents a stable equilibrium point, whereas the triangular shape represents an unstable equilibrium point.

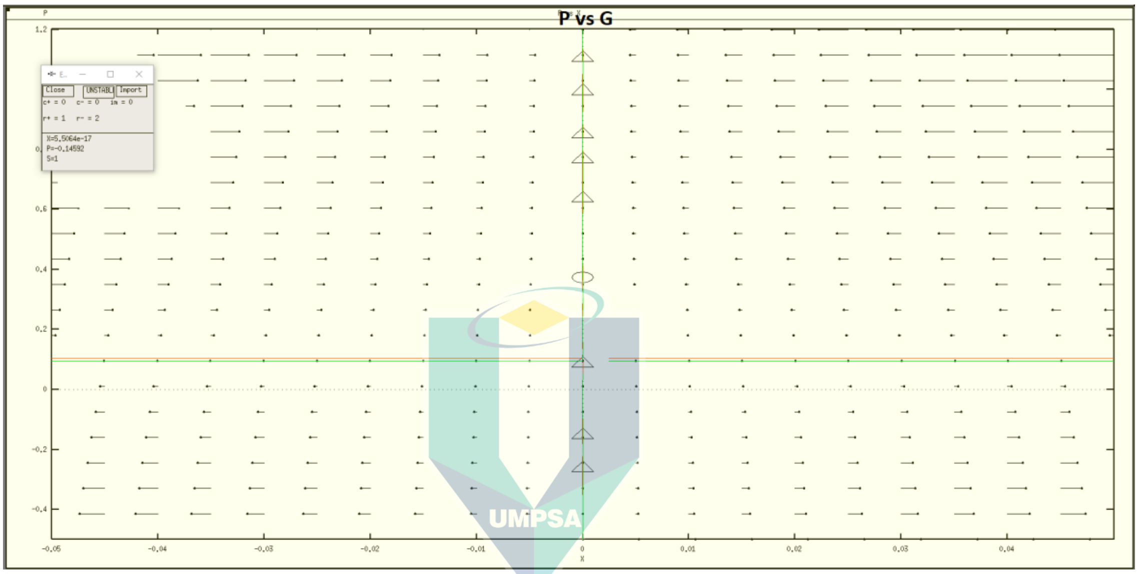

```
c+ = 0   c- = 0   im = 0
r+ = 1   r- = 2
X=5.5064e-17
P=-0.14592
S=1
```

Figure 4.2 Direction fields, nullclines, and equilibrium points of variable *p* against *g*.

Figure 4.3 displays the stability study involving variables *s* and *g*, where the value of the variable *p* was set to 1. There were eleven equilibrium points in this study, two of which were stable (oval-shaped), while the remaining nine were unstable (triangular shaped). The stable equilibrium points were coordinated at (0, 1, 0.91) and (0, 1, 0.4). From these two studies, it can be concluded that the fermentation ethanol production model using Equations 4.2–4.4 had three stable points located at (0, 0.37, 1), (0, 1, 0.91), and (0, 1, 0.4).

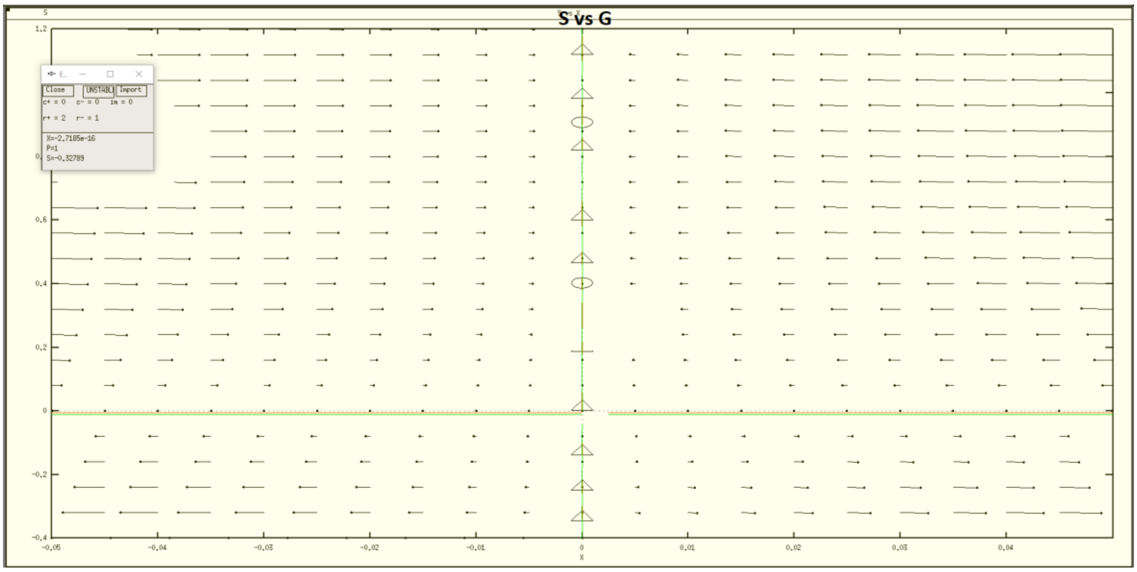

```
c+ = 0   c- = 0   im = 0

r+ = 2   r- = 1

X=-2.7185e-16
P=1
S=-0.32789
```

Figure 4.3 Direction fields, nullclines, and equilibrium points of variable *s* against *g*.

The results of the analysis in this section can be used to examine the dynamical systems of the Phisalaphong et al. (2006) model.

4.5 Parameter Analysis

The purpose of parameter analysis in the current study was to examine the behaviour of the parameters of Phisalaphong et al. (2006) model in connection to ethanol production. This analysis was conducted using a simulation method. The non-dimensional parameter values for Phisalaphong et al. (2006) model are found in Table 4.3. Those values were obtained by employing Equation 4.5 together with the values presented in Table 4.1.

Table 4.3 Parameter values for the non-dimensional Phisalaphong et al. (2006) model.

Parameters	**Values**
σ	34.6222
α	1.4149
β	0.0007
λ	8.7134
ϕ	1.4914
ρ	0.0756
γ	9.6657
κ	10.5712
Y_{MS}	2.7793
Y_{PS}	1.2606

The non-dimensional model was solved using the Runge-Kutta method of the fourth order. The computations do not require units and can be interpreted as a scale because this model is non-dimensional. Therefore, the initial concentrations of microbes, ethanol, and substrate were set at 0.1, 0, and 1, respectively. The three graphs in Figure 4.4 respectively illustrate the microbial growth, substrate consumption, and ethanol formation of a non-dimensional model under previously stated conditions. Based on Figure 4.4, the microbe approached 0.2970 units concentration on a time scale of 10. During the same time frame, roughly 78.16 per cent of the substrate was consumed during the fermentation process, yielding an ethanol concentration of 0.0946 units.

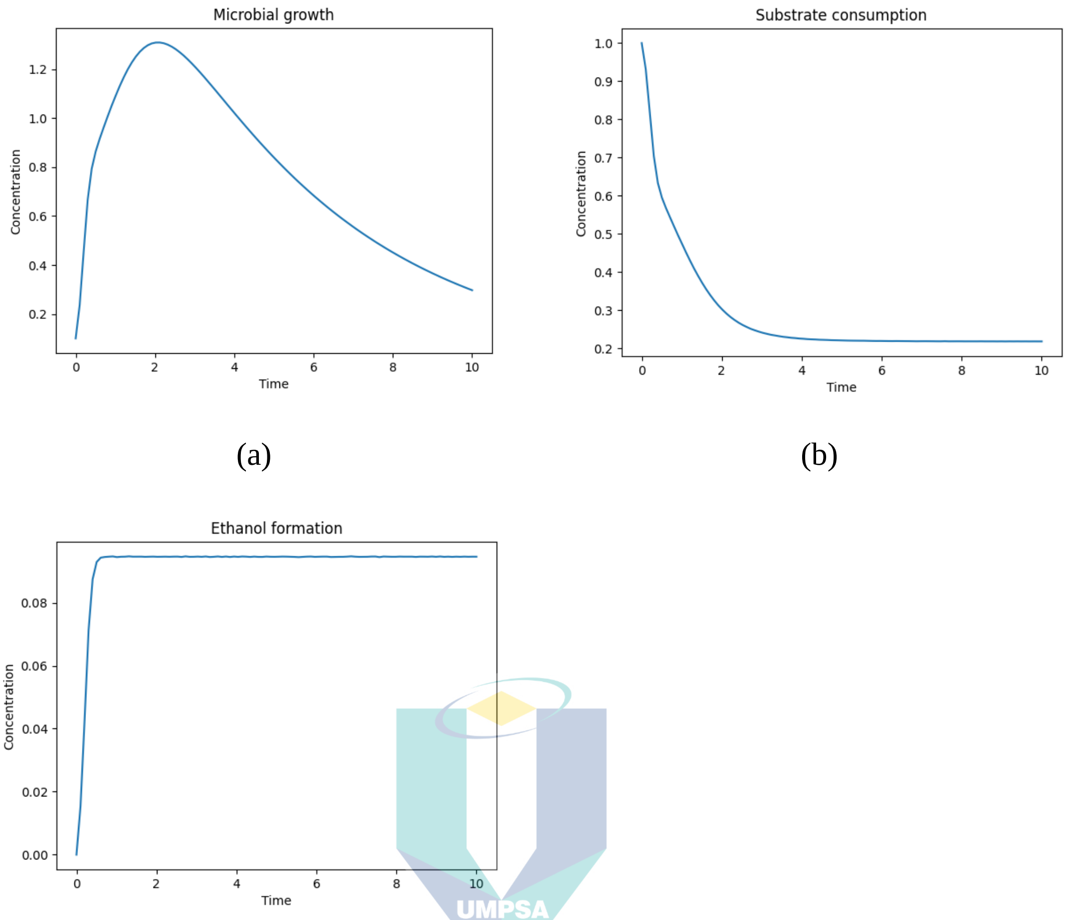

(a) (b)

(c)

Figure 4.4 The (a) microbial growth, (b) substrate consumption, and (c) ethanol formation using non-dimensional Phisalaphong et al. (2006) model.

This study experimented with different values of λ parameter, which were 10, 20, and 30. Figure 4.5 depicts the subsequent analysis of λ parameter for the model of the fermentation system. The arrows in the three graphs of Figure 4.5 illustrate the effect of increasing the parameter values. Figure 4.5 (a) demonstrates that the increase of λ rapidly dropped the concentration of microbes. This demonstrates that λ parameter inhibited the growth of microbes during the fermentation process. As shown in Figure 4.5 (b), this inhibitory effect increased the microbe’s substrate consumption. The concentration of remaining substrate at the end of fermentation with the greatest λ value ($\lambda = 30$) was the highest compared to other λ values. Furthermore, this inhibitory will have an indirect effect on ethanol production as shown in Figure 4.5 (c). Increasing the λ value from 10 to 30 will decrease the ethanol concentration at the end of fermentation.

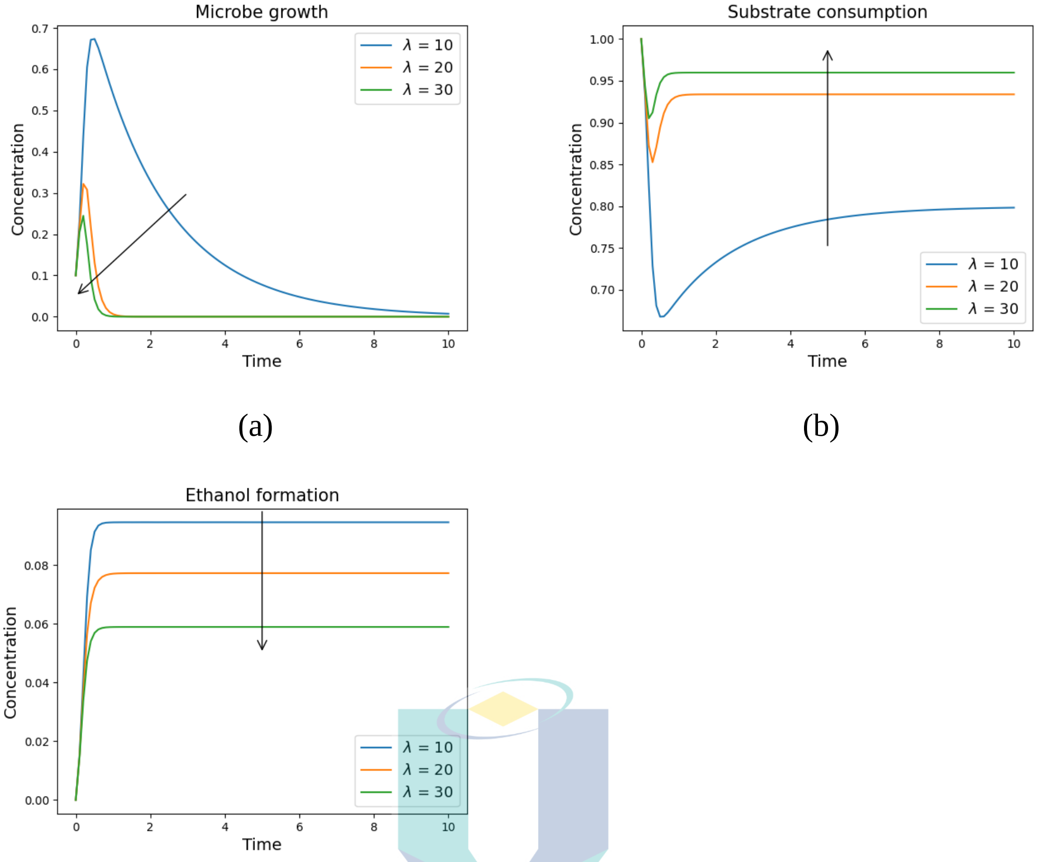

(a) (b)

(c)

Figure 4.5 The effect of the parameter λ to (a) microbial growth, (b) substrate consumption, and (c) ethanol formation.

The second examined parameter was σ. Figure 4.6 reveals that despite σ parameter was analysed using the same value as λ parameter, it yielded different results. As depicted in Figure 4.6 (a) and (b), increasing the value of σ parameter increases the exponential phase of microbial growth while accelerating the rate of substrate consumption. Comparing the values of σ = 10 to σ = 30 in Figure 4.6 (c), the concentration of ethanol produced through fermentation was the same. However, the production of ethanol with σ = 30 was quicker when compared to other values (i.e., σ = 10 and σ = 20). This indicates that increasing the σ parameter value boosts ethanol production.

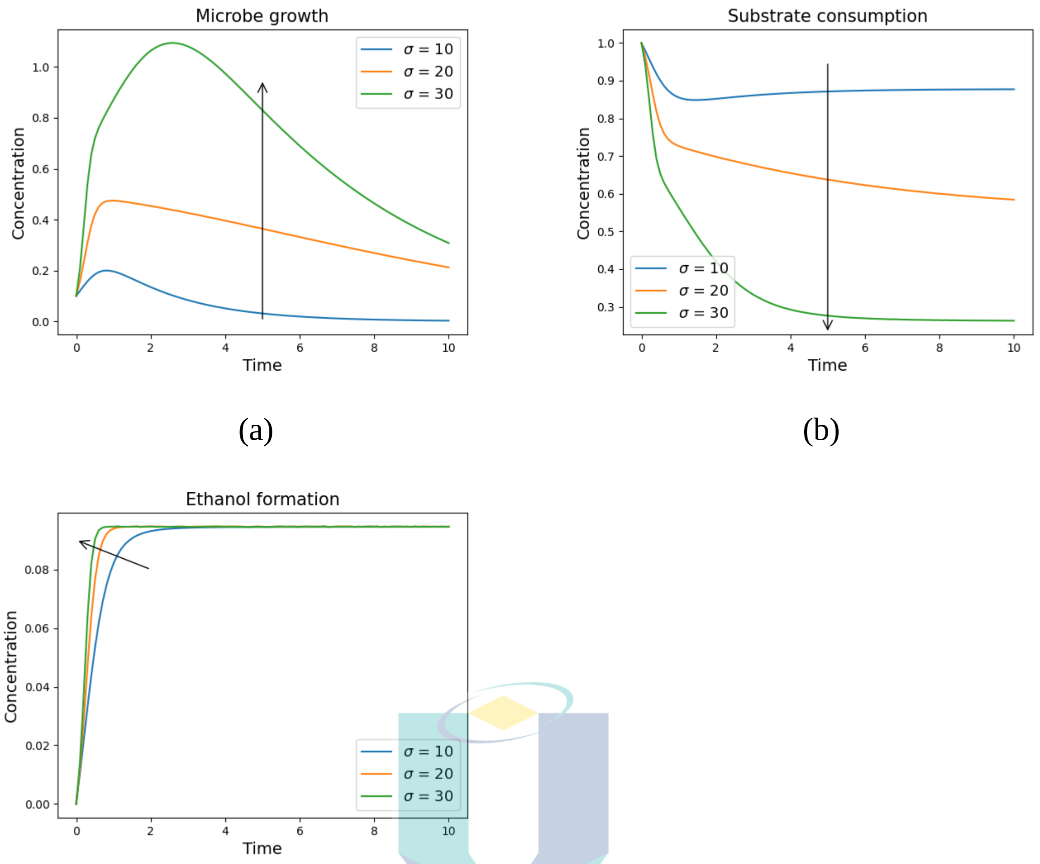

(a) (b)

(c)

Figure 4.6 The effect of the parameter σ to (a) microbial growth, (b) substrate consumption, and (c) ethanol formation.

The analysis of parameter analysis in the fermentation process continued with the investigation of α parameter. This analysis was conducted by setting α values to 10, 20, and 30, as illustrated in Figure 4.7. Figure 4.7 (a) illustrates that the rate of microbe reduction in the fermentation tank was proportional to the value of α parameter. Moreover, in Figure 4.7 (b), only 8.07 percent of the total substrate concentration was utilised for α , which had a value of 30, whereas 11.70 percent of α had a value of 10. This also indirectly impacted ethanol production as illustrated in Figure 4.7 (c). Compared to the beginning of the study, the value of α = 1.4149 was capable of producing up to 0.0946 units of ethanol concentration. When α = 30, production was restricted to 0.0854 units. It implies that an increase in α value will increase the inhibitory effect on ethanol production.

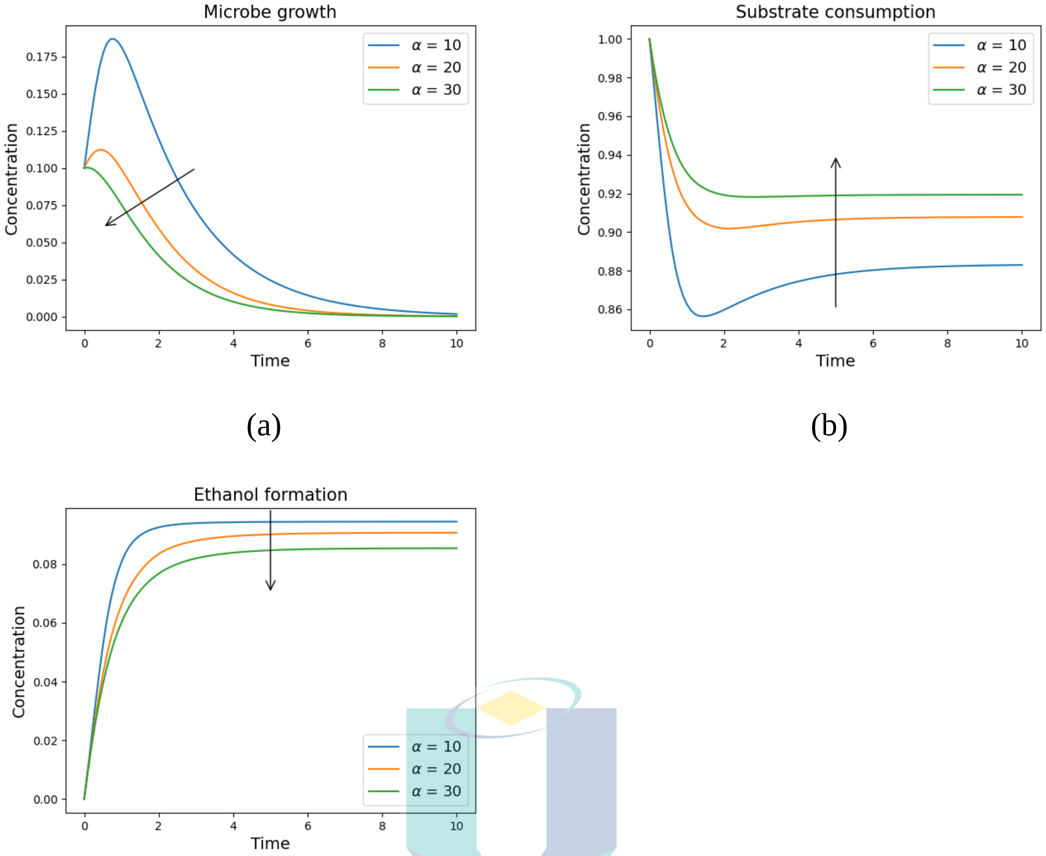

(a)

(b)

(c)

Figure 4.7 The effect of the parameter α to (a) microbial growth, (b) substrate consumption, and (c) ethanol formation.

The next parameter under evaluation was κ parameter, for which the values 10, 20, and 30 were examined. Figure 4.8 (a) demonstrates the positive correlation between microbial growth and κ values. However, increasing κ values increased substrate consumption rates (see Figure 4.8 (b)), but decreased the ethanol production (see Figure 4.8 (c)). The accumulated concentration of ethanol for $\kappa = 30$ was 0.05 units, with 95.29 per cent of the substrate concentration being consumed. This indicates that the increase in κ parameter increases the inhibitory effect on ethanol production.

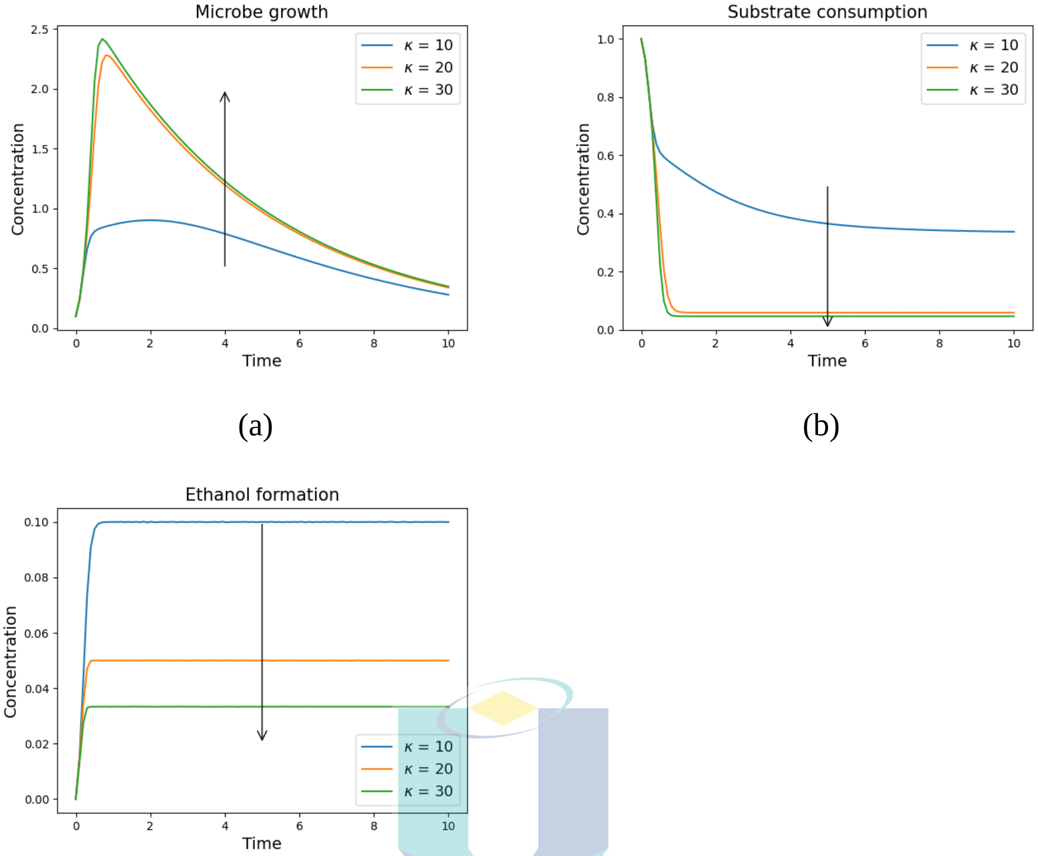

(a) (b)

(c)

Figure 4.8 The effect of the parameter κ to (a) microbial growth, (b) substrate consumption, and (c) ethanol formation.

Subsequently, an evaluation was conducted on γ parameter, specifically those with values of 10, 20, and 30, as depicted in Figure 4.9. The findings of this study demonstrated that increasing γ parameter had minimal impact on microbial growth (see Figure 4.9 (a)) and on substrate (see Figure 4.9 (b)). However, when γ parameter on a time scale of 2 (as depicted in the enlarged graph), it is evident that an increase in the parameter values from 10 to 30 resulted in an apparent rise in microbial growth, followed by a decrease in substrate consumption. On the contrary, the production of ethanol showed an obvious pattern of decline as γ values increased.

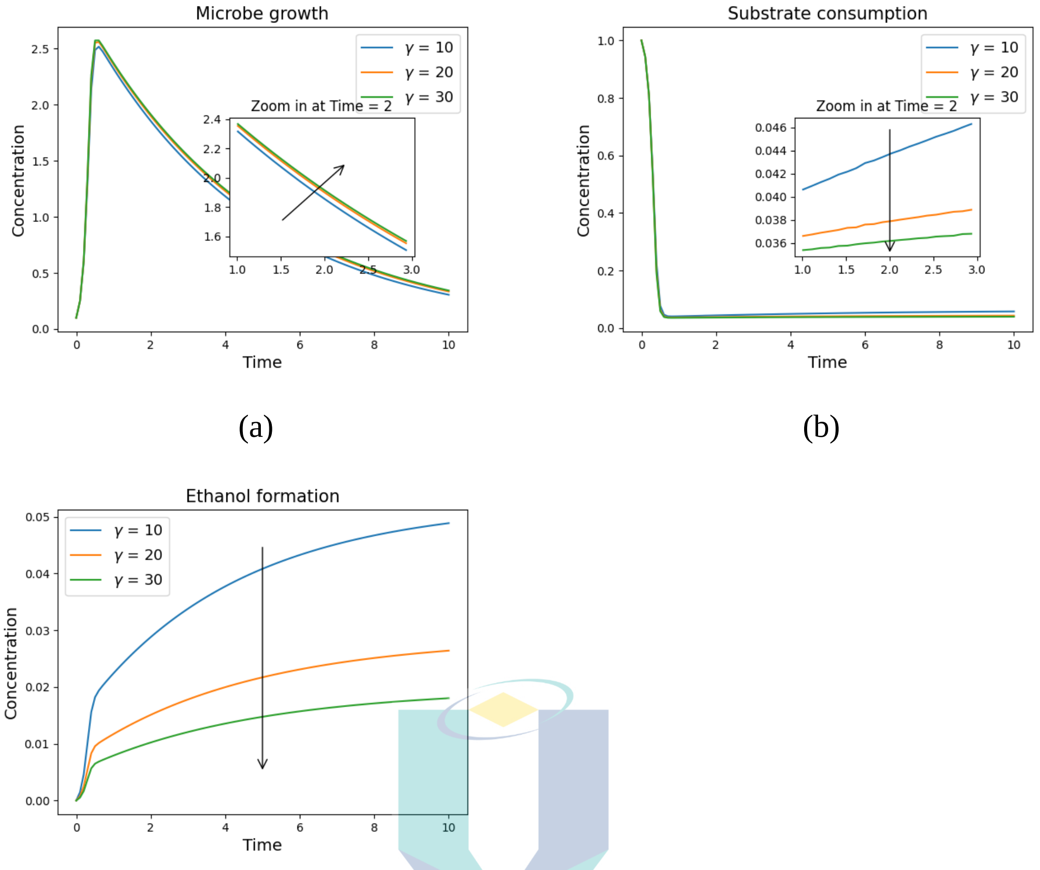

(a) (b)

(c)

Figure 4.9 The effect of the parameter γ to (a) microbial growth, (b) substrate consumption, and (c) ethanol formation.

Another investigated parameter using the same parameter values as γ parameter was β parameter (see Equation 4.3). Similar to the findings of γ parameters study, the study on β parameter revealed the same pattern of results when the parameter values were increased. The rate of microbial growth exhibited a positive correlation with β values (Figure 4.10 (a)), indicating that an increase in β values led to an increase in the growth rate. However, a decline in substrate consumption and ethanol production were observable, as depicted in Figure 4.10 (b) and Figure 4.10 (c), respectively. In addition, compared to the quantity of ethanol accumulated through fermentation for γ parameter values, $\beta = 10$ produced approximately 0.0946 units, while γ parameter of the same value produced up to 0.0489 units of ethanol. This indicates that β parameter is less inhibiting than γ parameter.

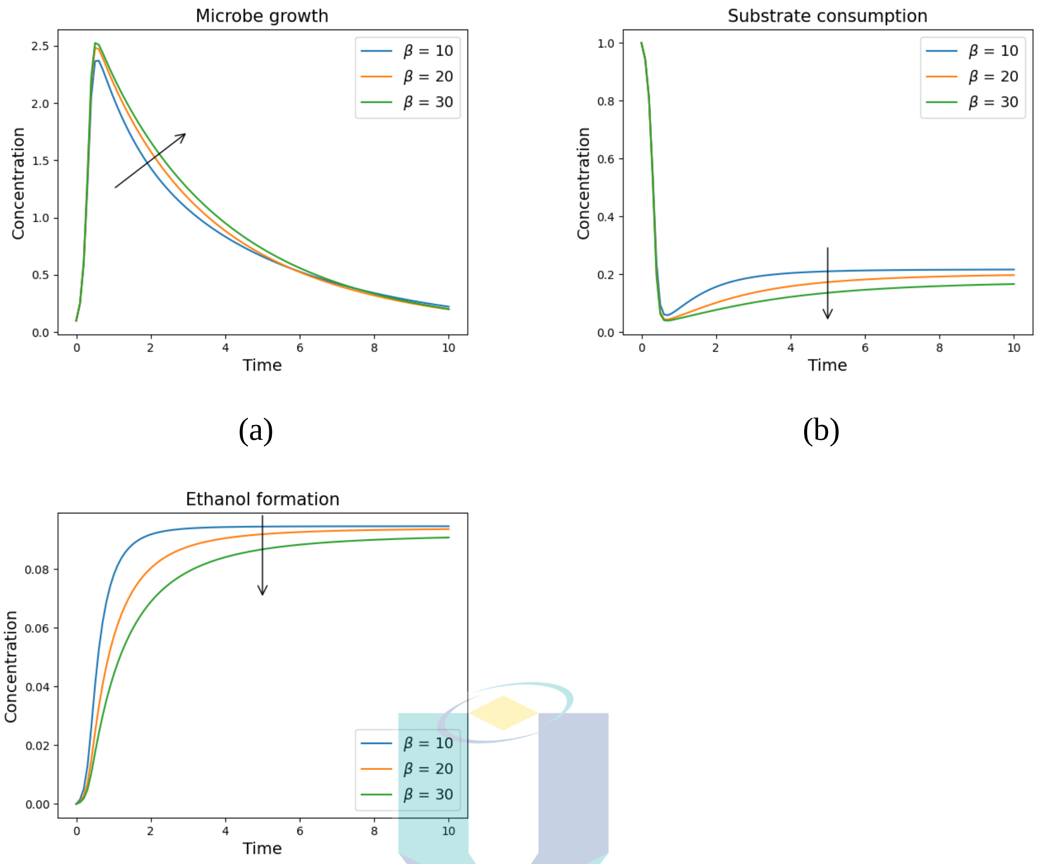

(a)

(b)

(c)

Figure 4.10 The effect of the parameter β to (a) microbial growth, (b) substrate consumption, and (c) ethanol formation.

Figure 4.11 illustrates the effect of raising the Y_{MS} parameter value on the ethanol fermentation process. The value of this study parameter is no different from other parameters. However, when compared to other parameters, this particular parameter exhibits distinct outcomes. Figure 4.11 (a) illustrates that the increase of Y_{MS} has led to an initial rise in the rate of microbial growth during the first 5.05 units of time, followed by a subsequent decline in microbial growth. The substrate consumption presented in Figure 4.11 (b) also exhibits two distinct patterns in response to the increment of the Y_{MS} parameter value. The observed trend in substrate consumption during the first 3.33 units of time exhibits an upward pattern. After that time, however, the rate of substrate consumption decreased. The outcome of increasing Y_{MS} values for ethanol production is also depicted in Figure 4.11 (c). Despite the absence of the Y_{MS} parameter at a value of

10 because of overlap, it has been observed that a rise in the Y_{MS} value leads to a reduction in the ethanol concentration after the first 5.05 units of time. Based on Equation 4.4, the parameter Y_{MS} serves as the denominator in the equation. It is noted that an increase in the value of the denominator leads to a decrease in the rate of substrate consumption during the fermentation process.

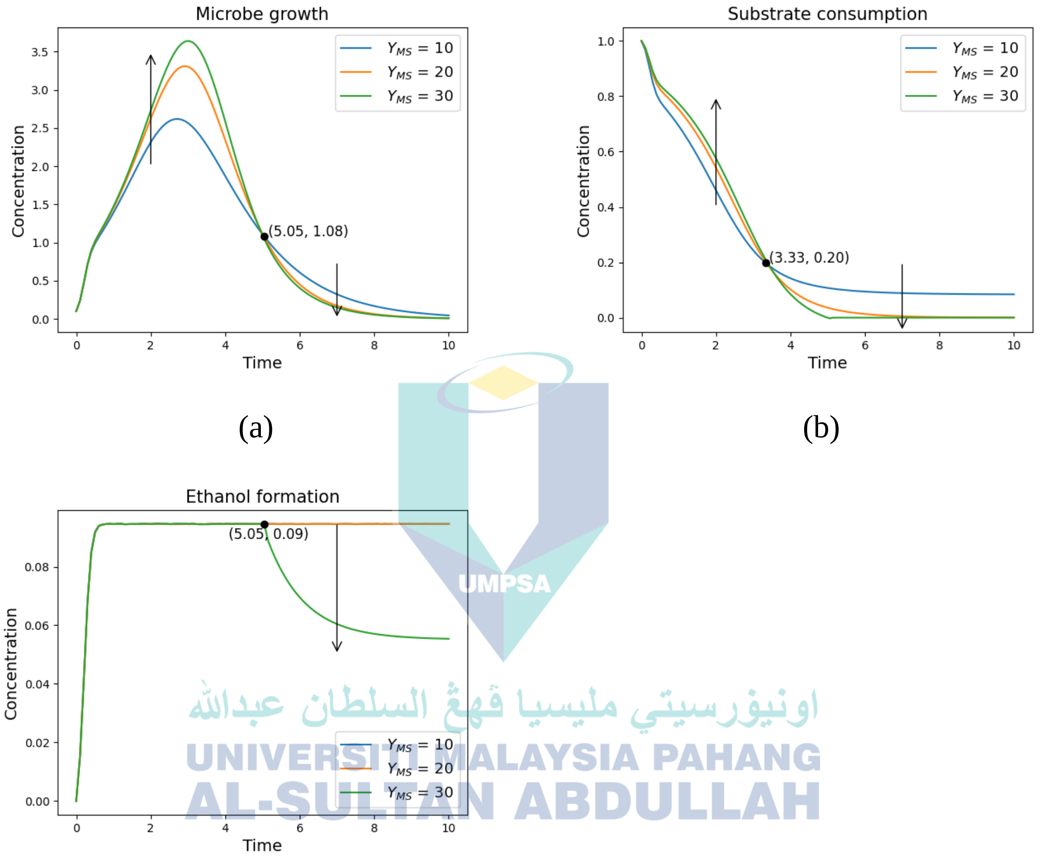

(a)

(b)

(c)

Figure 4.11 The effect of the parameter Y_{MS} to (a) microbial growth, (b) substrate consumption, and (c) ethanol formation.

Figure 4.12 shows the simulation results of the difference in Y_{PS} values. In general, the change in Y_{PS} parameter values do not yield significant effects on the general operation of the ethanol production through fermentation. The distinction among Y_{PS} parameter values can merely be discerned by microbial growth, as depicted in Figure 4.12 (a). During the initial two units of time of fermentation, there was a slight incremental trend in the rate of microbial growth as Y_{PS} value increased. In contrast, when analysing Figure 4.12 (b) and Figure 4.12 (c), it is observed that Y_{PS} parameter did not exhibit notable differences in terms of substrate consumption and ethanol production throughout the three simulations conducted with distinct parameter values. Thus, it can be concluded that Y_{PS} parameter has no effect on the ethanol production through fermentation.

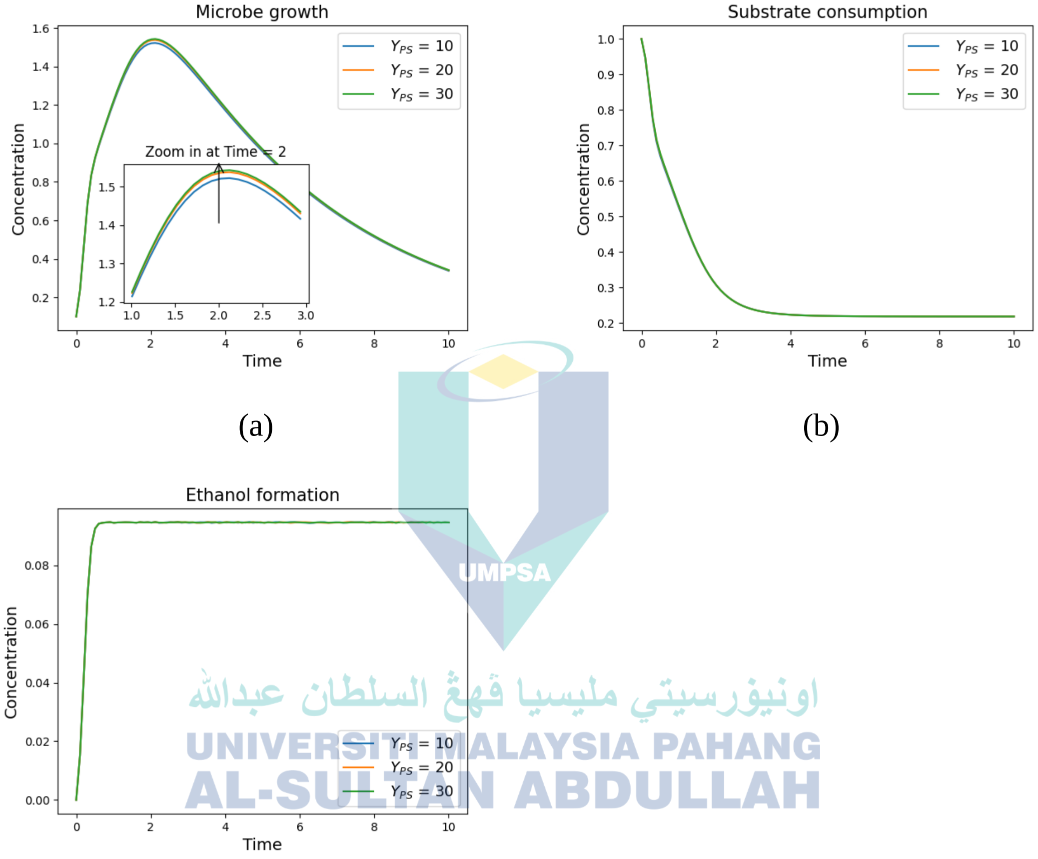

(a)

(b)

(c)

Figure 4.12 The effect of the parameter Y_{PS} to (a) microbial growth, (b) substrate consumption, and (c) ethanol formation.

According to Figure 4.13 and Figure 4.14, ϕ and ρ parameters also had an inhibiting impact on the fermentation-based ethanol production process. Regardless of the values employed for ϕ and ρ parameters, increasing the values lowered the microbe growth rate, as shown in Figure 4.13 (a) and Figure 4.14 (a). ϕ and ρ parameters also reduced the consumption of substrates, as displayed in Figure 4.13 (b) and Figure 4.14

(b). Therefore, the production of ethanol decreased as the values of ϕ and ρ parameters increased.

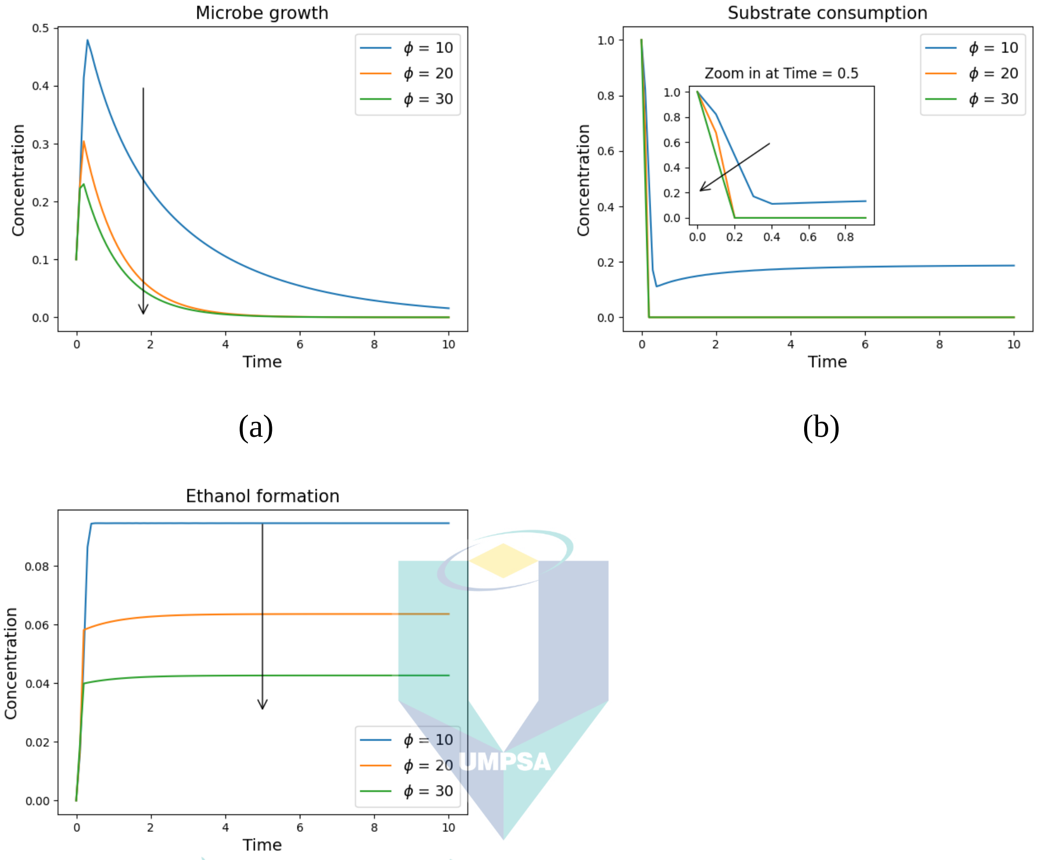

(a) (b)

(c)

Figure 4.13 The effect of the parameter ϕ to (a) microbial growth, (b) substrate consumption, and (c) ethanol formation.

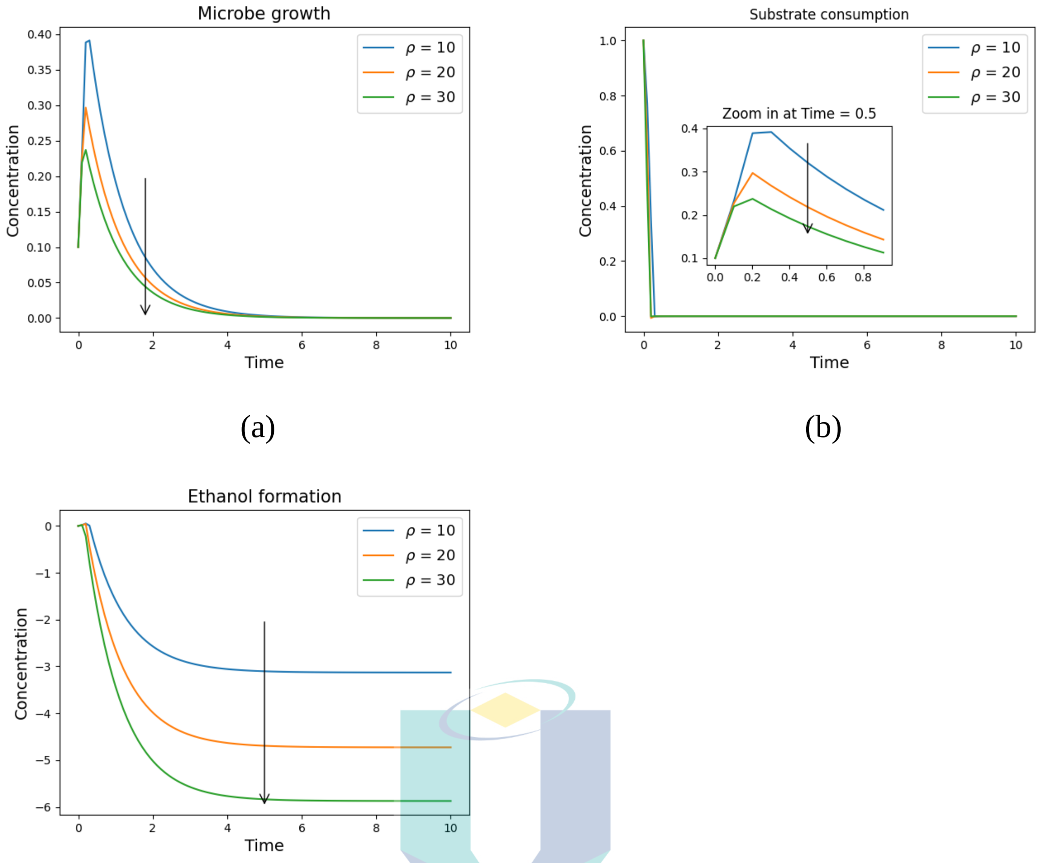

(a)

(b)

(c)

Figure 4.14 The effect of the parameter ρ to (a) microbial growth, (b) substrate consumption, and (c) ethanol formation.

The impacts of parameters on ethanol production are summarised in Table 4.4, similar to the earlier studies on parameters impacts. According to the table, σ was the only parameter exhibiting a beneficial impact on the production of ethanol, Y_{PS} did not have a significant impact, whereas the remaining eight parameters hindered the production of ethanol through fermentation.

Table 4.4 The impact of parameters in ethanol production

Parameters	Impact on Ethanol Production
λ	Inhibiting impact
σ	Boosting impact
α	Inhibiting impact
κ	Inhibiting impact
γ	Inhibiting impact
β	Inhibiting impact
Y_{MS}	Inhibiting impact
Y_{PS}	Impactless
ϕ	Inhibiting impact
ρ	Inhibiting impact

4.6 Conclusion

The objective of this chapter was to gain a deeper mathematical understanding of Phisalaphong et al. (2006) model. In the very beginning of this chapter, a technique of parameter fitting was performed to determine the values of each parameter in the model. Two forms of mathematical analysis were performed to gain a deeper understanding of the kinetics of this model, namely stability analysis and parameter analysis. The stability analysis of the non-dimensional model by Phisalaphong et al. (2006) revealed three stable points. These points serve as tools to examine the dynamical systems of this model. The parameter analysis revealed that only σ parameter had a positive impact on ethanol production. On the other hand, Y_{PS} parameter did not have a significant impact, while the remaining eight parameters were found hindering the production of ethanol through fermentation. Next, the current study proceeds with Phisalaphong et al. (2006) extended model. The purpose of the expanded models was to explore particle movement during the fermentation process.

CHAPTER 5

MATHEMATICAL MODELS

5.1 Introduction

Phisalaphong et al. (2006) model formulated a kinetic model incorporating inhibitory effects in ethanol production. However, the model could not spatially predict the microbe, substrate, and ethanol distribution in a tank. Hence, this chapter focuses on extending Phisalaphong et al. (2006) reaction model. The extension aims to consider the particle movement factor in a fermentation reactor. Three types of particle movement models related to the coupled diffusion-reaction equation, the coupled advection-diffusion-reaction equation, and the coupled fluid dynamics-advection-diffusion-reaction equation are presented.

5.2 Diffusion-reaction Model

This study focused on two types of fermentation, non-shaking fermentation and shaking fermentation (refer to Section 2.6). Non-shaking fermentation is characterised by the fermentation process in a reactor without a stirrer (agitator). This type of fermentation is used because bioethanol production occurs under anaerobic conditions (Serafim & Lanças, 2019). According to Takahashi & Aoyagi (2018), increasing the gas-liquid contact area of the surface culture can boost the oxygen supply to the cells by shaking the reactor. This is also one of the inhibitory effects that can lower ethanol production, according to Abdul Halim (2016). In short, it is important to study non-shaking fermentation as an alternative to shaking fermentation. This section proposed a mathematical model for non-shaking fermentation, employing diffusion-reaction coupling, which was an extension of Phisalaphong et al. (2006) model (see Equations 5.1, 5.2, and 5.3).

$$\frac{\partial M\left(x,t\right)}{\partial t}=D\frac{\partial^2 M}{\partial x^2}+\frac{\mu_{max}SM}{K_{SM}+S+S^2/K_{IM}}\left(1-\frac{P}{P_M}\right)-K_dM \tag{5.1}$$

$$\frac{\partial P\left(x,t\right)}{\partial t}=D\frac{\partial^2 P}{\partial x^2}+\frac{v_{max}SM}{K_{SP}+S+S^2/K_{IP}}\left(1-\frac{P}{P_P}\right) \tag{5.2}$$

$$\begin{aligned}\frac{\partial S\left(x,t\right)}{\partial t}=D\frac{\partial^2 S}{\partial x^2}-\frac{1}{Y_{MS}}\left[\frac{\mu_{max}SM}{K_{SM}+S+S^2/K_{IM}}\left(1-\frac{P}{P_M}\right)-K_dM\right]\\ -\frac{1}{Y_{PS}}\left[\frac{v_{max}SM}{K_{SP}+S+S^2/K_{IP}}\left(1-\frac{P}{P_P}\right)\right]-mM\end{aligned} \tag{5.3}$$

The interpolation of diffusion element ($\partial^2/\partial x^2$) on microbe (M), ethanol (P), and substrate (S) is a system of nonlinear Partial Differential Equations (PDE) that reflects spatial coordinate (x) and time observation (t) as two independent variables. Table 5.1 lists the parameters and their values related to the proposed model. The values of these parameters were determined through the process of fitting parameters, explained in Chapter 4. Meanwhile, D values were the diffusion parameter to be studied.

Table 5.1 Parameters in the diffusion-reaction model.

Parameters	Description	Values	Units
D	Diffusivity coefficient	0.1/0.3/0.5/0.7/0.9	$cm^2\ h^{-1}$
μ_{max}	Maximum specific rate for microbial growth	0.779	h^{-1}
v_{max}	Maximum specific rate for ethanol production	50.1142	h^{-1}
K_{SM}	Substrate half-saturation coefficient for microbial growth	257.9958	$g\ L^{-1}$
K_{SP}	Substrate half-saturation coefficient for ethanol production	26.3216	$g\ L^{-1}$
K_{IM}	Substrate inhibition coefficient in microbial growth	182.3467	$g\ L^{-1}$
K_{IP}	Substrate inhibition coefficient in ethanol production	0.1221	$g\ L^{-1}$
P_M	Product inhibition coefficient in microbial growth	31.2110	$g\ L^{-1}$
P_P	Product inhibition coefficient in ethanol production	25.7261	$g\ L^{-1}$
K_d	Microbial death rate	0.0225	h^{-1}
Y_{MS}	Yield coefficient for the substrate used on microbial growth	2.7793	dimensionless
Y_{PS}	Yield coefficient for the substrate used on ethanol production	1.2606	dimensionless
m	Maintenance coefficient of microbial	0.0017	h^{-1}

Figure 5.1 illustrates the diagram of a fermentation tank used in this study, where $0 \le x \le 10$ centimetres. The diagram was designed to examine the diffusion of *M*, *P*, and *S* particles in the tank.

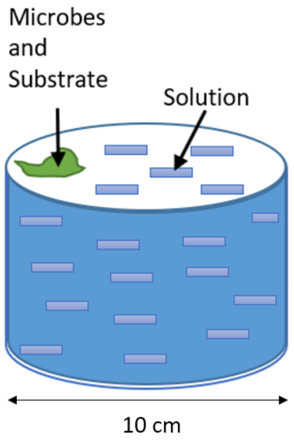

Figure 5.1 The diagram of a fermentation tank.

Since data on the initial conditions for each space (location) were not available from Abdul Halim (2016), the gamma distribution was applied to depict the initial distribution of each particle in the tank, as described in Equation 5.4,

$$\begin{aligned} M(x,0) &= 3.8757 \times \frac{x^{\omega-1} e^{-x/\psi}}{\psi^{\omega}\Gamma(\omega)} \text{ g L}^{-1} \\ P(x,0) &= 0.0 \text{ g L}^{-1} \\ S(x,0) &= 87 \times \frac{x^{\omega-1} e^{-x/\psi}}{\psi^{\omega}\Gamma(\omega)} \text{ g L}^{-1} \end{aligned} \tag{5.4}$$

where ω is shape parameter and ψ is scale parameter of the distribution. In order to get the initial condition illustrated in Figure 5.1, the value of ω was set to 8, while ψ was 0.25. Figure 5.2, Figure 5.3, and Figure 5.4 show the initial conditions of microbes, substrate, and ethanol in this study, respectively.

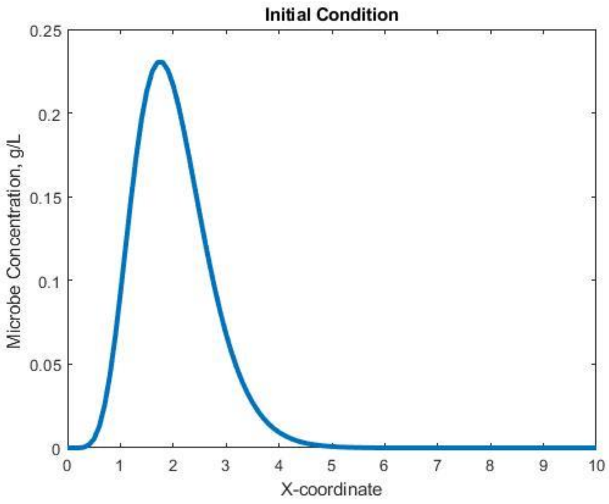

Figure 5.2 Initial condition of microbe concentration in a reactor.

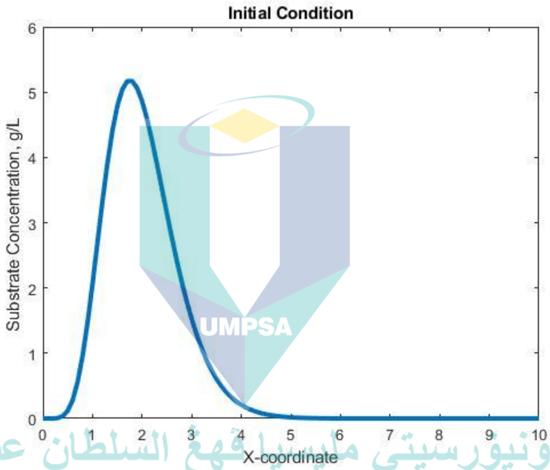

Figure 5.3 Initial condition of substrate concentration in a reactor.

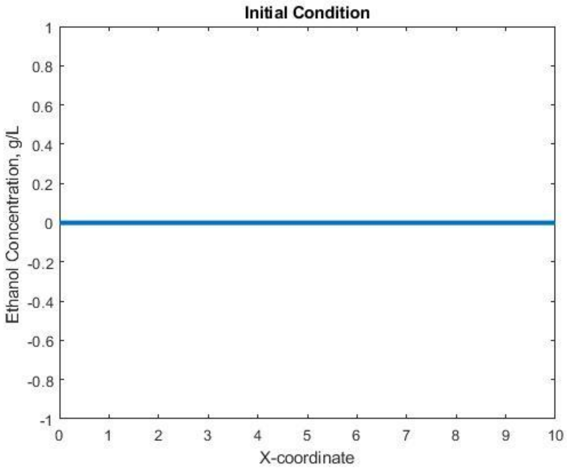

Figure 5.4 Initial condition of ethanol concentration in a reactor.

In addition, the boundary conditions were set, as shown in Equation 5.5, to represent a state where there was no outgoing or incoming flux on the left or right sides of the reactor.

$$\begin{aligned} &\frac{\partial M(0,t)}{\partial x}=0; \qquad \frac{\partial P(0,t)}{\partial x}=0; \qquad \frac{\partial S(0,t)}{\partial x}=0; \\ &\frac{\partial M(10,t)}{\partial x}=0; \qquad \frac{\partial P(10,t)}{\partial x}=0; \qquad \frac{\partial S(10,t)}{\partial x}=0; \end{aligned} \tag{5.5}$$

The solution to this model could be obtained using FVM, with a more comprehensive explanation provided in Chapter 3. In addition, this model enables the analysis of D parameter, denoting particle diffusivity during the fermentation process.

5.3 Advection-diffusion-reaction Model

This section demonstrates the extension of the earlier mathematical model in the non-shaking fermentation section with the advection element, $\partial/\partial x$. The agitation inspired this model in fermentation which considers the advection effect on the ethanol production system. This model, also known as the shaking fermentation model, integrated the velocity coefficient parameter (U), which are represented in Equations 5.6, 5.7, and 5.8.

$$\frac{\partial M}{\partial t}=D\frac{\partial^2 M}{\partial x^2}+\frac{\mu_{max}SM}{K_{SM}+S+S^2/K_{IM}}\left(1-\frac{P}{P_M}\right)-K_dM-U\frac{\partial M}{\partial x} \tag{5.6}$$

$$\frac{\partial P}{\partial t}=D\frac{\partial^2 P}{\partial x^2}+\frac{v_{max}SM}{K_{SP}+S+S^2/K_{IP}}\left(1-\frac{P}{P_P}\right)-U\frac{\partial P}{\partial x} \tag{5.7}$$

$$\begin{aligned}\frac{\partial S}{\partial t}=D\frac{\partial^2 S}{\partial x^2}-\frac{1}{Y_{MS}}\left[\frac{\mu_{max}SM}{K_{SM}+S+S^2/K_{IM}}\left(1-\frac{P}{P_M}\right)-K_dM\right] \\ -\frac{1}{Y_{PS}}\left[\frac{v_{max}SM}{K_{SP}+S+S^2/K_{IP}}\left(1-\frac{P}{P_P}\right)\right]-mM-U\frac{\partial S}{\partial x}\end{aligned} \tag{5.8}$$

This model employed the same parameters, initial conditions, and boundary conditions as the diffusion-reaction model described in the previous subsection. This information makes it possible to conduct a comparative study between non-shaking fermentation and shaking fermentation. Similar to the previous model, this could be solved using FVM, as discussed in Chapter 3.

A coupled advection-diffusion-reaction model could be used to investigate the velocity coefficient (U). The current study did not only disclose the effect of increasing the velocity coefficient (U), but also recommend the optimal parameters to optimise the ethanol production process.

5.4 Coupled Fluid dynamics-advection-diffusion-reaction Model

The previous section highlighted the importance of advection factors in the production of ethanol through fermentation. However, assigning a scalar value to this element does not accurately capture the hydrodynamic effects occurring in stirred reactors. This section aims to present a mathematical model that incorporates a velocity profile of the agitator that is more representative of real-world conditions. This study suggested integrating velocity profiles obtained from fluid dynamics into a previously proposed advection-diffusion-reaction model. Furthermore, to enhance the scope of the investigation, the present study was carried out in a two-dimensional domain.

A baffle is a plate or series of plates that are placed within the reactor to create a barrier that directs the flow of the fluid in a specific pattern. The difference between a tank with a baffle and a tank without a baffle is depicted in Figure 5.5. In their fluid dynamics study, Saikali et al. (2021) validated water velocity profiles in an unbaffled reactor. Meanwhile, Labík et al. (2018) and Wyrobnik et al. (2022) agreed that unbaffled reactors are more suitable for shear-sensitive microbes, promising research with a reactor without a baffle.

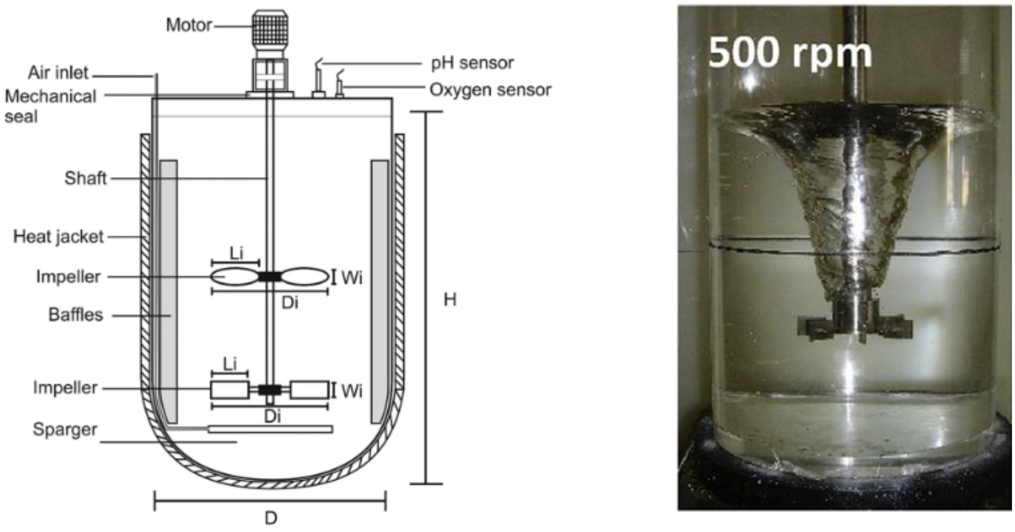

(a) (b)

Figure 5.5 The difference between (a) a tank with baffles and (b) an unbaffled tank. Source: (a) Afedzi et al. (2022), (b) Labik et al. (2018)

In Chapter 2, the continuity equation and the Navier-Stokes equation are introduced as fundamental equations employed for a description of fluid flow within the reactor tank. To bridge the gap on unbaffled tank, the current study proposed a mathematical model for the production of ethanol in the stirred, unbaffled tank bioreactor This proposed model integrates both the continuity equation and the Navier-Stokes equation. The resulting equation, known as the fluid dynamics-advection-diffusion-reaction equation, served as the foundation for the current study.

$$\frac{\partial U}{\partial x}+\frac{\partial V}{\partial y}=0 \tag{5.9}$$

$$\frac{\partial U}{\partial t}=-\left(U\frac{\partial U}{\partial x}+V\frac{\partial U}{\partial y}\right)+vis\left(\frac{\partial^2 U}{\partial x^2}+\frac{\partial^2 U}{\partial y^2}\right)-\frac{1}{\rho}\frac{\partial pr}{\partial x} \tag{5.10}$$

$$\frac{\partial V}{\partial t}=-\left(U\frac{\partial V}{\partial x}+V\frac{\partial V}{\partial y}\right)+vis\left(\frac{\partial^2 V}{\partial x^2}+\frac{\partial^2 V}{\partial y^2}\right)-\frac{1}{\rho}\frac{\partial pr}{\partial y} \tag{5.11}$$

$$\frac{\partial M}{\partial t} = -\left(U\frac{\partial M}{\partial x} + V\frac{\partial M}{\partial y}\right) + D\left(\frac{\partial^2 M}{\partial x^2} + \frac{\partial^2 M}{\partial y^2}\right) + \text{Reaction}(M) \tag{5.12}$$

$$\frac{\partial P}{\partial t} = -\left(U\frac{\partial P}{\partial x} + V\frac{\partial P}{\partial y}\right) + D\left(\frac{\partial^2 P}{\partial x^2} + \frac{\partial^2 P}{\partial y^2}\right) + \text{Reaction}(P) \tag{5.13}$$

$$\frac{\partial S}{\partial t} = -\left(U\frac{\partial S}{\partial x} + V\frac{\partial S}{\partial y}\right) + D\left(\frac{\partial^2 S}{\partial x^2} + \frac{\partial^2 S}{\partial y^2}\right) + \text{Reaction}(S) \tag{5.14}$$

where

$$\text{Reaction}(M) = \frac{\mu_{max} SM}{K_{SM} + S + S^2/K_{IM}}\left(1 - \frac{P}{P_M}\right) - K_d M \tag{5.15}$$

$$\text{Reaction}(P) = \frac{v_{max} SM}{K_{SP} + S + S^2/K_{IP}}\left(1 - \frac{P}{P_P}\right) \tag{5.16}$$

$$\begin{aligned}\text{Reaction}(S) = &-\frac{1}{Y_{MS}}\left(\frac{\mu_{max} SM}{K_{SM} + S + S^2/K_{IM}}\left(1 - \frac{P}{P_M}\right) - K_d M\right)\\ &-\frac{1}{Y_{PS}}\left(\frac{v_{max} SM}{K_{SP} + S + S^2/K_{IP}}\left(1 - \frac{P}{P_P}\right)\right) - mM\end{aligned} \tag{5.17}$$

The model contained two-dimensional spatial coordinates (x, y) and time observation (t), at three independent variables, namely $0 \le x \le 1$ metre, $0 \le y \le 1$ metre, and $0 \le t \le 100$ hours. U and V denote the velocity components in the x and y directions, while pr signifies the pressure in the solution. The variables vis and ρ describe the solution's viscosity and density, respectively. In this research, vis and ρ were set to 1×10^{-6} m^2 s^{-1} and 1000 kg m^{-3}, the same values employed in the study by Saikali et al. (2021), because the reactor tank was expected to be filled with water at room temperature.

Table 5.2 shows the parameters utilised in this study. To maintain consistency, all parameters relating to time were converted to second units and parameters relating to mass were converted to kilogramme units.

Table 5.2 The parameters value for the proposed model.

Parameters	**Values**	**Units**
D	0.01	$\mathrm{m\ s^{-1}}$
$\mu_{\max}$	2.1639×10^{-4}	$\mathrm{s^{-1}}$
$v_{\max}$	1.3921×10^{-2}	$\mathrm{s^{-1}}$
K_d	6.2500×10^{-6}	$\mathrm{s^{-1}}$
m	4.7222×10^{-7}	$\mathrm{s^{-1}}$
K_{SM}	2.5760×10^{-1}	$\mathrm{kg\ L^{-1}}$
K_{SP}	2.6320×10^{-2}	$\mathrm{kg\ L^{-1}}$
K_{IM}	1.8235×10^{-1}	$\mathrm{kg\ L^{-1}}$
K_{IP}	1.2210×10^{-4}	$\mathrm{kg\ L^{-1}}$
P_M	3.1211×10^{-2}	$\mathrm{kg\ L^{-1}}$
P_P	2.5726×10^{-2}	$\mathrm{kg\ L^{-1}}$
Y_{MS}	2.7793	dimensionless
Y_{PS}	1.2606	dimensionless

Figure 5.6 presents a cross-sectional view of the bioreactor where the agitator was at $x=0$ m. The shaded region represents the right-hand side of the cross-sectional bioreactor. It was assumed that the geometry was symmetric about $x=0$. Saikali et al. (2021) presented several velocity profiles of water in a bioreactor with different Reynolds numbers (Re), as shown in Figure 5.7 and Figure 5.8. For this study, these velocity profiles were used as a guide to figure out the boundary conditions. Figure 5.6–5.8 illustrated the boundary conditions employed in this study, and will aid in clarifying the domain's geometry.

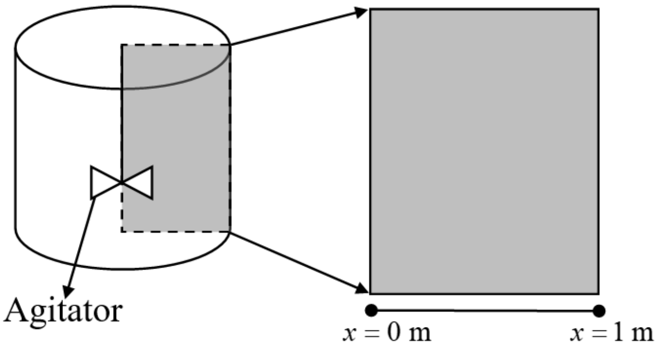

Figure 5.6 Cross-sectional view of the bioreactor.

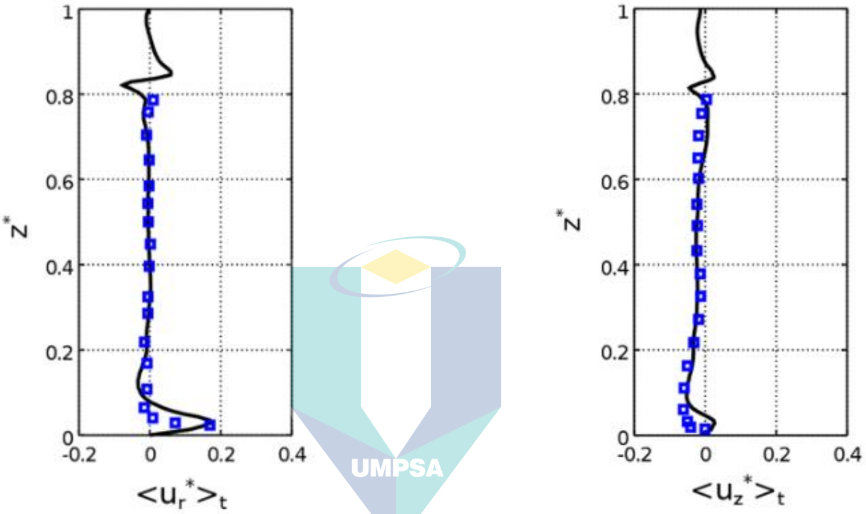

Figure 5.7 Velocity profiles in Saikali et al. (2021) for $Re \approx 7 \times 10^4$.

Source: Saikali et al. (2021)

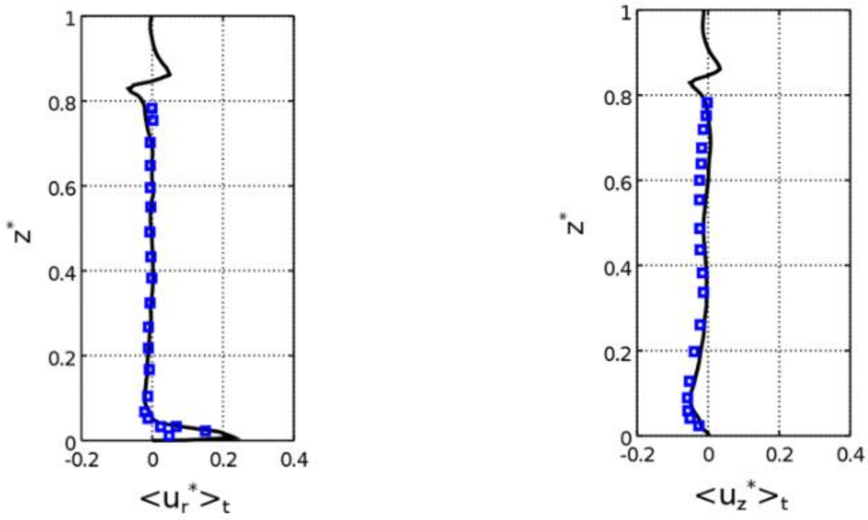

Figure 5.8 Velocity profiles in Saikali et al. (2021) for $Re \approx 8.6 \times 10^4$.
Source: Saikali et al. (2021)

Based on the velocity profiles shown in Figure 5.7 and Figure 5.8, Equations 5.18 and 5.19 were introduced to represent the boundary conditions at $x = 0$ m. The pressure boundary condition in Equation 5.20 is based on Bernoulli's principle. According to Childs (2011), the speed of a fluid increases, the pressure within the fluid decreases.

$$U(0,y,t) = 5 \times \left(500y \times e^{1+500y\times(0.80-1)}\right) \div 100 \qquad 5.18$$

$$V(0,y,t) = -0.3 \times \left(500y \times e^{1+500y\times(0.95-1)}\right) \div 100 \qquad 5.19$$

$$pr(0,y,t) = -\left(|U| + |V|\right) \qquad 5.20$$

These equations regarding boundary conditions on the left-side domain are displayed in Figure 5.9.

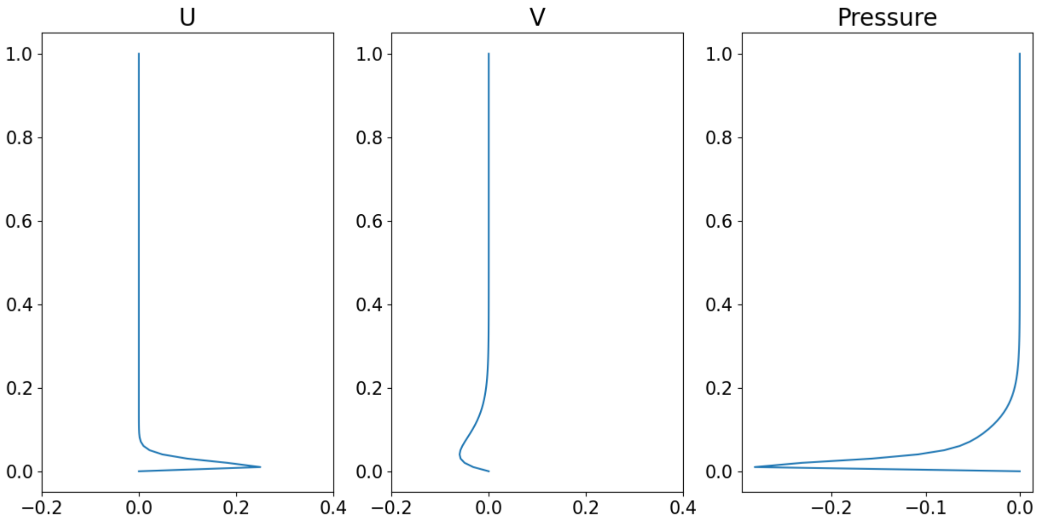

(a) (b) (c)

Figure 5.9 Boundary conditions at $x = 0$ for (a) U, (b) V and (c) pressure.

Next, a no slip boundary condition was set for the right and bottom domains. Equation 5.21 imposes the boundary condition for the domain on the right, whereas Equation 5.22 applies the boundary condition for the domain on the bottom.

$$U(1,y,t)=0; \qquad V(1,y,t)=0; \qquad pr(1,y,t)=0; \qquad 5.21$$

$$U(x,0,t)=0; \qquad V(x,0,t)=0; \qquad pr(x,0,t)=0; \qquad 5.22$$

According to Saikali et al. (2021), the vortex formed on the free surface resembles an inverted Gaussian profile, also referred to as an inverted normal distribution. Figure 5.10 demonstrates the profile for velocity and pressure.

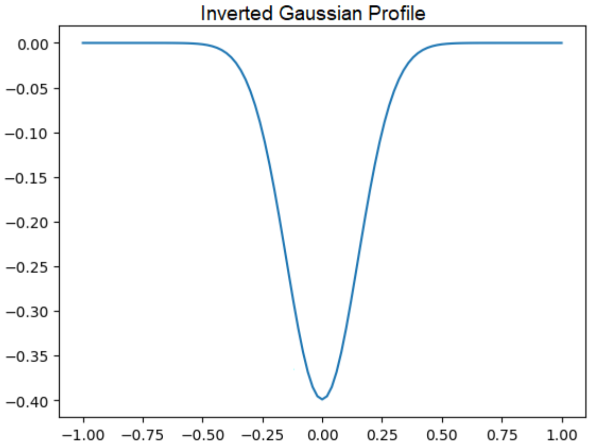

Figure 5.10 Inverted Gaussian profile for velocity and pressure.

This profile served as the upper boundary condition for the domain in this study. However, because the domain range was [0, 1], only half of this profile was considered. The upper-boundary condition for the variables *U*, *V*, and *pr* was represented by Equations 5.23, 5.24, and 5.25,

$$\frac{\partial U(x,1,t)}{\partial y} = -\frac{1}{\sigma_1\sqrt{2\pi}} e^{-\frac{1}{2}\left(\frac{x}{\sigma_1}\right)^2} \qquad 5.23$$

$$\frac{\partial V(x,1,t)}{\partial y} = -\frac{1}{\sigma_2\sqrt{2\pi}} e^{-\frac{1}{2}\left(\frac{x}{\sigma_2}\right)^2} \qquad 5.24$$

$$\frac{\partial pr(x,1,t)}{\partial y} = -\frac{1}{\sigma_3\sqrt{2\pi}} e^{-\frac{1}{2}\left(\frac{x}{\sigma_3}\right)^2} \qquad 5.25$$

where $\sigma = \sigma_1 = \sigma_2 = \sigma_3$ were the standard deviation of the normal distribution. Figure 5.11 depicts the three utilised standard deviation values. Chapter 6 will provide a more comprehensive details of standard deviation study.

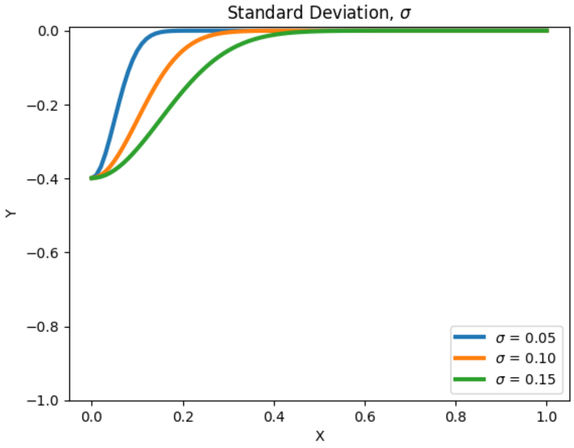

Figure 5.11 The standard deviation values were examined.

Given that the specific data regarding initial conditions for each space or location were not provided in the study conducted by Abdul Halim (2016), the utilisation of the normal distribution was employed in order to illustrate the dispersion of individual particles within the tank at the onset. The particles M, P, and S in a normal distribution along the domain (x, y) can be defined by Equation 5.26,

$$\begin{aligned} M(x,y,0) &= 3.8757 \times \text{NormalDistibution}(x,y) \text{ kgL}^{-1} \\ P(x,y,0) &= 0 \text{ kgL}^{-1} \\ S(x,y,0) &= 87 \times \text{NormalDistibution}(x,y) \text{ kgL}^{-1} \end{aligned} \qquad 5.26$$

where

$$\text{NormalDistibution}(x,y) = \frac{1}{2\pi\sigma_x\sigma_y\sqrt{1-Cov(x,y)}} e^{-\frac{g}{2\left(1-Cov(x,y)^2\right)}} \qquad 5.27$$

and

$$g = \frac{(x-\mu_x)^2}{{\sigma_x}^2} - \frac{2Cov(x,y)[x-\mu_x][y-\mu_y]}{\sigma_x\sigma_y} + \frac{(y-\mu_y)^2}{{\sigma_y}^2} \qquad 5.28$$

The symbols μ_x and μ_y represent the means for this distribution. These parameters were set to 0.50 to place the highest concentration of microbes and substrate at the start of fermentation, primarily in the centre of the domain. On the other hand, σ_x and σ_y were standard deviations. It attempted to determine the amount of dispersion between the mean values of variables M and S. These two parameters (σ_x and σ_y) were both set at 0.2. Figure 5.12, Figure 5.13, and Figure 5.14 illustrate the concentration distribution of M, S, and P in the tank at the beginning of the fermentation process.

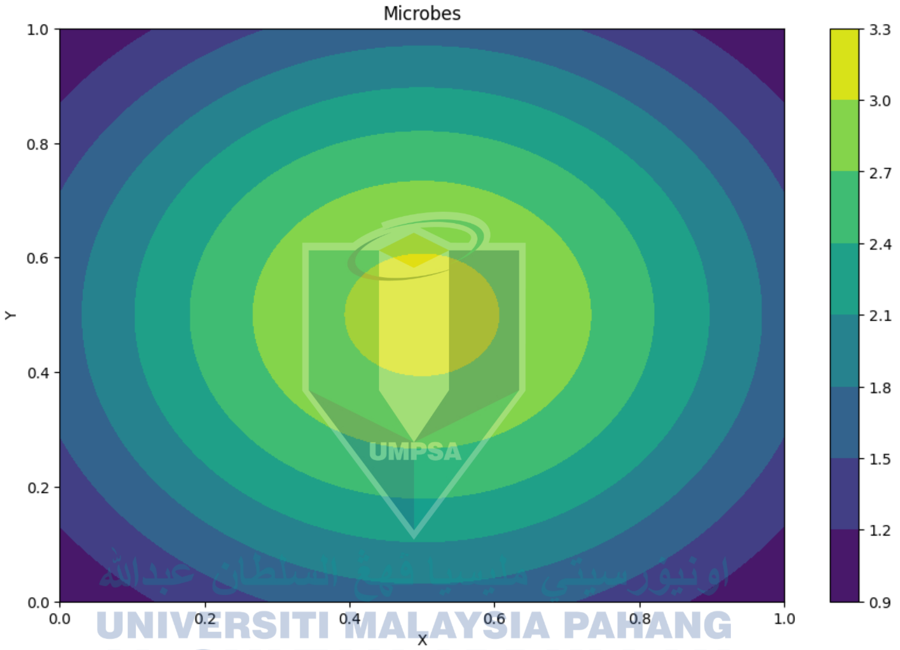

Figure 5.12 Initial condition of the variable M at the start of fermentation.

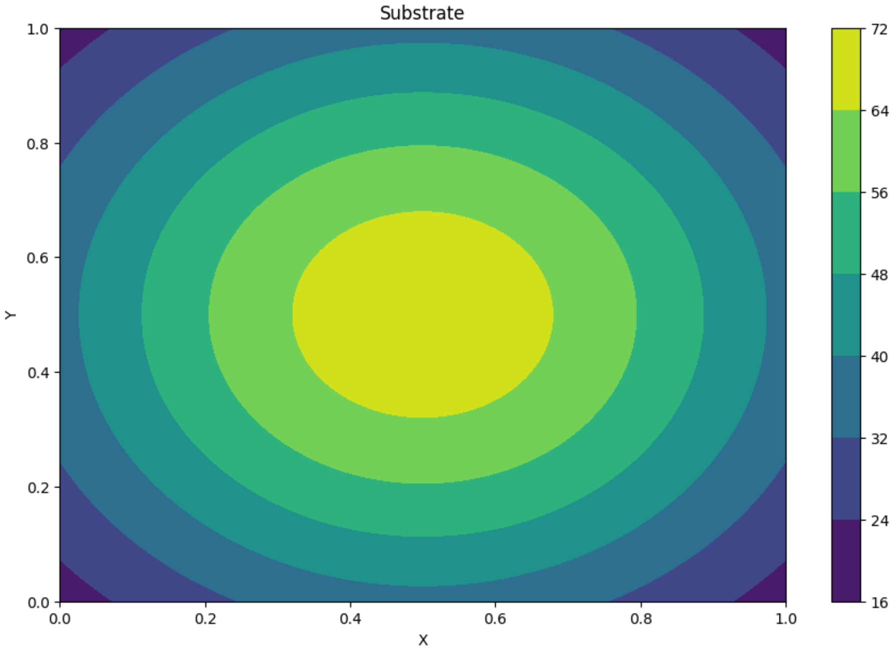

Figure 5.13 Initial condition of the variable S at the start of fermentation.

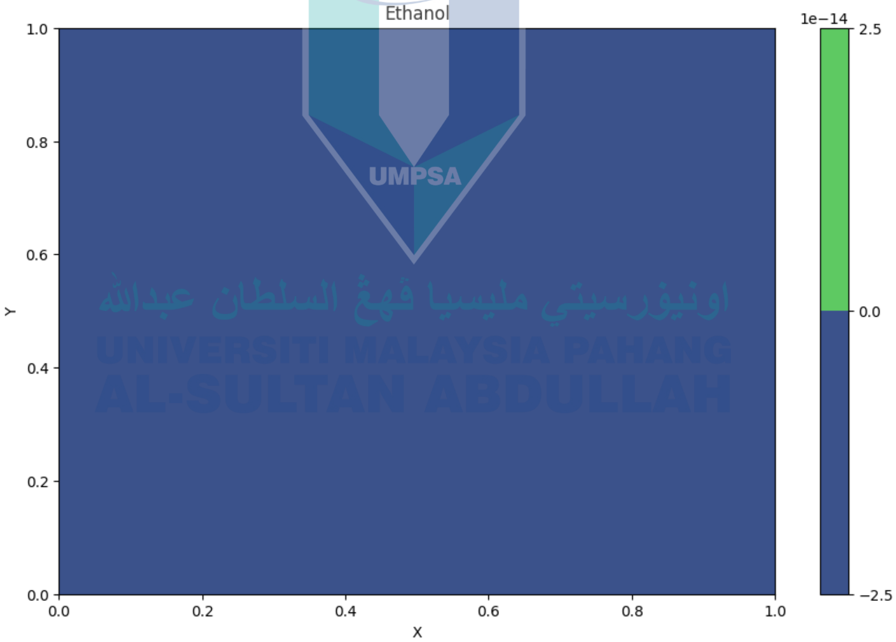

Figure 5.14 Initial condition of the variable P (ethanol) at the start of fermentation.

A Neumann-type boundary condition, equal to zero, was applied to the variables *M*, *P*, and *S* since no outflow or inflow happened on the left, right, bottom and top sides of the boundary. The boundary conditions for *M*, *P*, and *S* variables are listed in Equation 5.29.

$$\begin{aligned}
&\frac{\partial M(0,y,t)}{\partial x}=0; && \frac{\partial M(1,y,t)}{\partial x}=0;\\
&\frac{\partial M(x,0,t)}{\partial y}=0; && \frac{\partial M(x,1,t)}{\partial y}=0;\\
&\frac{\partial P(0,y,t)}{\partial x}=0; && \frac{\partial P(1,y,t)}{\partial x}=0;\\
&\frac{\partial P(x,0,t)}{\partial y}=0; && \frac{\partial P(x,1,t)}{\partial y}=0;\\
&\frac{\partial S(0,y,t)}{\partial x}=0; && \frac{\partial S(1,y,t)}{\partial x}=0;\\
&\frac{\partial S(x,0,t)}{\partial y}=0; && \frac{\partial S(x,1,t)}{\partial y}=0;
\end{aligned} \qquad 5.29$$

The model was solved using FVM. However, the use of 2D (x,y) domain required modification on the FVM grid, as explained in Chapter 3.

5.5 Conclusion

This study aimed to formulate a non-linear PDE model for ethanol production through fermentation by coupling diffusion-reaction into the model. The model specifically focused on non-shaking fermentation and extended to include an advection factor inspired by the agitation typically employed during fermentation. Thus, a model in the form of an advection-diffusion-reaction equation was formed. This chapter further broadened the study of the reactor condition by incorporating fluid dynamics factors into the model, which is referred to as the coupled fluid dynamics-advection-diffusion-reaction model.

CHAPTER 6

RESULT AND DISCUSSION

6.1 Introduction

This chapter highlights the results of the current study of including particle movement elements in the reaction model of Phisalaphong et al. (2006). The study is organised into three distinct subtopics, each corresponding to one of the three PDE systems discussed in Chapter 5. The first topic of discussion relates to the diffusion-reaction model, which is subsequently followed by a study of the advection-diffusion-reaction model. Then, an analytical discussion on mathematical models incorporating fluid dynamics into coupled diffusion-advection-reaction equations is provided. The current chapter gives a comprehensive analysis of the impact of the agitator position on the ethanol production, while also offering an optimal agitator position to maximise the production of ethanol through fermentation.

6.2 Discussion on Diffusion-reaction Model

The diffusion-reaction model, together with the stated initial and boundary conditions, as described in Chapter 5, was solved using FVM for $0 \le t \le 100$ hours. Figure 6.1, Figure 6.2, and Figure 6.3 show the proposed model solutions for microbes, substrates, and ethanol, respectively. By setting D to 0.1 cm^2 h^{-1}, this model not only demonstrated the diffusivity process, but also depicted the inhomogeneous conditions that occurred in the reactor during the fermentation process, which eventually affected the ethanol production. Based on these figures, initially most of the particles, either microbes or substrate, were concentrated on the left of the reactor. However, the particles dispersed after the diffusivity and fermentation processes, even though they did not reach the right side of the reactor.

In particular, the initial microbe and substrate concentrations Figure 6.1 and Figure 6.2 were highly concentrated in the ranges of *x*-coordinate = [0.3, 5]. However, over a duration of five hours, the concentration showed an expansion within the *x*-coordinate intervals of [0, 7]. This phenomenon indicates that particles within the reactor migrated from areas of high concentration to a region of low concentration. In contrast to the declining trends observed in microbial and substrate concentrations over time, ethanol concentrations exhibited an increasing pattern. This can be due to the fact that ethanol is a by-product of microbial-substrate reactions, as visually depicted in Figure 6.3. Hence, ethanol production will occur in any area where microbes and substrates are present, even with limited diffusion across the reactor.

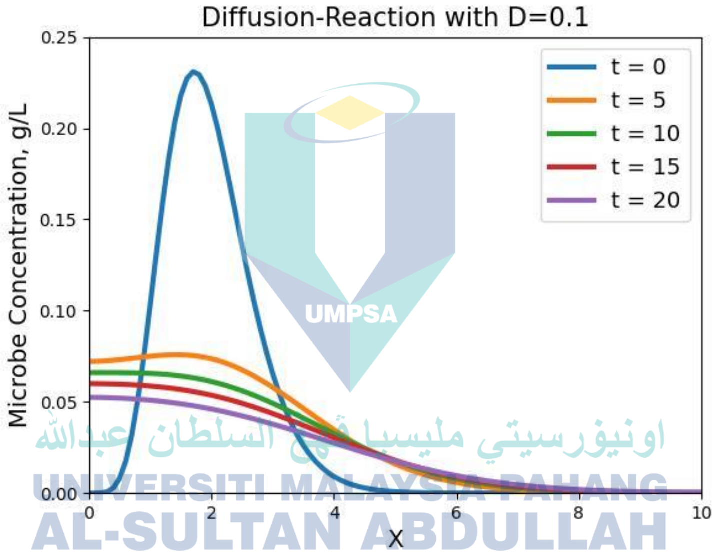

Figure 6.1 The diffusivity factor with *D* = 0.1 $cm^2 h^{-1}$ in microbial growth.

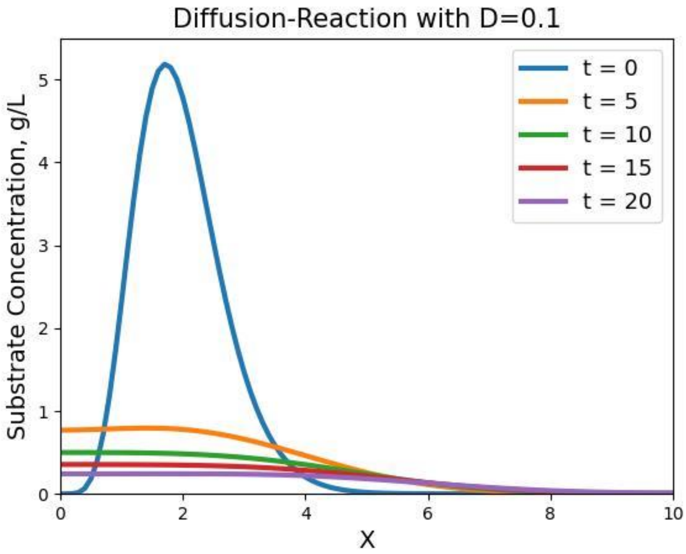

Figure 6.2 The diffusivity factor with $D = 0.1$ cm^2 h^{-1} in substrate consumption.

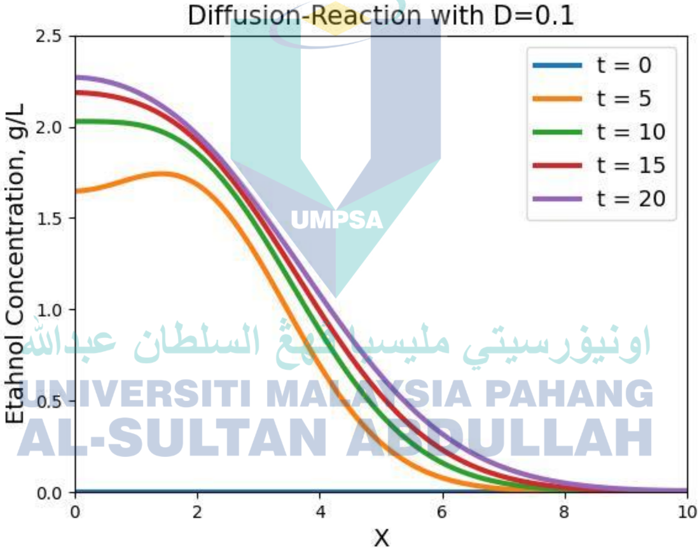

Figure 6.3 The diffusivity factor with $D = 0.1$ cm^2 h^{-1} in ethanol production.

This section also includes the analysis of the diffusion coefficient value of the fermentation system. The effects of increasing *D* values microbes, substrate, and ethanol in the reactor are depicted in Figure 6.4, Figure 6.5, and Figure 6.6, respectively. A simulation of the three variables during the first ten hours of fermentation with $D = 0.1$, 0.3, 0.5, 0.7, and 0.9 cm^2 h^{-1} revealed that increasing diffusivity flattered the concentration graph. This indicates that *D* could accelerate the process of obtaining a homogenous concentration in the reactor.

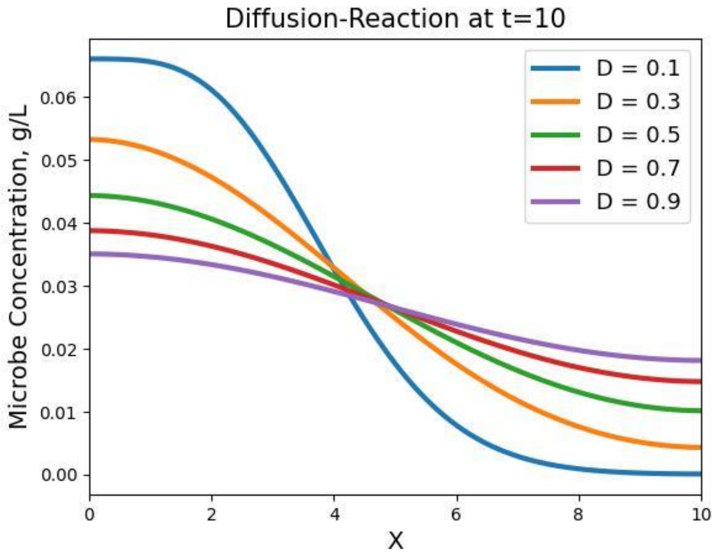

Figure 6.4 Evaluation of diffusion coefficient on microbial growth in the first 10 hours.

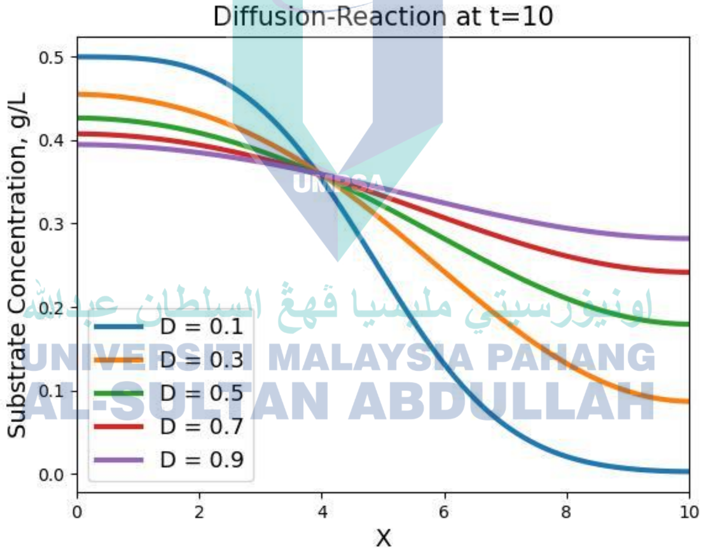

Figure 6.5 Evaluation of diffusion coefficient on substrate consumption in the first 10 hours.

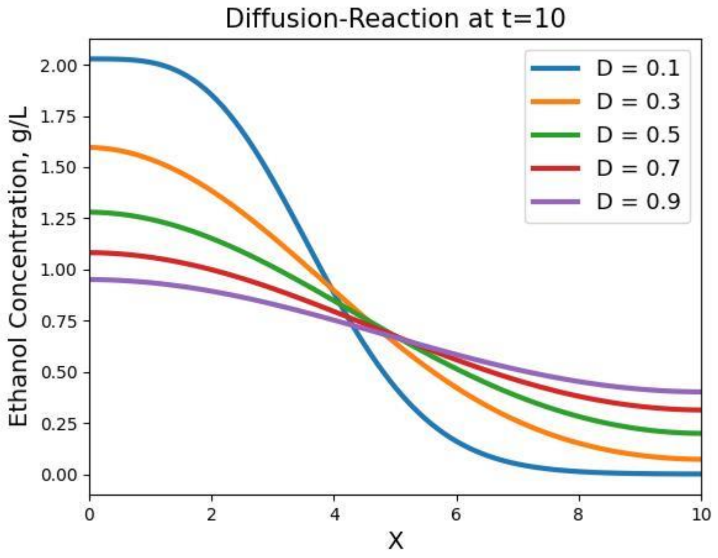

Figure 6.6 Evaluation of diffusion coefficient on ethanol production in the first 10 hours.

Diffusion is the random movement of naturally occurring particles, thereby beyond human control. Advection, on the other hand, is the movement due to the fluid's velocity. This movement can be controlled and manipulated by humans, such as by shaking fermentation tank. Therefore, a proposed model for ethanol production incorporated the influence of shaking on the production of ethanol presented in the upcoming sections.

6.3 Discussion on Advection-diffusion-reaction Model

The solutions for the advection-diffusion-reaction model for microbes, substrate, and ethanol are depicted in Figure 6.7, Figure 6.8, and Figure 6.9, respectively. This study utilised the same settings (initial and boundary conditions), parameter values, and methods as earlier studies (refer to Section 6.2). However, in order to analyse the existence of velocity (U) in the model, the diffusion coefficient (D) was set to 0.1 cm^2 h^{-1} and U to 0.1 cm h^{-1}. Figure 6.7, Figure 6.8, and Figure 6.9 illustrate the differences in the integral results between diffusion-reaction only and advection-diffusion-reaction models. Compared to microbial growth and substrate consumption, ethanol production exhibits remarkably different in particle movement. Nonetheless, given the presence of the advection component in the model, microbial concentrations, originally accumulated in the range of 0.3 to 5.0, were successfully dispersed across the *x*-coordinate within the first 20 hours. This is not observed in system models without an advection component (a model that only has diffusion components). It also occurred in the consumption of substrates. After twenty hours of fermentation, the substrate particles were successfully distributed across the reactor's spatial coordinates.

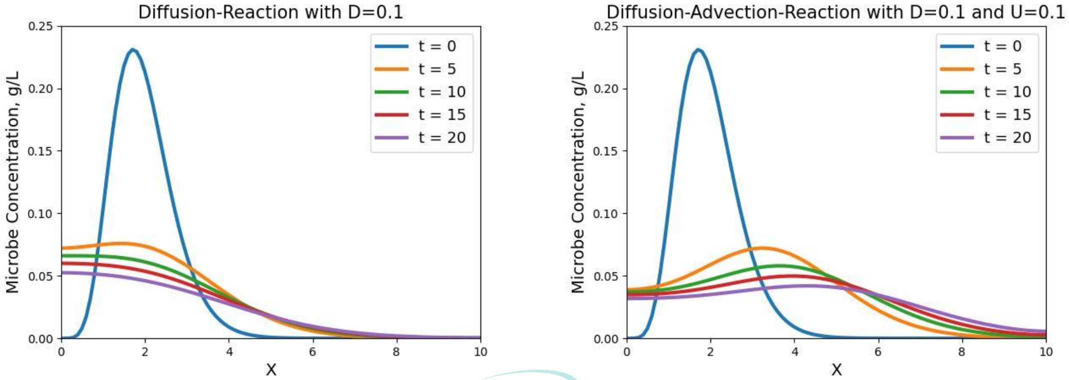

(a) (b)

Figure 6.7 Solution of microbial growth using (a) the diffusion-reaction model and (b) the advection-diffusion-reaction model.

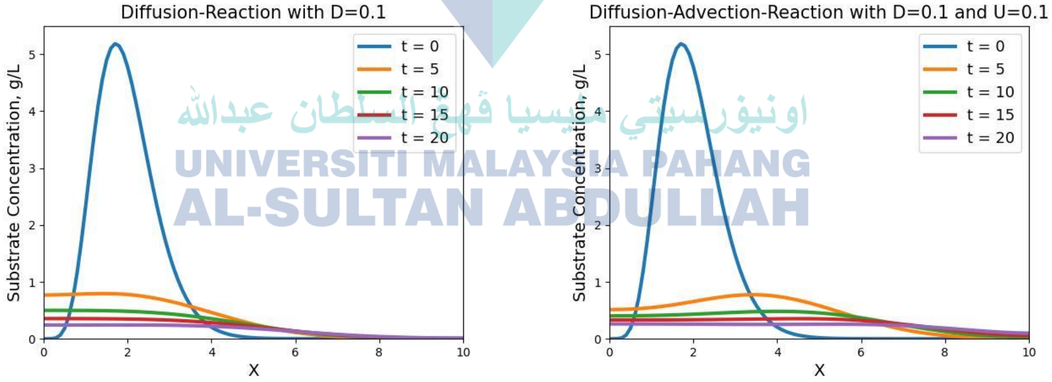

(a) (b)

Figure 6.8 Solution of substrate consumption using (a) the diffusion-reaction model and (b) the advection-diffusion-reaction model.

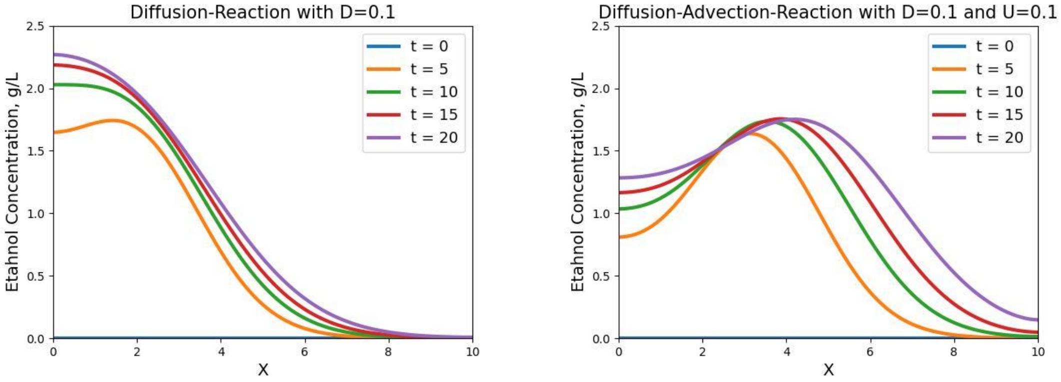

(a) (b)

Figure 6.9 Solution of ethanol production using (a) the diffusion-reaction model and (b) the advection-diffusion-reaction model.

Subsequently, a study was undertaken to determine the impact of the two models on the particle concentration value in the tank, as shown in Table 6.1. For this study, the first twenty hours of fermentation were selected. Assuming that the particles were distributed throughout the tank, the concentration was calculated using integrals by computing the area under the graph. Nevertheless, the movement of these particles over time increased the possibility that any mathematical function may not accurately capture their distribution. Consequently, the particle concentration was calculated using the trapezoidal rule described in Appendix D.

According to Table 6.1, the advection-diffusion-reaction model yielded higher particle concentration values than the diffusion-reaction model. This demonstrates that the influence of particle dispersion from advection can decrease tank inhomogeneity more quickly than diffusion alone. Hence, it can increase ethanol production, as shown in Figure 6.9 (b).

Table 6.1 Concentration of particles throughout the first 20 hours of fermentation for the two different models.

Models	Microbes (g L $^{-1}$)	Substrate (g L $^{-1}$)	Ethanol (g L $^{-1}$)
Diffusion-reaction	2.2299	15.1563	90.9305
Advection-diffusion-reaction	2.9189	22.6261	115.9547

A study on the variation in the value of the coefficient of velocity (U) was also conducted in this section. A total of five U values were examined, namely 0.1, 0.3, 0.5, 0.7, and 0.9 cm h^{-1}. Figure 6.10, Figure 6.11, and Figure 6.12 show the effects of increasing the value of U on the concentration of microbes, substrate, and ethanol, respectively, in the reactor. In the meantime, Table 6.2 the measured values of and the projected concentrations of three distinct particle types in the fermentation tank for the initial twenty-hour period. This estimation was also made using the trapezoidal rule described in Appendix D. The concentration of microbes exhibits a declining trend as U increases, and there is a decline in substrate consumption when the U value increases from 0.1 to 0.3. However, there was an observed rise in the total amount of remaining substrate after the first twenty-hour period of fermentation, as the U value increased from 0.3 to 0.9. According to a study conducted by Kamer (2004), the challenging aspect of the microbe's reaction with the substrate could perhaps be attributed to the high velocity of particle movement within the reactor. In addition, fermentation with a U coefficient of 0.1 cm h^{-1} has produced the most ethanol despite the fact that the amount of substrate remaining at the end of fermentation is not the smallest. This study reveals that the advection component has a substantial impact on the system for manufacturing ethanol. In addition, this study also provides recommendations for the optimal U value to produce the most ethanol, which is a U value of 0.1 cm h^{-1}.

Table 6.2 The concentration of particles with different U values.

U (cm h^{-1})	**Microbes (g L^{-1})**	**Substrate (g L^{-1})**	**Ethanol (g L^{-1})**
0.1	2.9189	22.6261	115.954
0.3	2.2037	19.8257	85.2278
0.5	2.1923	22.3784	82.0396
0.7	2.1854	23.8929	80.1374
0.9	2.1809	24.8588	78.9227

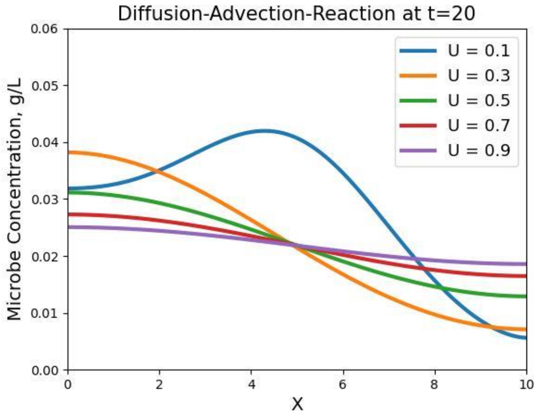

Figure 6.10 Evaluation of advection coefficient on microbial growth in the first 20 hours.

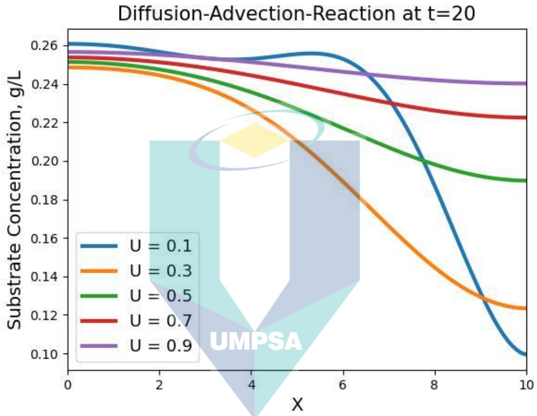

Figure 6.11 Evaluation of advection coefficient on substrate consumption in the first 20 hours.

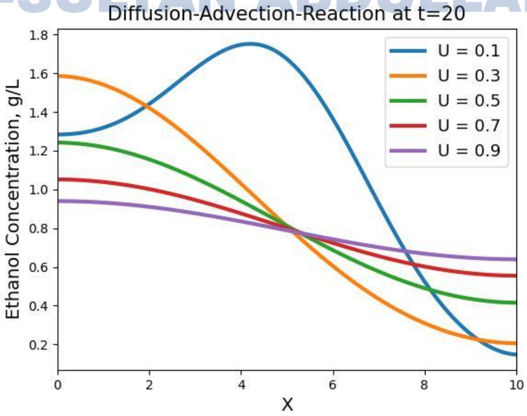

Figure 6.12 Evaluation of advection coefficient on ethanol production in the first 20 hours.

To conclude, compared to the diffusion-reaction-only model represented in Figure 6.9 (a) and the advection-diffusion-reaction model depicted in Figure 6.9 (b), fluid velocity advection can improve ethanol production. This is similar to the findings of Nasir et al. (2017), who found that shaking the reactor to create a homogenous mixture increase the production of ethanol.

6.4 Discussion on Fluid dynamics-advection-diffusion-reaction Model

This subsection provides a discussion of the study related to the integration of fluid dynamics into coupled advection-diffusion-reaction equations within mathematical models. Due to differences in the initial condition, boundary condition, and reactor geometry between this study and prior studies, certain modifications were implemented to solve the model in this particular subtopic. A time interval, (Δt) of 0.08 seconds was chosen to solve all of the equations in the proposed model. While the distance between cells in the x or y direction ($\Delta x, \Delta y$) has been set to 0.01 metres. The results of a five-minute simulation of the fermentation process are presented in Figure 6.13, Figure 6.14, and Figure 6.15. The arrows in the figures represent the velocity profile produced by the rotation of the agitator placed on the bottom of the tank surface, as implemented in the study by Saikali et al. (2021), with the length of the arrow indicating the magnitude of the velocity at a particular point. The standard deviation, σ was set to 0.05 in Equations 5.26–5.28.

The proposed model has the capability to approximately depict the motion of particles within the tank, contingent upon the speed of the agitator. As shown in Figure 5.12, the initial concentration of microbes was particularly high in the midsection of the tank, within the range [0.4, 0.6] of the domain. However, after five minutes of fermentation, the microbe concentration moved and dispersed throughout the tank, as depicted in Figure 6.13. Meanwhile, Figure 6.14 demonstrates that the concentration of the substrate, which was formerly concentrated in the centre of the domain, had shifted to the right side of the domain as a result of the movement of particles caused by the agitator speed. Figure 6.15 also depicts the occurrence of ethanol production during agitated fermentation when there was a difference in ethanol concentration levels within the tank.

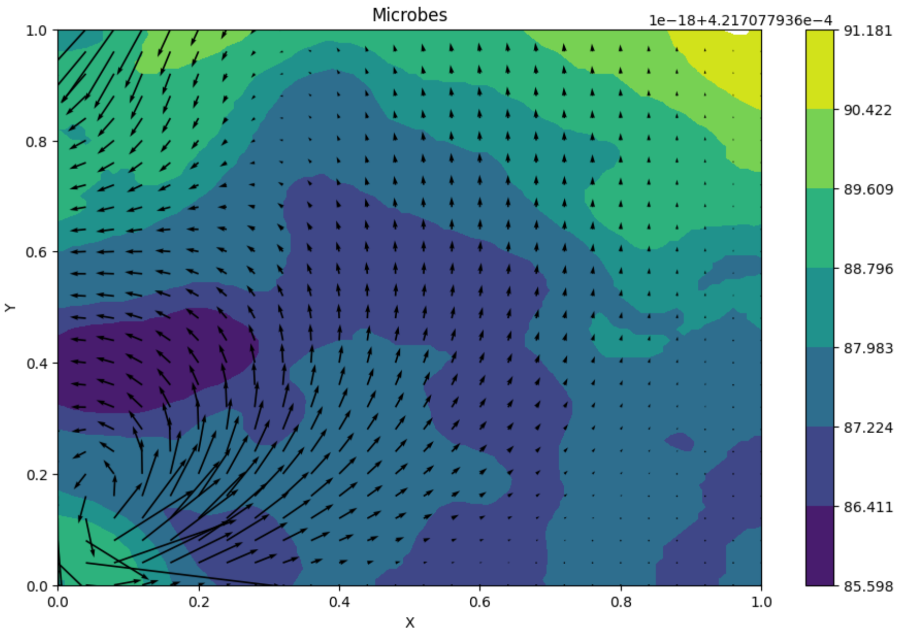

Figure 6.13 Microbe concentration after five minutes of fermentation.

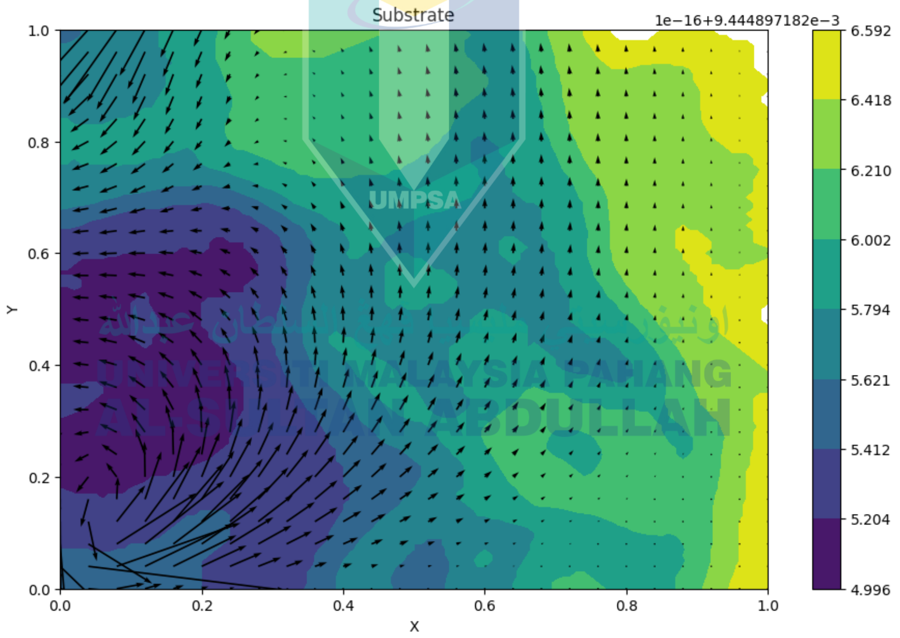

Figure 6.14 Substrate concentration after five minutes of fermentation.

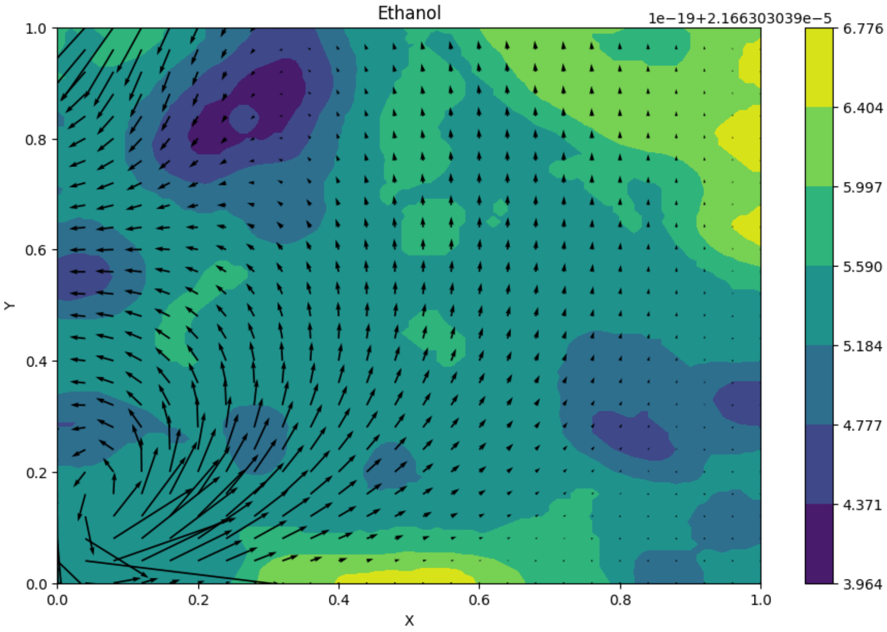

Figure 6.15 Ethanol concentration after five minutes of fermentation.

Table 6.3 contains the concentrations of variables *M*, *S*, and *P* during the first five minutes of fermentation. In the tank, the concentration of microbes and ethanol increased, while the concentration of substrate decreased slightly. This is consistent with the conclusions of the earlier chapters, which state that microbes and ethanol will increase at the beginning of fermentation when substrate is present.

Table 6.3 Particle concentration in the first 5 minutes of fermentation.

Minutes	**Microbes (kg L $^{-1}$)**	**Substrate (kg L $^{-1}$)**	**Ethanol (kg L $^{-1}$)**
0	3.8757	87	0
5	3.8769	86.8319	0. 19916

The study of the free surface vortex at the upper boundary condition of the domain using the σ parameter is also included in this section. As presented in Figure 5.11, σ values of 0.05, 0.10, and 0.15 were chosen for this study. Table 6.4 presents the concentration values of *M*, *S*, and *P* for the first five minutes of the fermentation process with different σ. When the σ value increased, each type of particle variable exhibited a decreasing trend. The vortex area on the free surface also expanded as σ value increased. According to Saikali et al. (2021), the area of the free surface vortex increases as the

Reynolds number (Re), increases. Agarwal et al. (2021) also state that Re is directly proportional to the agitator's rotational speed. On the basis of these two reports and the trends presented in Table 6.4, it can be concluded that increasing the σ value associated with the agitator's rotational speed will decrease ethanol production.

Table 6.4 Particle concentration in the first 5 minutes of fermentation with different σ.

Standard Deviation, σ	**Microbes (kg L $^{-1}$)**	**Substrate (kg L $^{-1}$)**	**Ethanol (kg L $^{-1}$)**
0.05	3.8769	86.8319	0.19916
0.10	3.8755	86.8001	0.19915
0.15	3.8696	86.6661	0.19912

In light of the findings of this study, the following section includes an investigation into the agitator's speed towards the ethanol production system.

6.5 Agitator's Speed in the Ethanol Production System

The analysis of the agitator's speed was conducted by incorporating Ag parameter as a speed coefficient into Equations 5.18 and 5.19, which was the left boundary condition equation. The following equations define the equation for the boundary condition at $x = 0$.

$$U(0,y,t) = Ag \times 5 \times \left(500y \times e^{500y\times(0.80-1)+1}\right) \div 100 \tag{6.1}$$

$$V(0,y,t) = Ag \times -0.3 \times \left(500y \times e^{500y\times(0.95-1)+1}\right) \div 100 \tag{6.2}$$

$$pr(0,y,t) = -\left(|U| + |V|\right) \tag{6.3}$$

This study experimented with the different settings of the Ag parameter, which were 0.4, 0.6, 0.8, 1, 3, and 5. The fermentation period was set at 5 minutes, consistent with earlier studies. In the meantime, σ parameter was set to 0.05 because, according to previously conducted studies, this value produced the most ethanol. The results of the Ag parameter value investigation on the ethanol production system are summarised in Table 6.5.

In general, the production of ethanol happened as a result of the microbe's interaction with the substrate. However, a pattern of decreasing microbial concentration has been observed with increasing Ag values. This may be due to the sheer force of the agitator destroying the microbes, which resulted in a decrease in ethanol production. This shows that increasing the value of Ag will reduce ethanol production.

Table 6.5 Study of Ag parameter values towards ethanol production yield.

Ag	**Microbes (kg L $^{-1}$)**	**Substrate (kg L $^{-1}$)**	**Ethanol (kg L $^{-1}$)**
0.4	3.8795	86.8885	0.199170
0.6	3.8789	86.8743	0.199168
0.8	3.8781	86.8557	0.199164
1.0	3.8769	86.8319	0.199160
3.0	3.8414	86.0384	0.199010
5.0	3.6967	82.8101	0.198340

6.6 Effect Of Agitator Position on Ethanol Yield

In addition to analysing the effect of agitator speed on the chemical reaction in the tank, fluid dynamics studies have focused on geometric parameters that can influence the mixing performance. There are also studies on the types of agitators conducted by Echaroj et al. (2020) and the positions of agitators carried out by Sahin et al. (2022). Saikali et al. (2021) used a magnetic rod installed at the bottom of the tank as an agitator. Meanwhile, Agarwal et al. (2021) evaluated the flow behaviour of two Rushton turbines.

Figure 6.16 illustrates the positional difference between the agitators used by Saikali et al. (2021) and Agarwal et al. (2021) in their studies.

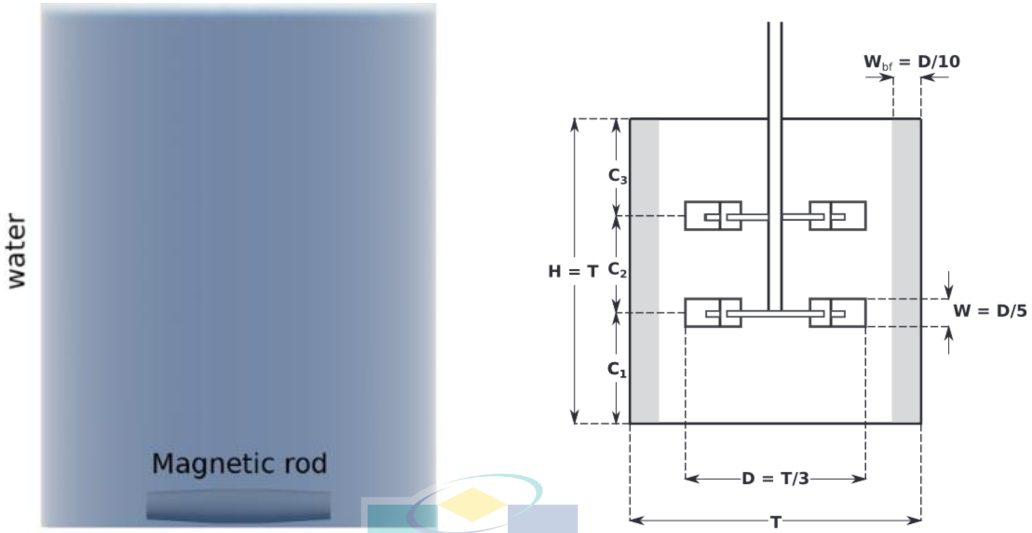

(a) (b)

Figure 6.16 The variation between the two agitator positions utilised by (a) Saikali et al. (2021) and (b) Agarwal et al. (2021).

Source: (a) Saikali et al. (2021), (b) Agarwal et al. (2021)

Modifying Equations 5.18 and 5.19, the position of the agitator was modified to resemble the agitator used by Agarwal et al. (2021). Below is a list of equations representing the new left boundary condition.

$$U(0,y,t) = 5 \times \left(500(y-0.5)^2 \times e^{500(y-0.5)^2 \times (0.80-1)+1}\right) \div 100 \qquad 6.4$$

$$V(0,y,t) = -0.3 \times \left(500(y-0.5)^2 \times e^{500(y-0.5)^2 \times (0.95-1)+1}\right) \div 100 \qquad 6.5$$

$$pr(0,y,t) = -\left(|U| + |V|\right) \qquad 6.6$$

Figure 6.17 presents the new boundary condition for the left side. In this study, two agitators were positioned at the approximate coordinates $y = 0.4$ and $y = 0.6$.

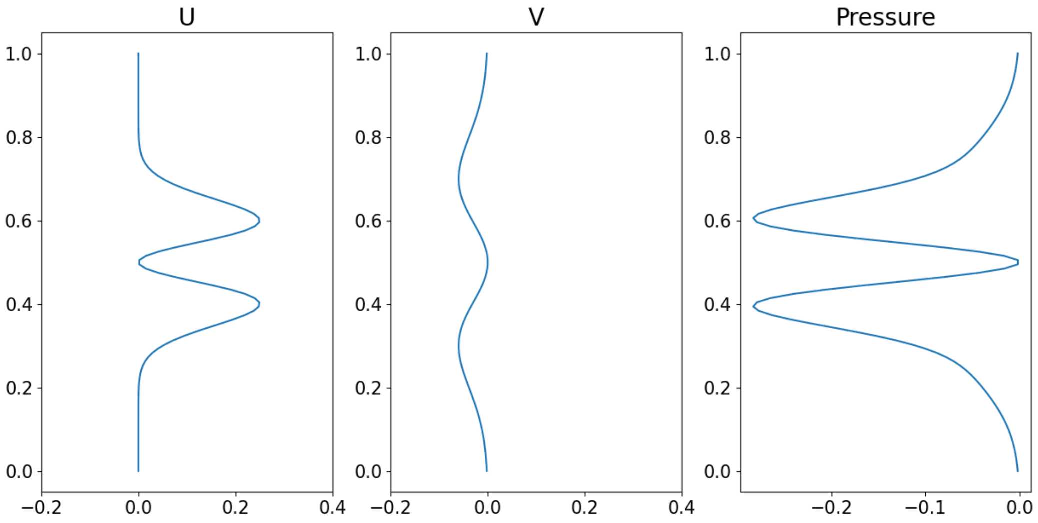

Figure 6.17 The new left-side boundary conditions for U , V and pr .

Figure 6.18, Figure 6.19, and Figure 6.20 illustrate the fermentation results for microbes, substrate, and ethanol using the new agitator position, with the fermentation period and σ parameter kept at 5 minutes and 0.05, respectively. The source of the velocity profile, represented by a magnitude arrow, caused the formation of two vortices in the tank as illustrated in Figure 6.18–Figure 6.20. One vortex was located at the lower part of the agitator, and the other was at the top. This demonstrates that Equations 6.4–6.6 can produce comparable results to the study conducted by Agarwal et al. (2021). However, the movement produced will only move the particles to the right side of the domain, or more specifically, towards the tank wall. This may not reduce the factor of inhomogeneity.

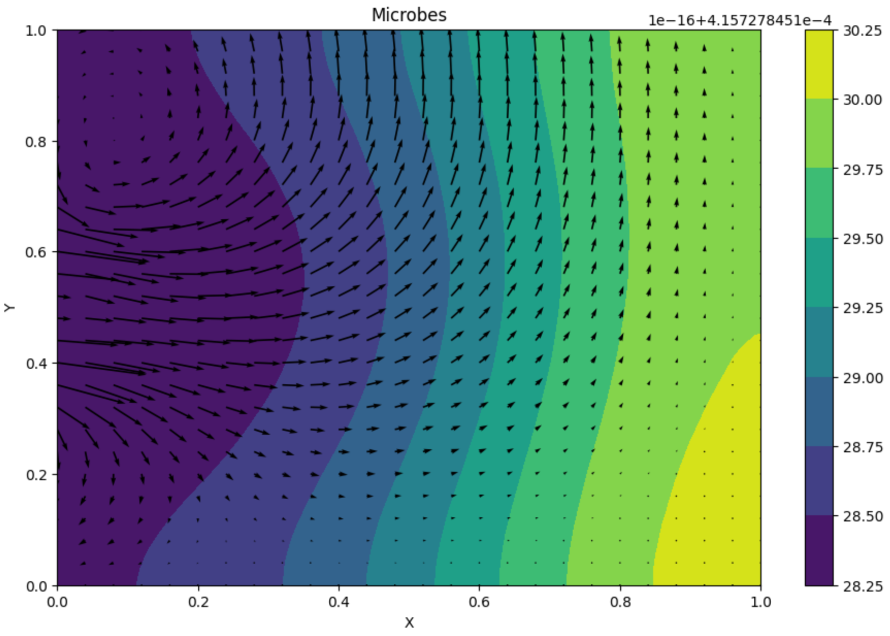

Figure 6.18 Microbe concentration using the new agitator position.

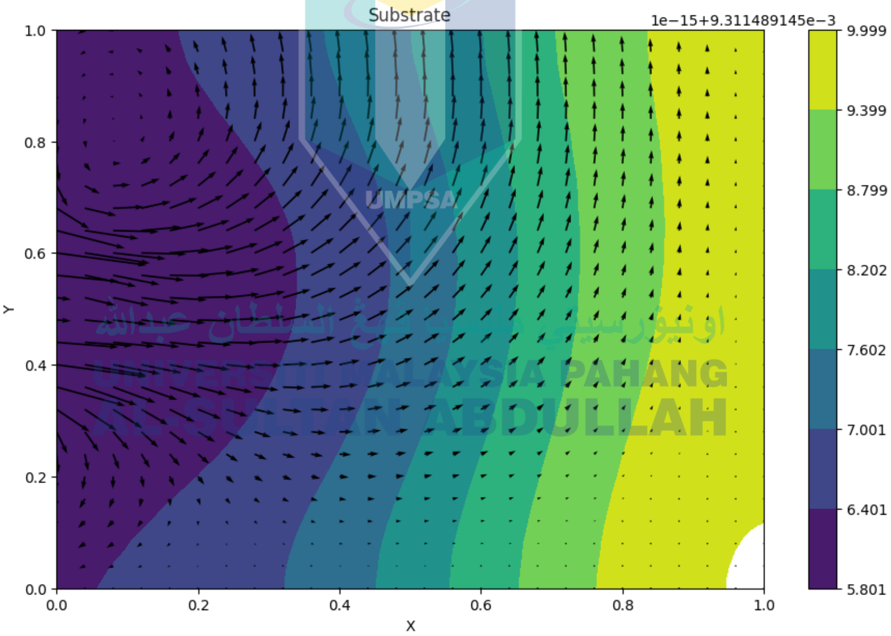

Figure 6.19 Substrate concentration using the new agitator position.

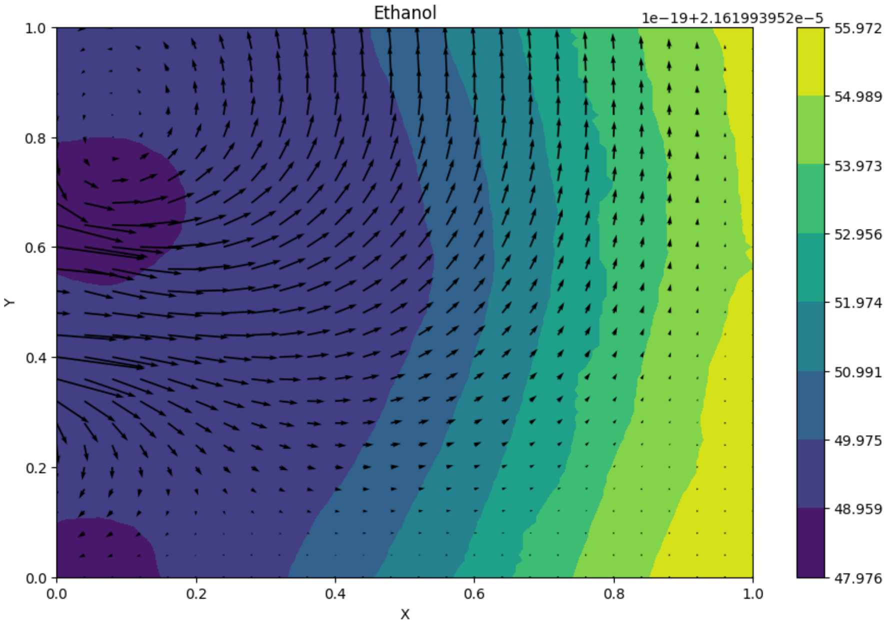

Figure 6.20 Ethanol concentration using the new agitator position.

Table 6.6 compares the particle concentration from Saikali et al. (2021) and Agarwal et al. (2021), particularly in different agitation positions, as illustrated in Figure 6.16. The current study found that all particles, whether microbes, substrate, and ethanol, had a higher concentration when the fermentation process was conducted using the agitator position described by Saikali et al. (2021) rather than the agitator position described by Agarwal et al. (2021). This suggests that the mixing approach of Saikali et al. (2021) can produce more ethanol than the mixing method of Agarwal et al. (2021). Even with the presence of substrate, the microbial concentration decreased from the initial concentration for the agitation fermentation position used by Agarwal et al. (2021) (microbes had an initial concentration of 3.8757 g/L, however, decreased to 3.8220 g/L). This could be because the mixing results created by the agitation position of Agarwal et al. (2021) only produce a particle movement pattern that pushes towards the tank wall, which is the right side of the domain. Nevertheless, this movement cannot solve the inhomogeneity issue in the tank, thus inhibit the fermentation process.

Table 6.6 Particle concentration using different agitation positions.

Agitation Position	Microbes (kg L $^{-1}$)	Substrate (kg L $^{-1}$)	Ethanol (kg L $^{-1}$)
Initial concentration	3.8757	87	0
Saikali et al. (2021)	3.8769	86.8319	0. 19916
Agarwal et al. (2021)	3.8220	85.6055	0.19892

On the basis of the research presented in this section, a recommendation can be made to obtain the maximum amount of ethanol, namely that a five minute fermentation process in the same vessel as Saikali et al. (2021), with σ of 0.05 in the free surface vortex section, and Ag value of 1 is capable of producing the greatest amount of ethanol.

6.7 Conclusion

This chapter aimed to discuss the inclusion of the particle movement elements into the reaction model of Phisalaphong et al. (2006). The first model discussed in this chapter was the coupled diffusion-reaction model. The diffusivity impact in the model was analysed and the result demonstrated that diffusivity had a minor effect on microbial growth, consumption of the substrate, and also in ethanol production. Motivated by the agitation employed in fermentation, the model was extended by including the advection parameter. Contrary to its diffusivity outcome, even though the advection coefficient was comparatively low, the model demonstrated an apparent change to the ethanol production system. Additionally, the development of this model not only confirms that the study of optimal advection value would enhance the value of ethanol production, but it could also illustrate that the presence of a high advection value will decrease ethanol production, as previous research has demonstrated.

Furthermore, this chapter also provided a more comprehensive analysis of the coupled fluid dynamics-advection-diffusion-reaction model. The fluid velocity represented by the Navier-Stokes equation was selected. In the early stages of the study, the velocity profile from Saikali et al. (2021) was used as the boundary condition of this study in order to determine the actual speed in the unbaffled tank. The proposed model successfully depicted the condition of particles dispersed throughout the tank. This reduced the inhomogeneity factor in the tank. With the effective solution of this model, a deeper understanding of the free surface vortex in relation to ethanol production could be gained. The free surface vortex was represented by a normal distribution function. The standard deviations of the normal distribution function were analysed to investigate the free surface vortex. According to this study, the smallest standard deviation of 0.05 can yield the highest ethanol concentration. This also indicates that a vortex with a large surface area will inhibit the production of ethanol. Also, the speed of the agitator was analysed in this chapter. The study revealed that increasing the speed of the agitator in the tank will kill microbes and influence the production of ethanol.

This chapter also includes a study of the agitator's position. A comparison was made between the agitator used in the study by Agarwal et al. (2021) and the agitator described by Saikali et al. (2021). Agarwal et al. (2021) use double-Rushton turbines as agitators, whereas Saikali et al. (2021) employ a magnetic stirrer. Fermentation using agitators such as double-Rushton turbines was unable to reduce the inhomogeneity factor in the tank, resulting in a decrease in ethanol production, according to a study of the first five-minute process. This study can provide recommendations for maximising ethanol production. For example, to achieve a homogeneous solution, the fermentation vessel must be stirred. In addition, the quicker the reduction of inhomogeneity in the bioreactor, the lower the death rate of microbes and the higher the chance of an increase in ethanol production. However, excessive agitation will also increase the shear force against the microbes, resulting in their death.

CHAPTER 7

CONCLUSIONS AND RECOMMENDATIONS

7.1 Conclusion

The process of ethanol production by fermentation has been employed for centuries in the production of alcoholic beverages and, more recently, in the field of renewable energy. Ethanol plays a crucial role in the production of biofuels, providing a cleaner and more environmentally friendly option compared to traditional fossil fuels. Consequently, the use of ethanol has the capacity to foster the establishment of an ecologically sustainable energy system.

The goal of this study is to uncover novel findings in the area of fermentation-based ethanol production. The identification of three stable points in the stability study can be utilised as predictive techniques for determining the long-term dynamics of ethanol production systems. The fermentation process will ultimately reach stable equilibrium points. Having knowledge of this value may provide an approximation of the ethanol production process.

Furthermore, it is believed that the results of parameter analysis would also lead to a rise in ethanol production. Increasing the model's sigma value has a beneficial effect on ethanol production. This study highlights the necessity of decreasing eight hindering parameters in order to attain the highest yield in ethanol production.

The proposed model in this work, which combines fluid dynamics, advection, diffusion, and reactivity, can be utilised to forecast ethanol production in various tanks. Similar to the simulations presented in this study, employing this approach could assist in avoiding unnecessary expenditures during the actual fermentation process. Additionally, it has the potential to greatly decrease the duration of testing needed during the fermentation process.

7.2 Recommendations

Several problems and topics requiring of additional research were encountered throughout this study. Regarding the presented results, there are a number of crucial issues and extensions that must be addressed.

This investigation was conducted using experimental data that only comprised time variables. In order to acquire a more precise model, it is recommended that future studies utilise sample data that include the geometric structure of a tank. In addition, it is also believed that a comprehensive exploration of fluid dynamics is necessary to broaden the scope of research in this field. The investigated model only predicted the fluid flow generated by a magnetic stirrer and two Rushton turbines. A comparison analysis conducted to examine the effects of these two different kinds of agitators on ethanol production would reveal contrasting results. Meanwhile, a variety of agitators have been utilised in the industry. It is recommended to do further investigation on various kinds of agitators that have the capability of increasing ethanol output. Last but not least, it is important to note that this mathematical study focused on batch fermentation approaches. Thus, it is strongly suggested that this mathematical model be adjusted so that it can be used for fed-batch or continuous fermentation.

REFERENCES

Abdul Halim, N. (2016). *Optimization of Bioethanol Production From Oil Palm Trunk Sap* [Doctoral thesis, Universiti Malaysia Pahang]. http://ecollib.ump.edu.my.ezproxy.ump.edu.my/id/eprint/3505

Afedzi, A. E. K., Rattanaporn, K., & Parakulsuksatid, P. (2022). Impeller selection for mixing high-solids lignocellulosic biomass in stirred tank bioreactor for ethanol production. *Bioresource Technology Reports*, *17*(October 2021), 100935. https://doi.org/10.1016/j.biteb.2021.100935

Agarwal, A., Singh, G., & Prakash, A. (2021). Numerical investigation of flow behavior in double-rushton turbine stirred tank bioreactor. *Materials Today: Proceedings*, *43*, 51–57. https://doi.org/10.1016/j.matpr.2020.11.208

Aiba, S., Shoda, M., & Nagatani, M. (1968). Kinetics of product inhibition in alcoholic fermentation. *Biotechnol Bioeng*, *11*, 846–864.

Bennett, T. (2012). *Transport by Advection and Diffusion*. John Wiley & Sons.

Birol, G., Doruker, P., Kirdar, B., İlsen Önsan, Z., & Ülgen, K. (1998). Mathematical description of ethanol fermentation by immobilised Saccharomyces cerevisiae. *Process Biochemistry*, *33*(7), 763–771. https://doi.org/10.1016/S0032-9592(98)00047-8

Bouzguenda, I., Alalouch, C., & Fava, N. (2019). Towards smart sustainable cities: A review of the role digital citizen participation could play in advancing social sustainability. *Sustainable Cities and Society*, *50*, 101627. https://doi.org/10.1016/j.scs.2019.101627

Brandon, J. (2003). Introduction to Applied Nonlinear Dynamical Systems and Chaos. In *The Mathematical Gazette* (Vol. 2, Issue 472). Springer-Verlag. https://doi.org/10.1007/b97481

Cheng, C., & Zheng, Z. (2021). Dynamics and spreading speed of a reaction-diffusion system with advection modeling West Nile virus. *Journal of Mathematical Analysis and Applications*, *493*(1), 124507. https://doi.org/10.1016/j.jmaa.2020.124507

Childs, P. R. N. (2011). Laws of Motion. In *Rotating Flow* (pp. 17–52). Elsevier.

https://doi.org/10.1016/B978-0-12-382098-3.00002-0

Das, D., & Pandit, S. (2021). *Industrial Biotechnology* (D. Das & S. Pandit (eds.); First edit). CRC Press. https://doi.org/10.1201/9780367822415

Derman, E., Abdulla, R., Marbawi, H., & Sabullah, M. K. (2018). Oil palm empty fruit bunches as a promising feedstock for bioethanol production in Malaysia. *Renewable Energy*, *129*, 285–298. https://doi.org/10.1016/j.renene.2018.06.003

Doble, M., Kruthiventi, A. K., & Gaikar, V. G. (2004). *Biotransforrnations and Bioprocesses*. CRC Press.

Ebrahimijahan, A., Dehghan, M., & Abbaszadeh, M. (2020). Compact local integrated radial basis functions (Integrated RBF) method for solving system of non–linear advection-diffusion-reaction equations to prevent the groundwater contamination. *Engineering Analysis with Boundary Elements*, *121*, 50–64. https://doi.org/10.1016/j.enganabound.2020.09.003

Echaroj, S., Ong, H. C., & Chen, X. (2020). Simulation of Mixing Intensity Profile for Bioethanol Production via Two-Step Fermentation in an Unbaffled Agitator Reactor. *Energies*, *13*(20), 5457. https://doi.org/10.3390/en13205457

Edwards, V. H. (1970). The influence of high substrate concentrations on microbial kinetics. *Biotechnology and Bioengineering*, *12*(5), 679–712. https://doi.org/10.1002/bit.260120504

Ermentrout, B. (2002). *Simulating, Analyzing, and Animating Dynamical Systems*. Society for Industrial and Applied Mathematics. https://doi.org/10.1137/1.9780898718195

Germec, M., Karhan, M., Demirci, A., & Turhan, I. (2022). Kinetic modeling, sensitivity analysis, and techno-economic feasibility of ethanol fermentation from non-sterile carob extract-based media in Saccharomyces cerevisiae biofilm reactor under a repeated-batch fermentation process. *Fuel*, *324*. https://doi.org/10.1016/j.fuel.2022.124729

Ghaly, A. E., & El-Taweel, A. A. (1997). Kinetic modelling of continuous production of ethanol from cheese whey. *Biomass and Bioenergy*, *12*(6), 461–472. https://doi.org/10.1016/S0961-9534(97)00012-3

Jeevan Kumar, S. P., Sampath Kumar, N. S., & Chintagunta, A. D. (2020). Bioethanol production from cereal crops and lignocelluloses rich agro-residues: prospects and challenges. *SN Applied Sciences*, *2*(10), 1673. https://doi.org/10.1007/s42452-020-03471-x

Kamer, S. (2004). *Effects of agitation, temperature, and bacterial cell concentration on Zymomonas mobilis fermentation of corn stover to ethanol* (Issue August). University o f Louisville.

Kono, T. (1968). Kinetics of microbial cell growth. *Biotechnology and Bioengineering*, *10*(2), 105–131. https://doi.org/10.1002/bit.260100202

Kono, T., & Asai, T. (1969). Kinetics of fermentation processes. *Biotechnology and Bioengineering*, *11*(3), 293–321. https://doi.org/10.1002/bit.260110304

Labík, L., Petričříček, R., Moucha, T., Brucato, A., Caputo, G., Grisafi, F., & Scargiali, F. (2018). Scale-up and viscosity effects on gas–liquid mass transfer rates in unbaffled stirred tanks. *Chemical Engineering Research and Design*, *132*, 584–592. https://doi.org/10.1016/j.cherd.2018.01.051

Langtangen, H. P., & Pedersen, G. K. (2016). Scaling of Differential Equations. In *Scaling of Differential Equations*. Springer International Publishing. https://doi.org/10.1007/978-3-319-32726-6

Levenspiel, O. (1980). The monod equation: A revisit and a generalization to product inhibition situations. *Biotechnology and Bioengineering*, *22*(8), 1671–1687. https://doi.org/10.1002/bit.260220810

Louie, K., Clark, H., & Newton, P. C. D. D. (1998). Analysis of differential equation models in biology: A case study for clover meristem populations. *New Zealand Journal of Agricultural Research*, *41*(4), 567–576. https://doi.org/10.1080/00288233.1998.9513340

Ma, L., & Tang, D. (2023). A diffusion-advection predator-prey model with a protection zone. *Journal of Differential Equations*, *375*, 304–347. https://doi.org/10.1016/j.jde.2023.08.004

Malek, A. B. M. A., Hasanuzzaman, M., Rahim, N. A., & Al Turki, Y. A. (2017). Techno-economic analysis and environmental impact assessment of a 10 MW biomass-based power plant in Malaysia. *Journal of Cleaner Production*, *141*, 502–513. https://doi.org/10.1016/j.jclepro.2016.09.057

Merger, J., Borzì, A., & Herzog, R. (2017). Optimal control of a system of reaction–diffusion equations modeling the wine fermentation process. *Optimal Control Applications and Methods*, *38*(1), 112–132. https://doi.org/10.1002/oca.2246

Mohd Azhar, S. H., Abdulla, R., Jambo, S. A., Marbawi, H., Gansau, J. A., Mohd Faik, A. A., & Rodrigues, K. F. (2017). Yeasts in sustainable bioethanol production: A review. *Biochemistry and Biophysics Reports*, *10*(February), 52–61. https://doi.org/10.1016/j.bbrep.2017.03.003

Monod, J. (1949). THE GROWTH OF BACTERIAL CULTURES. *Annual Review of Microbiology*, *3*(1), 371–394. https://doi.org/10.1146/annurev.mi.03.100149.002103

Moroney, T. J. (2006). *An investigation of a finite volume method incorporating radial basis functions for simulating nonlinear transport* [Queensland University of Technology]. https://api.semanticscholar.org/CorpusID:126292842

Nagarajan, S., Stella, L., Lawton, L. A., Irvine, J. T. S., & Robertson, P. K. J. (2017). Mixing regime simulation and cellulose particle tracing in a stacked frame photocatalytic reactor. *Chemical Engineering Journal*, *313*, 301–308. https://doi.org/10.1016/j.cej.2016.12.016

Nasir, A., Rahman, S. S., Hossain, M. M., & Choudhury, N. (2017). Isolation of Saccharomyces cerevisiae from pineapple and orange and study of metal's effectiveness on ethanol production. *European Journal of Microbiology and Immunology*, *7*(1), 76–91. https://doi.org/10.1556/1886.2016.00035

Phisalaphong, M., Srirattana, N., & Tanthapanichakoon, W. (2006). Mathematical modeling to investigate temperature effect on kinetic parameters of ethanol fermentation. *Biochemical Engineering Journal*, *28*(1), 36–43. https://doi.org/10.1016/j.bej.2005.08.039

Phuang, Z. X., Lin, Z., Liew, P. Y., Hanafiah, M. M., & Woon, K. S. (2022). The dilemma in energy transition in Malaysia: A comparative life cycle assessment of large scale solar and biodiesel production from palm oil. *Journal of Cleaner Production*, *350*. https://doi.org/10.1016/j.jclepro.2022.131475

Phukoetphim, N., Salakkam, A., Laopaiboon, P., & Laopaiboon, L. (2017). Kinetic models for batch ethanol production from sweet sorghum juice under normal and high gravity fermentations: Logistic and modified Gompertz models. *Journal of Biotechnology*, *243*, 69–75. https://doi.org/10.1016/j.jbiotec.2016.12.012

Quiroz-Pérez, E., Gutiérrez-Antonio, C., & Vázquez-Román, R. (2019). Modelling of production processes for liquid biofuels through CFD: A review of conventional and intensified technologies. *Chemical Engineering and Processing - Process Intensification*, *143*(December 2018), 107629. https://doi.org/10.1016/j.cep.2019.107629

Roca, E., Flores, J., Núñez, M. J., & Lema, J. M. J. M. (1996). Ethanolic fermentation by immobilized Saccharomyces cerevisiae in a semipilot pulsing packed-bed bioreactor. *Enzyme and Microbial Technology*, *19*(2), 132–139. https://doi.org/10.1016/0141-0229(95)00191-3

Sahin, F., Kaya, A., Alic, E., & Aydin, O. (2022). Investigation of effect of a mechanical agitator on pool boiling heat transfer. *International Communications in Heat and Mass Transfer*, *139*, 106433. https://doi.org/10.1016/j.icheatmasstransfer.2022.106433

Saikali, E., Bois, G., Rodio, M. G., Bieder, U., Burlot, A., & Bertrand, M. (2021). Validation of the hydrodynamics in a turbulent un-baffled vortex reactor at two different stirring Reynolds numbers. *Nuclear Engineering and Design*, *384*, 111450. https://doi.org/10.1016/j.nucengdes.2021.111450

Serafim, F. A. T., & Lanças, F. M. (2019). Sugarcane Spirits (Cachaça) Quality Assurance and Traceability: An Analytical Perspective. In *Production and Management of Beverages*. Elsevier Inc. https://doi.org/10.1016/b978-0-12-815260-7.00011-0

Setford, P. C., Jeffery, D. W., Grbin, P. R., & Muhlack, R. A. (2019). Mathematical modelling of anthocyanin mass transfer to predict extraction in simulated red wine fermentation scenarios. *Food Research International*, *121*(December 2018), 705–713. https://doi.org/10.1016/j.foodres.2018.12.044

Sokmez, E., Taymaz, I., & Eker Kahveci, E. (2022). Performance evaluation of direct ethanol fuel cell using a three-dimensional CFD model. *Fuel*, *313*, 123022. https://doi.org/10.1016/j.fuel.2021.123022

Takahashi, M., & Aoyagi, H. (2018). Practices of shake-flask culture and advances in monitoring CO2 and O2. *Applied Microbiology and Biotechnology*, *102*(10), 4279–4289. https://doi.org/10.1007/s00253-018-8922-8

Tesfaw, A., & Assefa, F. (2014). Current Trends in Bioethanol Production by Saccharomyces cerevisiae : Substrate, Inhibitor Reduction, Growth Variables, Coculture, and Immobilization. *International Scholarly Research Notices*, *2014*, 1–11. https://doi.org/10.1155/2014/532852

Tosun, I. (2007). *Modelling in transport phenomena : a conceptual approach*. Elsevier.

Tse, T. J., Wiens, D. J., & Reaney, M. J. T. T. (2021). Production of Bioethanol—A Review of Factors Affecting Ethanol Yield. *Fermentation*, *7*(4), 268. https://doi.org/10.3390/fermentation7040268

Tseng, M. M., & Wayman, M. (1975). Kinetics of yeast growth: inhibition-threshold substrate concentrations. *Canadian Journal of Microbiology*, *21*(7), 994–1003. https://doi.org/10.1139/m75-147

Um, B.-H., & Hanley, T. R. (2008). A Comparison of Simple Rheological Parameters and Simulation Data for Zymomonas mobilis Fermentation Broths with High Substrate Loading in a 3-L Bioreactor. *Applied Biochemistry and Biotechnology*, *145*(1–3), 29–38. https://doi.org/10.1007/s12010-007-8105-z

Wyrobnik, T. A., Oh, S., Ducci, A., & Micheletti, M. (2022). Engineering characterization of the novel Bach impeller for bioprocessing applications requiring low power inputs. *Chemical Engineering Science*, *252*. https://doi.org/10.1016/j.ces.2021.117263

Yano, T., & Koga, S. (1969). *Dynamic Behavior of the Chemostat Subject*. *XI*(2), 139–153.

APPENDICES

Appendix A: Non-dimensional Phisalaphong et al. (2006) model.

The model proposed by Phisalaphong et al. (2006) is represented by Equations 2.1, 2.2, and 2.3

$$\frac{dM}{dt} = \mu_{max} SM \left(K_{SM} + S + \frac{S^2}{K_{IM}} \right)^{-1} \left(1 - \frac{P}{P_M} \right) - K_d M \qquad 2.1$$

$$\frac{dP}{dt} = v_{max} SM \left(K_{SP} + S + \frac{S^2}{K_{IP}} \right)^{-1} \left(1 - \frac{P}{P_P} \right) \qquad 2.2$$

$$\frac{dS}{dt} = -\frac{1}{Y_{MS}} \left(\frac{dM}{dt} \right) - \frac{1}{Y_{PS}} \left(\frac{dP}{dt} \right) - mM \qquad 2.3$$

can be modified into a non-dimensional model using the following transformations

$$M = g\left(K_{IM}\right), \qquad P = p\left(\frac{v_{\max} K_{IP}}{K_d}\right), \qquad S = s\left(K_{IM}\right), \qquad t = \tau\left(\frac{1}{K_d}\right).$$

Then, for Equation 2.1,

$$\frac{dM}{dt} = \mu_{max} SM \left(K_{SM} + S + \frac{S^2}{K_{IM}} \right)^{-1} \left(1 - \frac{P}{P_M} \right) - K_d M$$

$$\frac{dgK_{IM}}{d\tau\left(\frac{1}{K_d}\right)} = \mu_{max} sK_{IM}\, gK_{IM} \left(K_{SM} + sK_{IM} + \frac{\left(sK_{IM}\right)^2}{K_{IM}} \right)^{-1} \left(1 - \left(\frac{pv_{max} K_{IP}}{K_d P_M} \right) \right) - K_d gK_{IM}$$

$$\frac{dg}{d\tau} = \frac{\mu_{max} sK_{IM}\, gK_{IM}}{K_{IM}} \left(\frac{1}{K_d} \right) \left(K_{SM} + sK_{IM} + \frac{\left(sK_{IM}\right)^2}{K_{IM}} \right)^{-1} \left(1 - \left(\frac{pv_{max} K_{IP}}{K_d P_M} \right) \right) - \frac{K_d gK_{IM}}{K_{IM}} \left(\frac{1}{K_d} \right)$$

$$\frac{dg}{d\tau}=\frac{\mu_{max}sgK_{IM}}{K_d}\left(K_{SM}+sK_{IM}+s^2K_{IM}\right)^{-1}\left(1-\left(\frac{pv_{max}K_{IP}}{K_dP_M}\right)\right)-g$$

Let $\sigma=\frac{\mu_{\max}}{K_d}$

$$\frac{dg}{d\tau}=\frac{\mu_{max}}{K_d}sgK_{IM}\left(K_{SM}+sK_{IM}+s^2K_{IM}\right)^{-1}\left(1-p\left(\frac{v_{max}K_{IP}}{K_dP_M}\right)\right)-g$$

$$\frac{dg}{d\tau}=\frac{\sigma sgK_{IM}}{K_{SM}+sK_{IM}+s^2K_{IM}}\left(1-p\left(\frac{v_{max}K_{IP}}{K_dP_M}\right)\right)-g$$

Let $\lambda=\frac{v_{\max}K_{IP}}{K_dP_M}$

$$\frac{dg}{d\tau}=\frac{\sigma sgK_{IM}}{K_{SM}+sK_{IM}+s^2K_{IM}}(1-p\lambda)-g$$

$$\frac{dg}{d\tau}=(1-\lambda p)\sigma\frac{sgK_{IM}}{K_{SM}+sK_{IM}+s^2K_{IM}}-g$$

$$\frac{dg}{d\tau}=(1-\lambda p)\sigma\frac{sx}{\frac{K_{SM}+sK_{IM}+s^2K_{IM}}{K_{IM}}}-g$$

$$\frac{dg}{d\tau}=(1-\lambda p)\sigma\frac{sg}{\frac{K_{SM}}{K_{IM}}+\frac{sK_{IM}}{K_{IM}}+\frac{s^2K_{IM}}{K_{IM}}}-g$$

$$\frac{dg}{d\tau}=(1-\lambda p)\sigma\frac{sg}{\frac{K_{SM}}{K_{IM}}+s+s^2}-g$$

Let $\alpha = \dfrac{K_{SM}}{K_{IM}}$.

Finally, the non-dimensional form of Equation 2.1 can be derived as shown in the following equation.

$$\frac{dg}{d\tau} = (1-\lambda p)\sigma \frac{sg}{\alpha + s + s^2} - g$$

In the case of Equation 2.2,

$$\frac{dP}{dt} = v_{max} SM \left(K_{SP} + S + \frac{S^2}{K_{IP}} \right)^{-1} \left(1 - \frac{P}{P_P} \right)$$

$$\frac{dp\left(\dfrac{v_{max}K_{IP}}{K_d}\right)}{d\tau\left(\dfrac{1}{K_d}\right)} = v_{max} sK_{IM}\, gK_{IM} \left(K_{SP} + sK_{IM} + \frac{(sK_{IM})^2}{K_{IP}} \right)^{-1} \left(1 - \frac{p\left(\dfrac{v_{max}K_{IP}}{K_d}\right)}{P_P} \right)$$

$$\frac{dp}{d\tau} = \frac{v_{max} sK_{IM}\, gK_{IM}}{\left(\dfrac{v_{max}K_{IP}}{K_d}\right)} \left(\frac{1}{K_d}\right) \left(K_{SP} + sK_{IM} + \frac{(sK_{IM})^2}{K_{IP}} \right)^{-1} \left(1 - \frac{p\left(\dfrac{v_{max}K_{IP}}{K_d}\right)}{P_P} \right)$$

$$\frac{dp}{d\tau} = v_{max} sK_{IM}\, gK_{IM} \frac{K_d}{v_{max}K_{IP}} \left(\frac{1}{K_d}\right) \left(K_{SP} + sK_{IM} + \frac{(sK_{IM})^2}{K_{IP}} \right)^{-1} \left(1 - p\left(\frac{v_{max}K_{IP}}{K_d P_P}\right) \right)$$

Let $\kappa = \dfrac{v_{\max} K_{IP}}{K_d P_P}$

$$\frac{dp}{d\tau}=\frac{sgK_{IM}K_{IM}}{K_{IP}}\left(K_{SP}+sK_{IM}+\frac{(sK_{IM})^2}{K_{IP}}\right)^{-1}(1-p\kappa)$$

$$\frac{dp}{d\tau}=\frac{sgK_{IM}{}^2}{K_{IP}\left(K_{SP}+sK_{IM}+\frac{(sK_{IM})^2}{K_{IP}}\right)}(1-p\kappa)$$

$$\frac{dp}{d\tau}=\frac{sg}{K_{IP}\left(K_{SP}+sK_{IM}+\frac{(sK_{IM})^2}{K_{IP}}\right)}\times K_{IM}{}^2\times(1-p\kappa)$$

$$\frac{dp}{d\tau}=\frac{sg}{K_{IP}\left(K_{SP}+sK_{IM}+\frac{(sK_{IM})^2}{K_{IP}}\right)}\times\frac{1}{\frac{1}{K_{IM}{}^2}}\times(1-p\kappa)$$

$$\frac{dp}{d\tau}=\frac{sg}{\frac{K_{IP}}{K_{IM}{}^2}\left(K_{SP}+sK_{IM}+\frac{(sK_{IM})^2}{K_{IP}}\right)}\times(1-p\kappa)$$

$$\frac{dp}{d\tau}=\frac{sg}{\frac{K_{IP}K_{SP}}{K_{IM}{}^2}+\frac{sK_{IM}K_{IP}}{K_{IM}{}^2}+\frac{K_{IP}}{K_{IM}{}^2}\frac{s^2K_{IM}{}^2}{K_{IP}}}\times(1-p\kappa)$$

$$\frac{dp}{d\tau}=\frac{sg}{\frac{K_{IP}K_{SP}}{K_{IM}{}^2}+s\frac{K_{IP}}{K_{IM}}+s^2}\times(1-p\kappa)$$

Let $\gamma = \frac{K_{SP}K_{IP}}{{K_{IM}}^2}$ & $\beta = \frac{K_{IP}}{K_{IM}}$

and Equation 2.2 can be expressed in non-dimensional form as illustrated below.

$$\frac{dp}{d\tau} = (1-\kappa p)\frac{sg}{\gamma+\beta s+s^2}$$

Relating to Equation 2.3,

$$\frac{dS}{dt} = -\frac{1}{Y_{MS}}\left(\frac{dM}{dt}\right) - \frac{1}{Y_{PS}}\left(\frac{dP}{dt}\right) - mM$$

$$\frac{dS}{dt} = -\frac{1}{Y_{MS}}\left(\mu_{max}SM\left(K_{SM}+S+\frac{S^2}{K_{IM}}\right)^{-1}\left(1-\frac{P}{P_M}\right) - K_d M\right) - \frac{1}{Y_{PS}}\left(v_{max}SM\left(K_{SP}+S+\frac{S^2}{K_{IP}}\right)^{-1}\left(1-\frac{P}{P_P}\right)\right) - mM$$

Y_{MS} and Y_{PS} are already in dimensionless form. So, these 2 parameters are left without making any changes.

$$\frac{dsK_{IM}}{d\tau\left(\frac{1}{K_d}\right)} = -\frac{\mu_{max}sK_{IM}gK_{IM}}{Y_{MS}}\left(K_{SM}+sK_{IM}+\frac{(sK_{IM})^2}{K_{IM}}\right)^{-1}\left(1-p\left(\frac{v_{max}K_{IP}}{P_M K_d}\right)\right) + \frac{K_d gK_{IM}}{Y_{MS}} - \frac{v_{max}sK_{IM}gK_{IM}}{Y_{PS}}\left(K_{SP}+sK_{IM}+\frac{(sK_{IM})^2}{K_{IP}}\right)^{-1}\left(1-p\left(\frac{v_{max}K_{IP}}{P_P K_d}\right)\right) - mgK_{IM}$$

$$\frac{ds}{d\tau}=-\frac{\mu_{max}sK_{IM}gK_{IM}}{Y_{MS}K_{IM}}\left(\frac{1}{K_d}\right)\left(K_{SM}+sK_{IM}+\frac{s^2K_{IM}{}^2}{K_{IM}}\right)^{-1}\left(1-p\left(\frac{v_{max}K_{IP}}{P_MK_d}\right)\right)+\frac{K_dgK_{IM}}{Y_{MS}K_{IM}}\left(\frac{1}{K_d}\right)$$
$$-\frac{v_{max}sK_{IM}gK_{IM}}{Y_{PS}K_{IM}}\left(\frac{1}{K_d}\right)\left(K_{SP}+sK_{IM}+\frac{s^2K_{IM}{}^2}{K_{IP}}\right)^{-1}\left(1-p\left(\frac{v_{max}K_{IP}}{P_PK_d}\right)\right)-\frac{mgK_{IM}}{K_{IM}}\left(\frac{1}{K_d}\right)$$

$$\frac{ds}{d\tau}=-\frac{\mu_{max}sgK_{IM}}{Y_{MS}}\left(\frac{1}{K_d}\right)\left(K_{SM}+sK_{IM}+s^2K_{IM}\right)^{-1}\left(1-p\left(\frac{v_{max}K_{IP}}{P_MK_d}\right)\right)+\frac{g}{Y_{MS}}$$
$$-\frac{v_{max}sgK_{IM}}{Y_{PS}}\left(\frac{1}{K_d}\right)\left(K_{SP}+sK_{IM}+\frac{s^2K_{IM}{}^2}{K_{IP}}\right)^{-1}\left(1-p\left(\frac{v_{max}K_{IP}}{P_PK_d}\right)\right)-\frac{mg}{K_d}$$

$$\frac{ds}{d\tau}=-\frac{\frac{sg}{Y_{MS}}\left(\frac{\mu_{max}}{K_d}\right)\times K_{IM}}{K_{SM}+sK_{IM}+s^2K_{IM}}\left(1-p\left(\frac{v_{max}K_{IP}}{P_MK_d}\right)\right)$$
$$-\frac{\frac{sg}{Y_{PS}}\left(\frac{v_{max}K_{IM}}{K_d}\right)}{K_{SP}+sK_{IM}+\frac{s^2K_{IM}{}^2}{K_{IP}}}\left(1-p\left(\frac{v_{max}K_{IP}}{P_PK_d}\right)\right)+\frac{g}{Y_{MS}}-\frac{m}{K_d}g$$

Let $\sigma=\frac{\mu_{\max}}{K_d}$, $\lambda=\frac{v_{\max}K_{IP}}{K_dP_M}$, $\kappa=\frac{v_{\max}K_{IP}}{K_dP_P}$, $\rho=\frac{m}{K_d}$

$$\frac{ds}{d\tau}=-\frac{1}{Y_{MS}}\frac{sg\sigma}{\frac{K_{SM}+sK_{IM}+s^2K_{IM}}{K_{IM}}}(1-p\lambda)$$
$$-\frac{1}{Y_{PS}}\frac{sg\left(\frac{v_{max}K_{IM}}{K_d}\right)}{\frac{K_{SP}K_{IP}}{K_{IP}}+s\frac{K_{IM}K_{IP}}{K_{IP}}+s^2\frac{K_{IM}{}^2}{K_{IP}}}(1-p\kappa)+\frac{g}{Y_{MS}}-\rho g$$

$$\frac{ds}{d\tau}=\frac{(p\lambda-1)}{Y_{MS}}\frac{sg\sigma}{\frac{K_{SM}}{K_{IM}}+s\frac{K_{IM}}{K_{IM}}+s^{2}\frac{K_{IM}}{K_{IM}}}+\frac{(p\kappa-1)}{Y_{PS}}\frac{sg\left(\frac{v_{max}K_{IM}}{K_{d}}\right)}{\frac{\left(K_{SP}K_{IP}+sK_{IM}K_{IP}+s^{2}K_{IM}{}^{2}\right)}{K_{IP}}}+\left(\frac{1}{Y_{MS}}-\rho\right)g$$

Let $\alpha=\frac{K_{SM}}{K_{IM}}$

$$\frac{ds}{d\tau}=\frac{(p\lambda-1)}{Y_{MS}}\frac{sg\sigma}{\alpha+s+s^{2}}+\frac{(p\kappa-1)}{Y_{PS}}sg\left(\frac{v_{max}K_{IM}}{K_{d}}\right)\div\frac{\left(K_{SP}K_{IP}+sK_{IM}K_{IP}+s^{2}K_{IM}{}^{2}\right)}{K_{IP}}$$
$$+\left(\frac{1}{Y_{MS}}-\rho\right)g$$

$$\frac{ds}{d\tau}=\frac{(\lambda p-1)}{Y_{MS}}\sigma\frac{sg}{\alpha+s+s^{2}}+\frac{(\kappa p-1)}{Y_{PS}}sg\left(\frac{v_{max}}{K_{d}}\right)\frac{K_{IM}{}^{2}}{K_{IM}}\times\frac{K_{IP}}{\left(K_{SP}K_{IP}+sK_{IM}K_{IP}+s^{2}K_{IM}{}^{2}\right)}$$
$$+\left(\frac{1}{Y_{MS}}-\rho\right)g$$

$$\frac{ds}{d\tau}=\frac{(\lambda p-1)}{Y_{MS}}\sigma\frac{sg}{\alpha+s+s^{2}}+\frac{(\kappa p-1)}{Y_{PS}}sg\left(\frac{v_{max}K_{IP}}{K_{d}K_{IM}}\right)\times\frac{K_{IM}{}^{2}}{\left(K_{SP}K_{IP}+sK_{IM}K_{IP}+s^{2}K_{IM}{}^{2}\right)}$$
$$+\left(\frac{1}{Y_{MS}}-\rho\right)g$$

$$\frac{ds}{d\tau}=\frac{(\lambda p-1)}{Y_{MS}}\sigma\frac{sg}{\alpha+s+s^{2}}+\frac{(\kappa p-1)}{Y_{PS}}sg\left(\frac{v_{max}K_{IP}}{K_{d}K_{IM}}\right)\div\frac{\left(K_{SP}K_{IP}+sK_{IM}K_{IP}+s^{2}K_{IM}{}^{2}\right)}{K_{IM}{}^{2}}$$
$$+\left(\frac{1}{Y_{MS}}-\rho\right)g$$

$$\frac{ds}{d\tau}=\frac{(\lambda p-1)}{Y_{MS}}\sigma\frac{sg}{\alpha+s+s^{2}}+\frac{(\kappa p-1)}{Y_{PS}}sg\left(\frac{v_{max}K_{IP}}{K_{d}K_{IM}}\right)\div\left(\frac{K_{SP}K_{IP}}{K_{IM}{}^{2}}+s\frac{K_{IM}K_{IP}}{K_{IM}{}^{2}}+s^{2}\frac{K_{IM}{}^{2}}{K_{IM}{}^{2}}\right)$$
$$+\left(\frac{1}{Y_{MS}}-\rho\right)g$$

Let $\gamma=\dfrac{K_{SP}K_{IP}}{K_{IM}{}^{2}}$, $\quad\phi=\dfrac{v_{\max}K_{IP}}{K_{d}K_{IM}}$

$$\frac{ds}{d\tau}=\frac{(\lambda p-1)}{Y_{MS}}\sigma\frac{sg}{\alpha+s+s^{2}}+\frac{(\kappa p-1)}{Y_{PS}}sg\phi\div\left(\gamma+s\frac{K_{IP}}{K_{IM}}+s^{2}\right)+\left(\frac{1}{Y_{MS}}-\rho\right)g$$

Let $\beta=\dfrac{K_{IP}}{K_{IM}}$.

The Equation 2.3 can therefore be transformed into a non-dimensional form, as shown in the following expression.

$$\frac{ds}{d\tau}=\frac{(\lambda p-1)}{Y_{MS}}\sigma\frac{sg}{\alpha+s+s^{2}}+\frac{(\kappa p-1)}{Y_{PS}}\phi\frac{sg}{\gamma+s\beta+s^{2}}+\left(\frac{1}{Y_{MS}}-\rho\right)g$$

Appendix B: Conditions of equilibrium points.

The equilibrium points depend on the certain condition as follows:

Condition 1

$(\rho \neq 0 \mid \lambda \neq 0 \;\&\; \sigma = 0) \;\&\; \kappa \neq 0 \mid \kappa = 0 \mid \kappa \neq 0 \;\&\; \lambda = 0 \;\&\; \rho = 0 \mid \kappa \neq 0 \;\&\; \lambda \neq 0 \;\&\; \rho = 0 \;\&\; \sigma \neq 0$

Condition 2

$\kappa \neq 0 \;\&\; \lambda = 0 \;\&\; \rho = 0$

Condition 3

$\kappa \neq 0 \;\&\; \lambda = 0 \;\&\; \rho = 0$

Condition 4

$\kappa \neq 0 \;\&\; \lambda \neq 0 \;\&\; \rho = 0 \;\&\; \sigma \neq 0$

Condition 5

$(\rho \neq 0 \mid \lambda \neq 0 \;\&\; \sigma = 0) \;\&\; z2 + \beta{*}z + \gamma \neq 0 \;\&\; z2 + z + \alpha \neq 0 \;\&\; \kappa \neq 0 \mid z2 + \beta{*}z + \gamma \neq 0 \;\&\; z2 + z + \alpha \neq 0 \;\&\; \kappa \neq 0 \;\&\; \lambda = 0 \;\&\; \rho = 0 \mid z2 + \beta{*}z + \gamma \neq 0 \;\&\; z2 + z + \alpha \neq 0 \;\&\; \kappa \neq 0 \;\&\; \lambda \neq 0 \;\&\; \rho = 0 \;\&\; \sigma \neq 0$

Condition 7

$\kappa \neq 0 \;\&\; \lambda \neq 0 \;\&\; \rho = 0 \;\&\; \sigma \neq 0$

Condition 8

$(\rho \neq 0 \mid \lambda \neq 0 \;\&\; \sigma = 0) \;\&\; \kappa \neq 0 \mid \kappa = 0 \mid \kappa \neq 0 \;\&\; \lambda = 0 \;\&\; \rho = 0 \mid \kappa \neq 0 \;\&\; \lambda \neq 0 \;\&\; \rho = 0 \;\&\; \sigma \neq 0$

Appendix C: Fourth-order Runge-Kutta methods.

The fourth-order Runge-Kutta method is given by

$$h_{i+1} = h_i + \frac{s}{6}\left(k_1 + 2k_2 + 2k_3 + k_4\right)$$

where

$$\begin{aligned} k_1 &= f\left(t_i, h_i\right) \\ k_2 &= f\left(t_i + \frac{s}{2}, h_i + \frac{s}{2}k_1\right) \\ k_3 &= f\left(t_i + \frac{s}{2}, h_i + \frac{s}{2}k_2\right) \\ k_4 &= f\left(t_i + s, h_i + sk_3\right) \end{aligned}$$

The variable s is the iterative step size and h_{i+1} is the approximation at $t_i + s$.

Appendix D: Estimating the Concentration of Particles.

Trapezoidal rule can be used to compute the particle concentration.

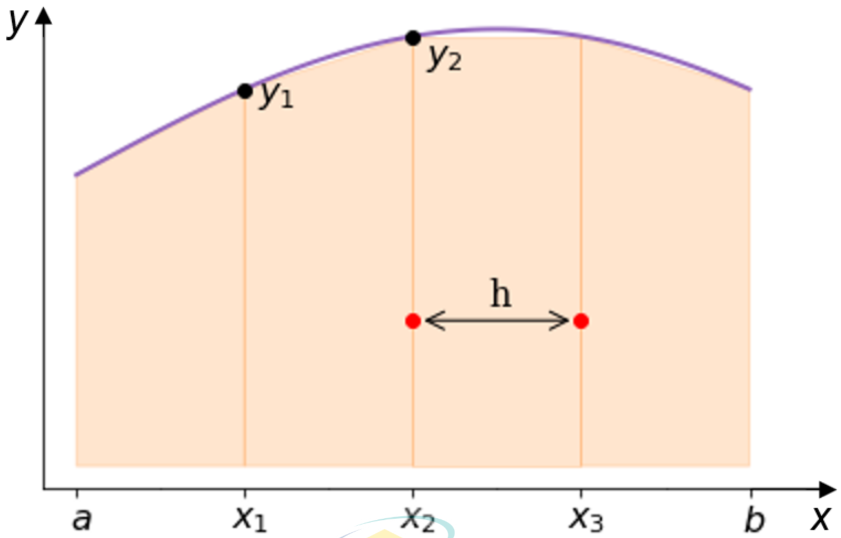

The trapezoidal rule is represented by the following equation.

$$\int_a^b y dx \approx \frac{b-a}{2n}\left[a+2\left(y_1+y_2+\ldots+y_{n-1}\right)+b\right]$$

where *n* is the number of subintervals and *h* is the equal trapezoidal width.